2016

The Influence of Soil Properties on Marsh Edge Erosion

Cody Lee Johnson
Louisiana State University and Agricultural and Mechanical College, cjoh296@lsu.edu

THE INFLUENCE OF SOIL PROPERTIES ON MARSH EDGE EROSION

A Thesis

Submitted to the Graduate Faculty of the
Louisiana State University and
Agricultural and Mechanical College
in partial fulfillment of the
requirements for the degree of
Masters of Science

in

Civil and Environmental Engineering

by
Cody L. Johnson
BS, Florida State University, 2010
December 2016

For Friends and Family

Acknowledgments

I want to first of all thank my parents, Christopher and Mary Johnson, who were always able to create a positive environment. I also need to thank the rest of my family and friends. Certainly, very little through me would be possible without their support and friendship.

I gratefully acknowledge the guidance and opportunities which my adviser Prof. Qin Chen has made available to me. Dr. Chen has figured for me as the model academician possessing the thoroughness required to pursue scientific research. I would also like to thank the other members of my thesis committee, Prof. Samuel Bentley and Prof. Celalettin Ozdemir, for their time, effort, and insight.

I am grateful to have worked with the other members of my research group, Arash Karimpour, Ke Liu, Agnimitro Chakrabarti, Ling Zhu, and Thomas Everett. Their patience and curiosity are an continual inspiration. I am also grateful to those members of the Louisiana State University's Department of Geology and Geophysics and the Coastal Studies Institute's Field Support team who ensured the success of all our field work.

This thesis is indebted to the work it has built upon and the expert opinions of practicing research professionals. A large part of the data analysis was pre-formatted and provided to me by Brady Couvillion of the USGS. His work analyzing the shoreline retreat rates and compiling accurate digital elevation maps formed the starting point for much of this research. I also had the opportunity to interact with other research specialists, Gregg Snedden and Hongqing Wang, within the USGS. Working with these professionals provided valuable experience for an initiate researcher.

This thesis and my graduate studies would not have been possible without the financial support of the Coastal Protection and Restoration Authority's Coastal Science Assistantship Program. Nor would it have been possible without the facilities and services provided by the Louisiana State University.

Table of Contents

List of Tables

List of Figures

Abstract

Coastal Louisiana exhibits some of the highest rates of land conversion to open water in the world. This is most apparent in Terrebonne Bay, Barataria Bay, and Breton Sound (Couvillion et al., 2011). The hypothesis is made that locally generated wind waves are responsible for the observed land loss.

Recent research has attempted to relate the marsh edge erosion rate to wave energy flux density. Under the appropriate assumptions, this relationship is modeled reasonably well by a linear relationship between erosion rate and wave energy flux. Such a model is a valuable tool for coastal resource management. A deficiency of some of the proposed models is the exclusion of the marsh's resistivity to erosion or, generally speaking, its strength.

Marsh edge strength is a complex function of abiotic, biotic, and geochemical factors. A plausible assumption however is that geotechnical soil properties form a governing set of parameters with respect to erosion. The inclusion of spatially varying, site-specific soil properties in addition to the hydrodynamic driving force is then a logical step towards improving any model of marsh edge erosion.

A parametric wave generation model is validated with an existing, observed wave record and a state-of-the-art numerical model. The parametric model is used to calculate wave energy flux at the marsh edge study sites in Terrebonne Bay, LA over 9 years. A key subset of soil parameters is identified from an extensive geotechnical and geological data set. The geotechnical data set was derived from a related field campaign in the Mississippi river delta's coastal region which has a simimlar age and sediment source.

The distribution of a proposed influential soil property in marsh edge strength (undrained shear strength) is used to demonstrate the site-specific differences in the relationship between observed marsh edge erosion and modeled wave energy flux density. Recommendations for the future success of modeling marsh edge erosion in the Mississippi river delta region are provided based on the applicability and suitability of the soil property framework and the method of modeling wave energy flux in Terrebonne Bay.

Chapter 1
Introduction

1.1 Background

1.1.1 Regional Geomorphic Setting

Before introducing the proper content of this thesis' research, i.e. wind wave attack on coastal marshes, a desctiption of the broader region's geomorphic setting and its attendant geomorphodynamic processes is required. The broader regional setting of this work is the lower Mississippi river delta (MRD) complex. Deltaic environments are subject to variable geomorphic processes. On the one hand, these processes are characterized by areas of erosion, subsidence, and generalized land loss while other areas exhibit a counter-balancing coastal progradation. The erosional geomorphodynamics of coastal deltaic settings may be exacerbated by anthropogenic influences (Day et al., 2000; Kirwan and Megonigal, 2013). This is evidently the case in Louisiana and this thesis' study area, i.e. Terrebonne Bay, LA (TE) (Penland et al., 2000; Couvillion et al., 2011).

The MRD has been studied extensively because of its economic importance and its rich natural systems. It exemplifies both the dynamics of deltaic coasts and the role human society plays in shaping these landscapes. The former is laid bare by the reconstruction of the MRD's Holocene geologic history ($\sim$ 12 ka to the present). This was an epoch of delta progradation whereby the Mississippi river's sediment discharge was sufficient to fill the nearshore accommodation space of the Gulf of Mexico (GoM). The delta lobes and landforms which resulted from this epoch can be seen in Figure 1.1 (Coleman et al., 1998).

The geomorphodynamics of the MRD's Holocene history is, in broad strokes, painted by the operation of the delta-switching process (Roberts, 1997, 1998; Coleman et al., 1998). Delta-switching is the process by which a river's main channel periodically and progressively alters its flow path in response to a decrease in the hydraulic efficiency of its present configuration. As a result, the depositional center of the river also periodically shifts its

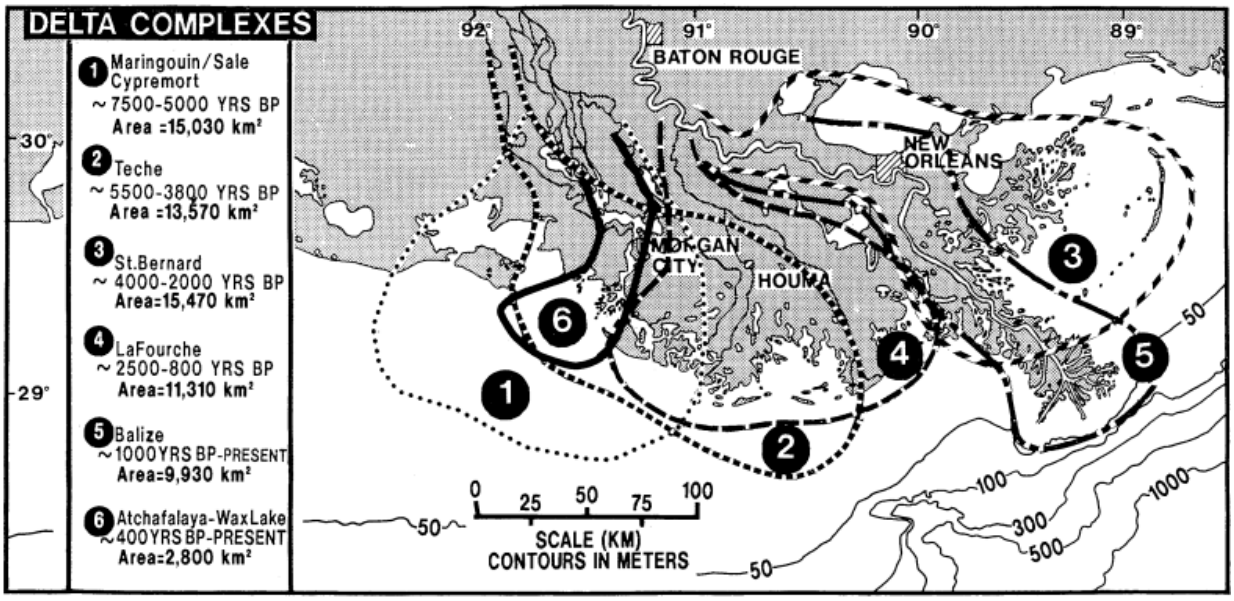

Figure 1.1: Succession of delta lobes formed by the Mississippi river over the course of the Holocene (Roberts, 1997).

location along the coast. This periodic switching of the Mississippi river, which operated on the order of 1000 years, has resulted in the complex of paleo-delta lobes which form the Louisiana coast as we know it today (see Figure 1.1 for a visualization of the relationship between the extent of the paleo-delta lobes and the Louisiana's current shoreline). From Figure 1.1 it can be seen that the older delta lobes typically have less sub-aerial land despite the larger lateral extent of their geological formation. While the actual processes and geomorphic responses of the Mississippi river's delta-cycle are recondite and variable, two idealized phases are easier to elucidate and important to this work.

The first geomorphodynamic phase, occurring when the delta is "active" and the river is discharging sediment into the area, is associated with periods of delta progradation and shoreline accretion. In the classic figure by Roberts (1997) this is termed the "fluvially-dominated regressive phase", where "regressive" refers to the movement of the shoreline into the ocean (see Figure 1.2). Once the river has changed course, i.e. once the delta has "switched", this region becomes "inactive" and receives a reduced fluvial sediment input commensurate with the displacement of the river mouth and any changes in long-shore drift. The second geomorphodynamic phase is generally a transgressive period where

landforms are converted to open water or are submerged. This phase is referred to as the "marine-dominated transgressive phase" in Figure 1.2. To speak loosely, the recently deposited sediment of the youngest delta lobe compacts and subsides significantly; barrier islands, consisting of sand delivered by the now "inactive" delta, shrink, are submerged and eventually become subaqueous shoals; while coastal wetlands, to the degree to which they are starved of sediment and/or are unable to maintain sufficient organic accretion, are converted to shallow coastal embayments (Reed, 1995).

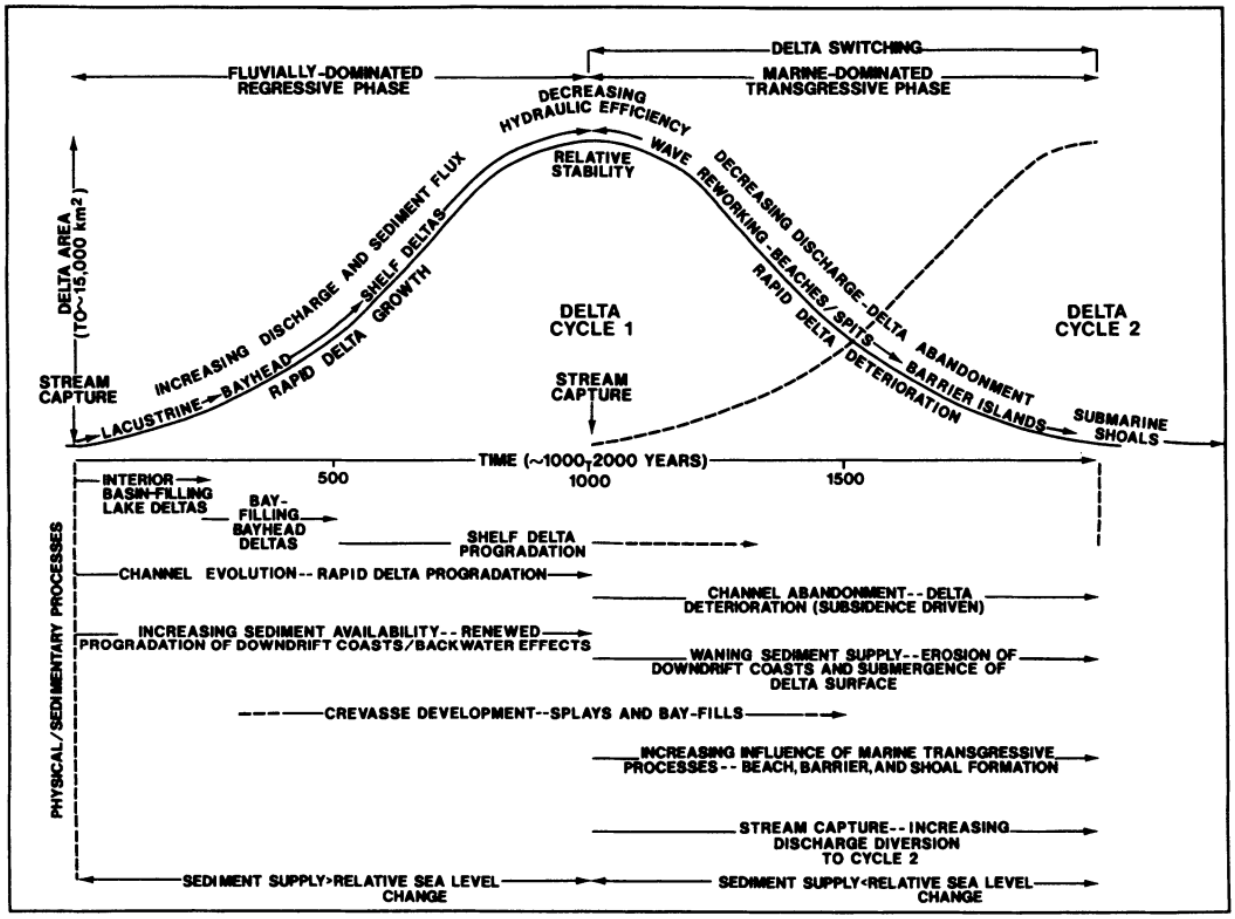

Figure 1.2: Idealized delta-switching process and the geomorphodynamics associated with each phase (Roberts, 1998).

As was mentioned above, coastal Louisiana is also conspicuous for exhibiting the effects of anthropogenic interventions. The more recent history of the Mississippi river (circa 200 years) tells the story of these interventions and the disturbances they have wrought on the land building dynamics of the delta-switching process (Alexander et al., 2012). The

most significant episode of this history, with respect to coastal geomorphodynamics, is the engineering of the Mississippi river, i.e. its channelization, stabilization, and up-river damming.

Prior to the navigational engineering of its primary channel, the Mississippi river was able to freely migrate about the coast. In this scenario, loci of high sediment delivery were naturally distributed in time and space. This, coupled with a greater gross sediment budget than that which is available at present (Blum and Roberts, 2009), resulted in a quasi-dynamic equilibrium between the GoM and the coast at geologic time and spatial scales. In other words, land-loss in areas which were more remote from the river mouth were eventually replenished with sediment once the Mississippi river's main channel switched locations.

The stabilization of the Mississippi river for navigational purposes spatially fixed its point of sediment discharge into the Gulf of Mexico. Coastal regions outside of the river's radius of influence are thus starved of the sediment which maintained their dynamic equilibrium. Further, the main channel of the Mississippi has been lined with levees for flood protection. This serves to disrupt the natural distribution of sediment into the nearshore coastal wetlands which at one point benefited from the suspended sediment which accompanied periodic tidal flooding. In some regions, the coastal wetlands are now unable to keep pace with RSLR (Day et al., 2011).

Up-river damming reduced the total sediment load of the Mississippi, i.e. the amount of sediment available to the entire MRD system for mineral accretion (Blum and Roberts, 2009). At the same time, the deepening of the main river channel increased its flow velocity, jettisoning sediment further from the coast and reducing actual deposition in the nearshore environment. In addition to these straight-forward reductions to the sediment budget, subsidence and accelerated sea-level rise have combined to increase accommodation space and negatively impact the coastal ecosystems. To make matters worse, local disturbances (e.g. increased wind wave attack, channel cutting for the oil and gas industry, hydrologic

impoundment of tidal marshes, etc.) are pervasive and generally promote erosion (Cahoon, 1994; Reed, 1995). In summary, multiple factors, spanning several temporal and spatial scales, have produced the unstable, eroding coastal geomorphic setting which is observed in the study area and the majority of coastal Louisiana today.

1.1.2 Coastal Land Loss in Louisiana

Recent work by the United States Geological Survey (USGS) assessed persistent land-to-water changes for coastal Louisiana over the years 1932 to 2010. Couvillion et al. (2011) reported concerning results: a total land-to-water area change of 4877 km^2 over this time period. This loss accounted for 25% of the total wetland area in 1932. The study analyzed multiple temporal periods and the most recent of those (1985 to 2010) displayed an accelerated land-loss rate of 43 km^2 yr^{-1}. Periods of intense tropical storm activity exhibited greater rates of land loss. The years containing hurricanes Katrina and Rita had a land-to-water area change of -562 km^2 (Barras, 2007; Couvillion et al., 2011). The increased hydrodynamic bottom shear stresses induced by hurricanes and high-energy storms have been suggested as a driver of wetland land-loss (Howes et al., 2010).

Land-loss in TE was observed to be higher than any of the other regions over the entire study period (Couvillion et al., 2011). Land-loss in TE over this time period amounted to approximately 1200 km^2. The only other region which showed comparable land-loss was the basin adjacent to TE, Barataria Bay (BA), which lost nearly 1090 km^2 of land during the same period. The average of the other coastal areas defined in the study amounted to roughly 310 km^2 and the maximum amongst them was 513 km^2 of land lost which was in Calcasieu-Sabine (Couvillion et al., 2011).

It is reasonable to assume that TE and BA were in a "marine-dominate transgressive phase" over this time period. TE and BA would fall under the category of rapidly deteriorating down-drift coasts in Figure 1.2. However, its is also safe to assume that other sections of the coast in the MRD region were subject to similar forcings associated with this phase of the delta cycle. It is then likely that local processes are responsible for the

observed variability in land loss between different regions.

Prior work by the USGS quantified the relative contribution of different land-loss processes and their disposition along Louisiana's coast (Penland et al., 2000). The quantitatively significant processes were identified as natural wave action, subsidence due to subsurface fluid withdrawal (oil and gas extraction), altered hydrology (impoundment of tidal marshes), and the direct removal of land by channelization. In total, 83.79% of land-loss between 1932 and 1990 were attributed to these factors. Out of these dominant mechanisms, natural wind wave action figured as the greatest factor, contributing to 26.21% of the total land-loss. Inspection of the spatial distribution of land-loss processes argues that natural wind wave attack is the dominate mode of land-loss in TE (see Figure 1.3) (Penland et al., 2000). Further, contemporaneous shoreline evolution and hydrodynamic data collected by Watzke (2004) suggest that the local waves generated by the passage of cold-fronts, a regular seasonal phenomenon in TE, drive salt marsh erosion.

Terrebonne Bay is fringed by extensive saline and brackish wetlands which are characteristic of Louisiana's low energy coast. Coastal wetlands are a often lauded as a natural resource. Recently, they are also becoming evaluated as such (Barbier et al., 2011). Coastal marshes provide a number of ecosystem services to communities in their immediate proximity, but they are also integral components of larger, more remote ecosystems. It is also recognized that coastal wetlands are significant in regulating global biogeochemical cycles. A few important ecosystem services which they provide are: their function as barriers to storm surge flooding by the dissipation of wave and flow energy (Chen and Zhao, 2012; Temmerman et al., 2013; Fagherazzi, 2014), the creation of invaluable habitat for myriad species, to act as spawning grounds for commercially important fisheries, fowling grounds for migratory birds, areas for recreational hunting and fishing, and the removal of carbon and nitrogen from biogeochemical nutrient cycles. Further, work by Twilley et al. (2016) argues that the anthropogenically driven dynamics of land loss and growth may play a significant role in the long-term sustainability of human settlements within the coastal

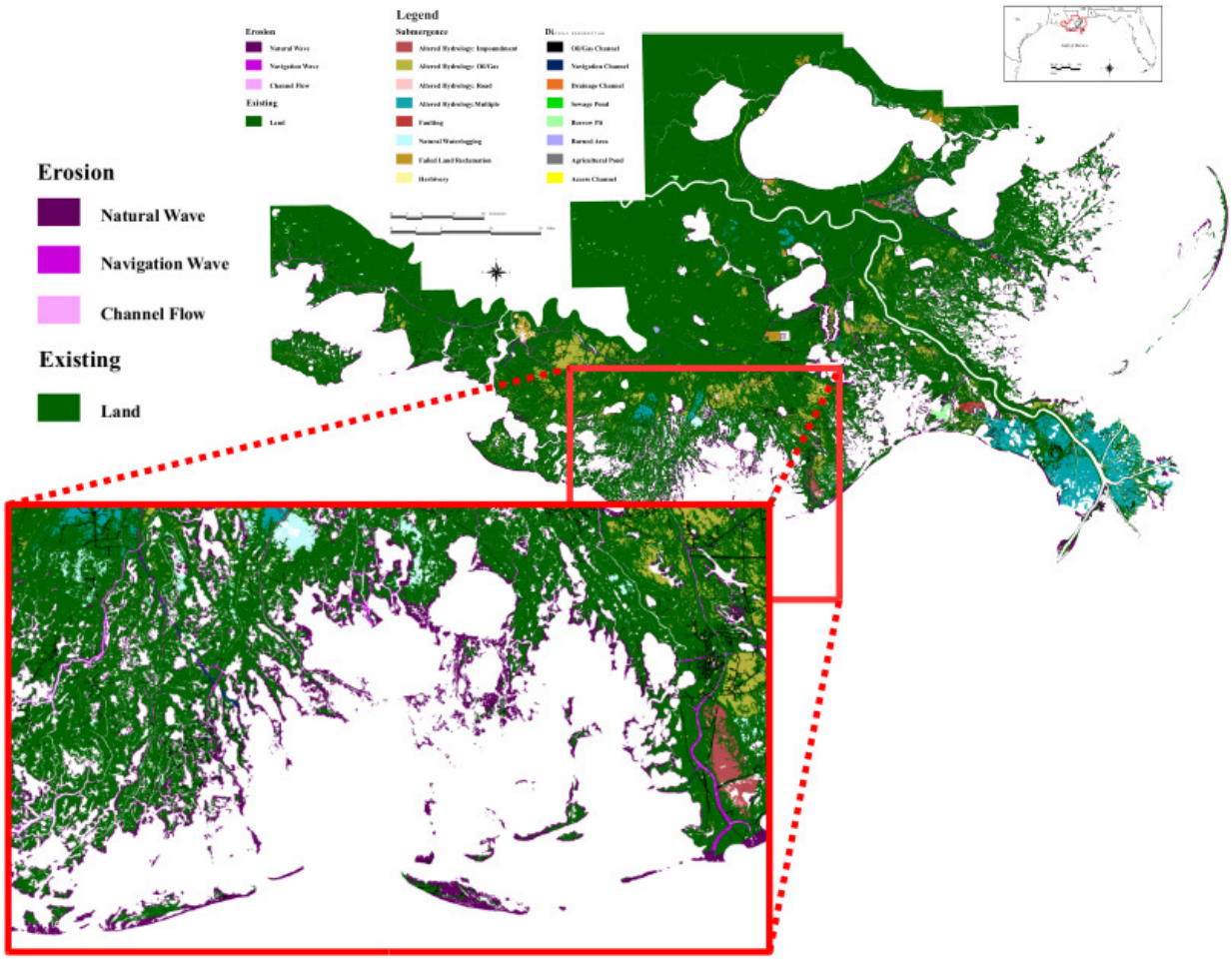

Figure 1.3: Spatial distribution of the different processes which are responsible for land-loss in Louisiana. The inset detail map shows Terrebonne Bay (modified from Penland et al. (2000)).

zone.

In light of these facts, the rapid rate of land loss in TE is very concerning. Wetland restoration and marsh creation are strategies which are currently being employed by the state of Louisiana. These projects are however extremely costly. In their last bi-decadal report, the state of Louisiana proposed to invest $50 billion over the next 50 years in these kind of projects (CPRA, 2012). These are expected funds and the projects were identified based on the previous generation of models. The need to improve the prediction of wetland loss is fundamental to optimizing the cost-benefit ratio of restoration projects. This thesis purports to examine the possibility of achieving this improvement by incorporating soil

properties into the relationship between wave attack and coastal marsh edge erosion.

1.2 Contemporary Related Studies

Salt marsh landscapes subject to wave forcing seem to be characterized by a similar geomorphology and processes despite the broad range of their important physical parameters (e.g. sedimentation rate, RSLR, tidal range, incident significant wave height, and dominate species of vegetation). The eroding marsh shoreline, the so-called marsh edge, is characterized by a vertical cliff-like face at the land-water interface (see Figure 1.4). This is referred to as the marsh scarp and is largely controlled by the tidal range. One can conceive of the scarp as being composed essentially of two layers. The upper layer is formed by living vegetation, their root systems, and sediment. This is sometimes called the root-mat. The root mat grades vertically downward into a relatively more homogeneous, more mineral sediment which is similar in composition to the adjacent tidal flats (see Figure 1.5).

Figure 1.4: Eroding marsh edge which exhibits the marsh scarp and its characteristic geometry (Fagherazzi et al., 2013).

Incident wave energy is expended doing work to the marsh scarp thus causing it to retreat laterally, i.e. erode (Tonelli et al., 2010). The erosion of the marsh scarp is characterized by two modes: continuous particle ablation and occasional mass failure events (mass slumping, toppling, or sliding) (Bendoni et al., 2014, 2016). The former mode refers to the displacement of sediment grains from the soil matrix. The latter mode is a more complex and less predictable process. It occurs through the undercutting of the root-mat

Figure 1.5: Vertical profile of the marsh scarp showing the root-mat and gradation into the mineral layer (Rodriguez, 2013).

by a vertical variation in the erosion rate of the marsh scarp. Once the mineral layer has eroded to a sufficient extent, the overlying root mat begins to overhang the scarp in a cantilever fashion. Figure 1.6 shows a schematic drawing of a marsh scarp and the overhanging root-mat. The extruded mass introduces tensional cracks into the marsh surface which may be sufficient to loose large blocks of the marsh. These modes have been observed in the laboratory (Feagin et al., 2009; Francalanci et al., 2013; Bendoni et al., 2014) and their outcome has been monitored in the field (Bendoni et al., 2016).

Schwimmer (2001) was the first to apply the method of relating incident wave energy flux density (W m^{-1}) to observed marsh edge erosion rate (m yr^{-1}). Schwimmer (2001) monitored erosion rates for salt marshes in Delaware Bay, DE and estimated the wave parameters based on reported wind, bathymetric, and fetch data with an unspecified wave model. Schwimmer (2001) proposed that wave energy flux density (from now on "wave

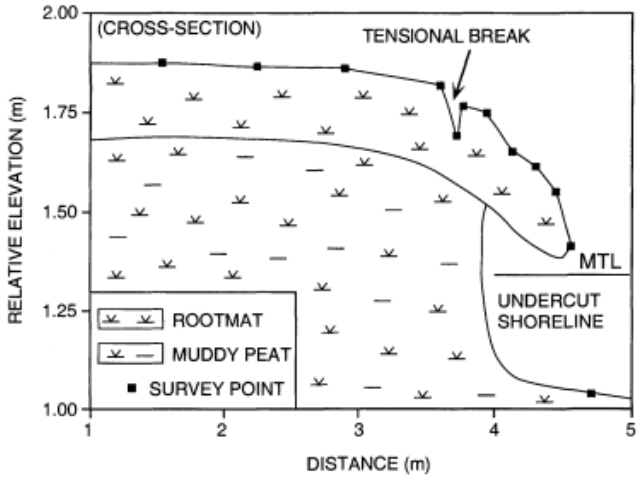

Figure 1.6: Schematic of the marsh scarp in the process of a mass failure event (modified from Schwimmer (2001)). The physical dimensions of the marsh scarp should not be taken as representative of a Louisiana marsh because this schematization is derived from salt marshes within Delaware Bay, DE.

power") was related to erosion rate in a power law fashion by Eq. (1.1).

$$R = \alpha P^{\beta} \tag{1.1}$$

where R is the erosion rate, P is the wave power, and $\alpha,\ \beta$ are site-specific regression coefficients (for Schwimmer's site they are 0.35 and 1.1, respectively). Mariotti and Fagherazzi (2010) modified Eq. (1.1) to include a critical wave power which the incident wave power must necessarily exceed in order to result in marsh erosion and assumed that $\beta = 1$.

Marani et al. (2011) attempted to theoretically derive a linear relationship between wave power and marsh edge erosion based on the Buckingham Π theorem. See Figure 1.7 for a cartoon relating the physical parameters which were considered influential by Marani et al. (2011). The symbology found in this diagram will be adhered to throughout this thesis. The functional relationship between Π-groups derived by Marani et al. is given as:

$$\frac{Rhc}{\overline{P_i}} = f\left(\frac{h}{d}\right) \tag{1.2}$$

where h is the marsh scarp height, c is the cohesion of the soil, $\overline{P_i}$ is the incident wave

power averaged over a sufficiently long and representative period, and d is the water depth at the marsh edge.

The key assumption made by Marani et al. (2011) is that $f\left(\frac{h}{d}\right)\frac{1}{c} \approx k$, where k is considered as a constant which must be determined through the calibration of wave power to marsh edge erosion observations on a site by site basis. This allows Marani et al. (2011) to express Eq. (1.2) as a linear relationship between a volumetric erosion rate per linear unit marsh and the mean incident wave power. The final result is Eq. (1.3).

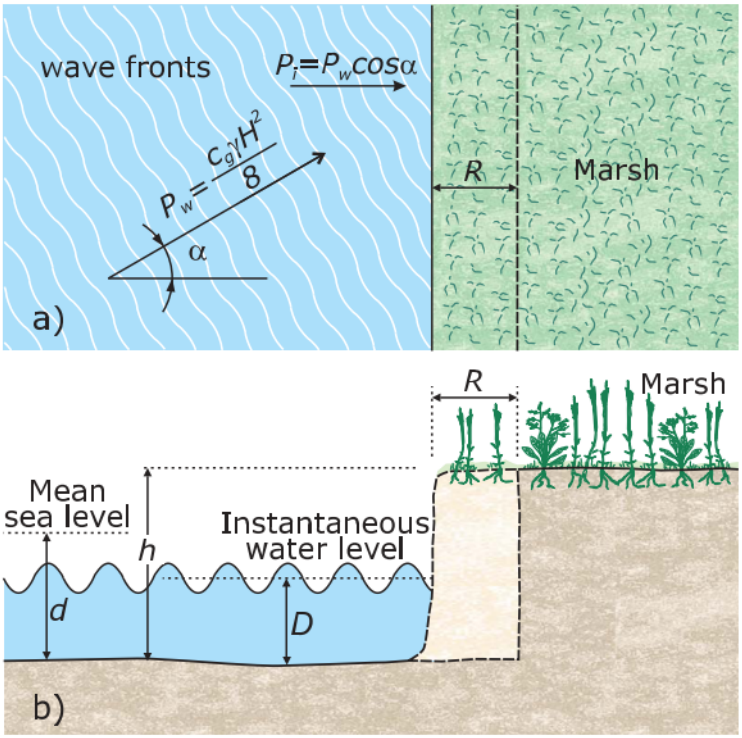

Figure 1.7: Schematic showing the physical variable of marsh edge erosion in cross-section and plan-view (modified from Marani et al. (2011)).

$$V = R \cdot h = k\overline{P_i} \tag{1.3}$$

where V is the volumetric erosion erosion rate per linear unit marsh.

Leonardi and Fagherazzi (2015) sought to model the high degree of spatial variation observed in the response of marsh shorelines to moderately uniform wave fields with a cellular automata model. Leonardi and Fagherazzi (2015) randomized the marsh's resistance

to erosion within each cell of the model and then varied the wave forcing between numerical experiments. They used Eq. (1.4) in order to simulate the erosion rate of each cell.

$$R = \alpha P^{\beta} \exp\left(-\frac{H_c}{H}\right) \tag{1.4}$$

where H_c is the so-called critical marsh height and H is wave height.

H_c was randomly generated from a probability density function with the same mean and standard deviation as field observations of marsh strength. While Leonardi and Fagherazzi (2015) were not attempting to relate observed erosion rates to wave power, their work advanced the capability of erosion models by proposing a method by which to incorporate soil properties. Equation (1.4) allows for a scaling of the erosion rate based on the marsh's strength (H_c) relative to the wave forcing (H). For example, no matter how energetic a certain wave field may be, if the marsh it is incident upon is exceedingly strong, i.e. has a high H_c value, no erosion will occur. This situation is similar to a scenario where waves which would erode a fragile marsh (low H_c) are instead impinging on a cliff face (high H_c). At the cliff face it is expected that little or no erosion would occur under the given forcing.

In the MRD region specifically, the Coastal Restoration and Protection Authority (CPRA) recently used aerial photography and GIS algorithms to analyze erosion rates between 2004 and 2012 at 1343 points along the entire coast of Louisiana (Allison et al., 2015). Following Marani et al. (2011) these rates were correlated to estimated mean wave power in order to determine the coefficient k in Eq. (1.3). Figure 1.8 shows the results of their analysis. The grouping of the data, i.e. the appearance of three separate trends in the data, suggests that the CPRA's analysis conflated areas which exhibit different geomorphic responses. This may be caused by spatial variability in the marsh's strength and is understandable considering the scale of their domain and analysis.

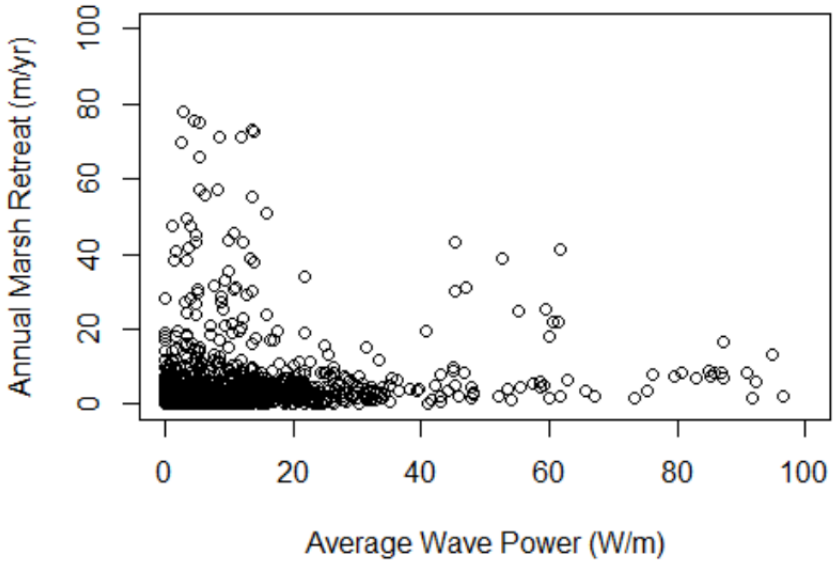

Figure 1.8: Observed erosion rates for the entire Louisiana coast versus hindcasted wave power for the years 2004 to 2012 (modified from Allison et al. (2015)).

1.3 Objectives

The scatter observed in Figure 1.8 could be due to many different natural factors present in the coastal environments analyzed, e.g. site specific vegetation properties, marsh platform elevation differences, or local hydrodynamics. The scatter could also be the result of unrealistic wave powers due to assumptions made in the wave model. One objective of this work is to explore the possibility of modeling erosion rates as a function of wave power on basin scale domains such as Terrebonne Bay. In order to accomplish this, the work done by Allison et al. (2015) will be refined by reducing the domain from the entire coast of Louisiana to Terrbonne Bay, LA. Further, the frequency-weighted method of calculating wave power (McLoughlin et al., 2014; Allison et al., 2015) will be replace with a time-series approach. These modifications will improve upon the wave power calculations. Establishing greater confidence in the wave power model will allow for the exploration of additional factors in order to explain the scatter in Figure 1.8.

With respect to these additional factors, it is reasonable to assume that geotechnical properties of the eroding marsh edge soil substrate form a governing set of parameters in regards to its geomorphic response. The other objective is then to explain this variability

by incorporating a geotechnical data set which is assumed representative of Louisiana's saline marsh edge soils. The proper consideration of marsh strength in the marsh edge's response, i.e. its erosion rate, to a given wave climate could collapse the data in Figure 1.8 into a linear relationship. The inclusion of the marsh's soil strength into Eq. (1.3) in a fashion similar to the work by Leonardi and Fagherazzi (2015) may be able to explain the variability in the erosion rates observed in Figure 1.8.

Chapter 2
Methods and Materials

2.1 Geotechnical Data

2.1.1 Study Area

A multi-disciplinary team from Louisiana State University conducted a series of field trips in order to collected baseline geological and geotechnical data from coastal regions of the MRD. The field campaign comprised four study areas: Lower Breton Sound (LBR), Lower Barataria Bay (LBA), Middle Breton Sound (MBR), and Middle Barataria Bay (MBA) (see Figure 2.1 for a regional map).

Breton Sound and Barataria Bay are two shallow coastal embayments immediately adjacent the lower stretches of the Mississippi river and its terminus into the GoM. Breton Sound is roughly 2470 km^2 in extent with almost 754 km^2 of wetlands. Barataria Bay is larger with a total area of 6330 km^2 and nearly 2500 km^2 of wetlands. Their open ocean boundaries are protected by degrading, low-elevation barrier island chains. The majority of their sub-aerial land is fresh, brackish, or saline marsh (Sasser et al., 2014). The dominate vegetation is typically *Spartina patens* or *Spartina alternaflora* with stands of *Distichlis spicata* and *Avicennia germinans*. Both basins suffer from a lack of sediment supply and have had their natural hydrology significantly altered.

These two basins are part of the Balize delta lobe (see Figure 1.1). The Mississippi river is actively depositing sediment within this basin. The initiation of the Balize delta's growth has been dated to approximately 1000 ybp. It is a relatively young delta within the MRD and is second only to the Atchafalaya which is very new by geological reckoning. The Balize delta is thought to overlap the tail end of the LaFourche lobe's cycle (Bomer et al., 2016; Hughes et al., 2016; White, 2016). The LaFourche lope forms the surficial stratigraphy of Terrebonne Bay. Considering the similarity in ages and sediment source (i.e. the MRD catchment), it is likely that the sediments of Breton Sound and Barataria

Bay are similar in character to those of Terrebonne Bay.

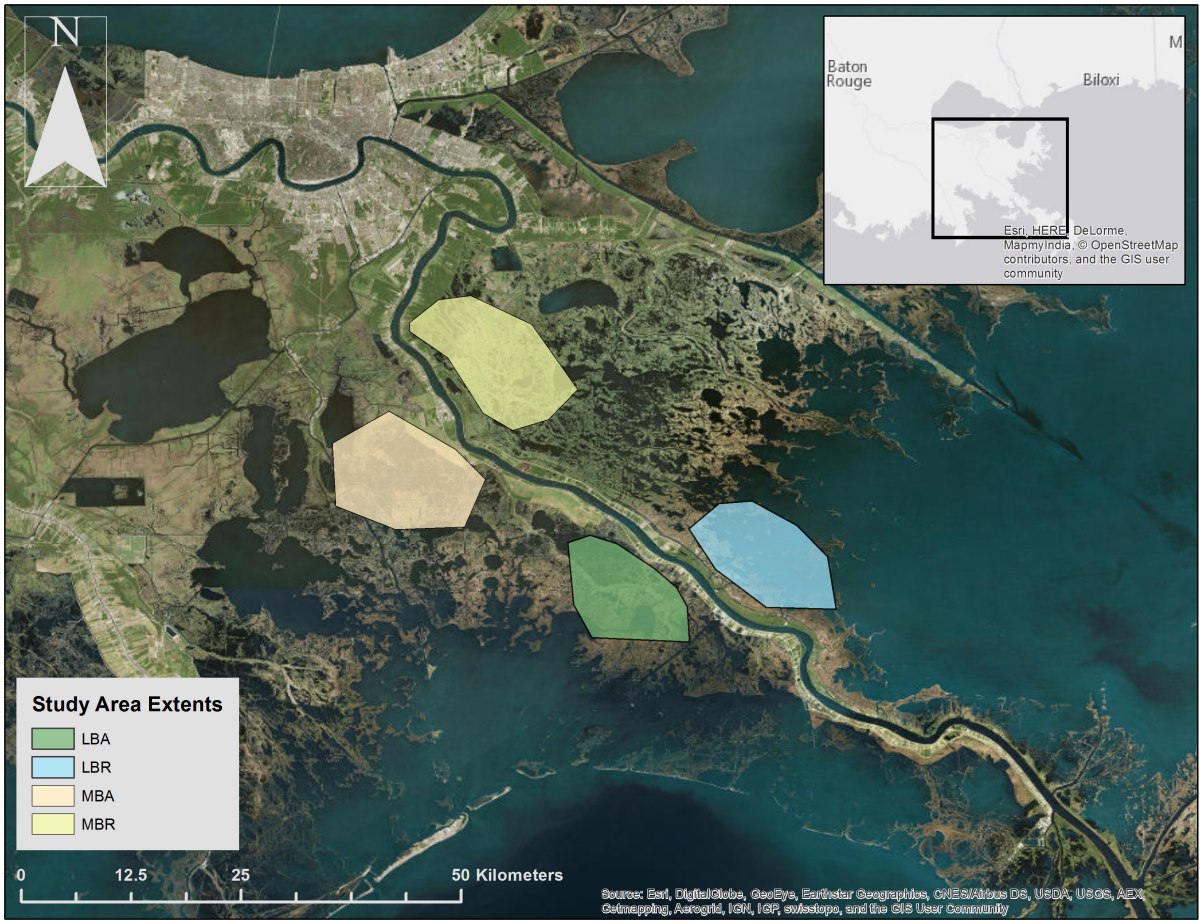

Figure 2.1: Regional map of the study areas in Breton Sound and Barataria Bay, LA.

2.1.2 Field Campaign

A total of 8 field trips between 2014 and 2015 were required to complete the objectives of the field campaign (see Table 2.1 for the trip logistics). The objective was to geologically and geotechnically characterize receiving basins for proposed large-scale river sediment diversions. The team consisted of graduate students from the Civil and Environmental Engineering, Coastal and Ocean Sciences, and Geology and Geophysics departments of Louisiana State University and the Coastal Studies Institute's field support staff.

Airboats were used to navigate the wetlands because many of the pre-selected sampling sites were not accessible by regular vessels. Typically, 6 to 7 sites could be sampled per day. At each study site a sediment core was sampled and in-situ measurements of undrained

shear strength were taken. The methodologies of these techniques are discussed in Section 2.1.3 and Section 2.1.5, respectively.

Table 2.1: Times and study areas investigated during geological/geotechnical field trips

Basin	dates	number of sites samples
LBR	4-15-2014 to 4-17-2014	14
LBR	6-3-2014 to 6-4-2014	11
LBA	8-10-2014 to 8-15-2014	25
MBA	2-11-2015 to 2-12-2015	6
MBA	3-16-2015 to 2-18-2015	19
MBR	3-30-2015 to 3-31-2015	12
MBR	5-13-2015	6
MBR	7-9-2015	7

2.1.3 Sediment Core Sampling

The sediment samples were extracted from the marsh in 6 m long by 7.5 cm in diameter thin-walled aluminum Shelby tubes. The tubes were driven into the marsh surface until their entire length was below ground or until the tube met with the depth of refusal, i.e. the depth where the Shelby tube is met with sufficient resistance to halt its progress. This depth was often deeper than the entire length of the tube (i.e. 6 m).

The average extracted core length and compaction for each basin are reported in Table 2.2 in order to provide an general sense of the sampling results. The greater average water depth over the core samples in the more coastal regions (LBA and LBR) may have been due to the tidal stage. However, this is unlikely because the times of the core extractions were evenly distributed throughout the day. It is possible that the elevations of the marsh platform in these regions is generally lower in the tidal frame.

The insertion of the Shelby tubes was accomplished with a vibra-coring rig. In order to extract the core after it was fully inserted, a motorized winch was attached to a tripod which was mounted on the bow of the air boat (see Figure 2.2 for an picture of the tripod and winch extracting a sediment core). Three or four people, aided by the winch, were able to safely extract the core. Most of the cores were taken within a 1 to 2 m of the marsh edge.

A few cores were extracted from the open water of the bay. In these locations co-located in-situ measurements were not possible.

After a vibr-acore sample was extracted, the core was cut into vertical sections of approximately 1.5 m in length. This was necessary because the entire core weighed a couple hundred kilograms and was 6 m long. The original dimensions of the core proved to be unwieldy in transportation. The sectioning was accomplished with a standard tube cutting tool. The open ends of the core were capped with plastic lids and sealed with electrical tape. The individual sections were labeled with markers indicating the coring site (e.g. LBA15), place in the soil column (e.g. 1 m - 2 m), and its in-situ orientation (i.e. upward). These indications allowed for the reconstruction of the core once they were transported to the laboratory. The core sections were secured in a custom container on the airboat. After the completion of the field work for a single trip (approximately 2 to 4 days), the cores were transferred to a pickup truck bed and transported to LSU's Department of Geology and Geophysics' on-campus refrigerated storage.

Table 2.2: Average core sampling conditions

Basin	Extracted Core Length (m)	Compaction (m)	Water Depth above Core (cm)
LBR	NA	1.3	17
LBA	4.3	1.3	3
MBR	NA	NA	0
MBA	NA	NA	1

(NA denotes that data was not available.)

It is the opinion of the author that the coring methodology might have been appropriate for geological analyses, but should be considered uncontrolled and inappropriate by the standards of geotechnical engineering (see ASTM D1587, D4220, and D4823). The objectives of some geological analyses, those of the current field campaign included, operate on larger scales than that of geotechnical engineering analyses. Therefore, geological work often does not require the same level accuracy than that of geotechnical engineering. Further, the results of geological work are often qualitative in nature, e.g. researchers

sketching the general stratigraphy of an area. The following is a list and discussion of possible sources of error which were introduced by the core sampling methodology (i.e. extraction, transportation, and storage).

Figure 2.2: Louisiana State University geology students and the Coastal Studies Institute's Field Support staff in the final stages of extracting a sediment core at a study site in MBR.

Mechanical vibration

Vibracoring relies on the mechanical vibration of the coring tube to penetrate into the soil. The process takes roughly 10 to 15 minutes and vigorously shakes the tube and the sediment it contains the entire time. The vibration undoubtedly results in a high degree of disturbance to the soil sample. The grains are displaced from their in-situ emplacement and artificial consolidation occurs as grain packing is increased (Grabowski (2014)).

Compaction

A second source of error is the so-called sampling compaction. It regularly occurred that the original 6 m of in-situ soil would result in a shorter recovered soil column (see Table 2.2). Thus, as a result, the exact in-situ depth of an analysis performed on the sampled core is difficult to know with certainty at the spatial scales relevant to the geotechnical analyses of this project (e.g. 10 cm). In other words, if a certain vertical interval is isolated in the soil column based on laboratory analyses (e.g. density measurements) performed on the compacted sample, then comparison to in-situ properties (e.g. undrained shear strength) at the same depth interval will be subject to a high degree of uncertainty. Further, the action of compaction disturbs the soil as well.

Sectioning

Cutting the core into sections resulted in an unrecoverable loss of sample material at the location of the cuts. This introduced discontinuities into the extracted soil column. This source of error is evident in the laboratory analyses at the sectioning locations (e.g. unrealistically low bulk density).

Transportation

The transportation of the cores was uncontrolled with respect to geotechnical standards (see ASMT D4220). The transportation container in both the airboat and the truck permitted a great amount vibration as the cores were transported to LSU. This undoubtedly disturbed, homogenized, and packed the samples further.

Storage

In some cases, the cores were stored in the refrigerator unit for months before being analyzed. Biological and biogeochemical properties of the sample were undoubtedly affected regardless of the reduced reaction rates induced by the refrigeration.

2.1.4 Laboratory Analyses

The sediment samples were transported to LSU for the purpose of laboratory analyses. The laboratory methods employed were bulk density measurements, grain size analyses,

high resolution imaging of split cores, laboratory undrained shear strength, critical shear stress, and organic content. The individual laboratory tests will be described in separate sections below.

As stated above, the core samples were kept in refrigerated storage prior to the tests. The cores were not tested in a systematic sequence. The number of tests to perform and the availability of the technicians dictated an irregular work schedule. Different tests were performed by different labs on campus. Data were reported as the sediment property versus the depth in the soil column at which it was measured. The results were organized by coring site and sediment receiving basin (e.g. Lower Breton Sound) and housed in an FTP server.

Laboratory Analysis Workflow

1. Density was measured with the Geotek Multi-Sensor Core Logger (MSCL).
2. The cores were cut horizontally at specified depths.
3. Undrained shear strength and critical shear stress were measured on the exposed sediment surface at these depths
4. The core sections were reconstructed and split length-wise into halves.
5. The entire core was imaged with the MSCL.
6. Sediment subsamples were taken at various depths from one half of the split core.
7. Grain size analyses were performed on the subsamples.
8. Organic content was measured on the subsamples.
9. The cores were placed back into storage for future research.

Density

Bulk density was determined with a Geotek Multi-Sensor Core Logger (MSCL). This logger allows for the rapid downcore determination of density with a coupled gamma source and detector. The gamma source-detector is calibrated with dummy slugs of known density. Beams of gamma rays are then passed though the core and the level of gamma detection is calibrated to bulk density. The spatial resolution is 5 mm. The MSCL is also capable of producing high-resolution imagery. The cores were imaged after they had been split

length-wise.

Granulometry

Grain size was determined with a LS 13 320 Laser Diffraction Particle Size Analyzer (0.04-2000 µm). Sediment cores were subsampled every 20 cm. The subsamples were washed with a 30% H_20_2 solution in order to remove large organic grains less they be falsely treated as sand grains. The cleaned subsamples were soaked with 20 mL of water and placed in a centrifuge for 4 minutes. The samples were then placed in the analyzer.

Organic content

In order to determine the organic content, loss of ignition tests were performed on the subsamples. The samples were dried at 60°C to a constant weight and then ground into a powder. 1.00 gram samples were weighed, put into a muffle furnace for 2 hours at 550°C, and then re-weighed. The difference in weight was registered as organic content.

2.1.5 In-situ Measurements

In-situ peak undrained shear strength (s_u) measurements were also taken at the coring sites. Shear strength is defined as the maximum shear stress applied to a soil continuum (or other continua) which when exceeded results in a failure of the soil. In the presence of shear stresses less than a soil's shear strength, only continuous deformation is expected to occur. Shear stress is a primary driver in geomorphic change. Soil shear strength is a function of physical, chemical, and biological factors within the soil itself. There are a variety of instruments to measure shear strength, but the hand-held shear vane is considered the best for rapid, quick, and reliable measurements (Grabowski, 2014).

The s_u measurements were made within 1 to 2 m of the sediment core samples. This was done to allow the in-situ measurements to be reasonably correlated with the laboratory tests based on downcore depth. Measurements were made every 0.5 m to a maximum depth of 3 m. The depth interval was determined by the extension rods of the device which were 0.5 m in length. The marsh surface was commonly flood by 5 to 30 cm of water which may have had an effect on the shear strength measurements. The presence and depth of

Figure 2.3: Photograph of partially submerged shear vane and water depth measurement.

water on the marsh surface also affected the subsurface depth at which the s_u readings were made, because the handle and display had to remain above the water. As a result the in-situ s_u readings were made at different depths between sites. The marsh surface was flooded more frequently at sites within LBA and LBR which are in closer proximity to the coast.

The s_u measurements were made with a handheld Geonor H-60 field inspection vane (see Figure 2.4). The H-60 field inspection vane consists of a four rectangular-bladed vane (24.5 mm in diameter by 50.8 mm in height), which is rotated at subsurface depths until a cylindrical section of soil is sheared at the vanes edges. The torque initiating failure is measured and calibrated to a shear stress, i.e. the peak undrained shear stress, based on the dimensions of the vane using a closed form equation following the ASTM D2573 standards. In addition to the undisturbed in-situ measurements, remolded shear strength ($s_{u,rem}$) measurements were taken following ASTM D2573. This entailed maintaining the

vane in the same location as it was for the undisturbed in-situ test and rotating the vane 50 times before taking another shear strength measurement.

As mentioned above, the maximum recorded torque is calibrated to the peak undrained shear strength based on the dimensions of the shear vane. For a rectangular vane with $\frac{H_v}{D_v} = 2$, the shear strength is calibrated by the following equation.

$$s_u = \frac{6T}{7\pi D_v^3} \tag{2.1}$$

where s_u is the peak undrained shear strength, T is the maximum measured torque, H_v is the vane height, and D_v is the vane diameter.

Figure 2.4: Geonor handheld field inspection vane.

2.2 Wave Power Model for Terrebonne Bay, LA

2.2.1 Study Area

Geomorphic setting

The basic geomophic dimensions of Terrebonne Bay, LA can be seen in Figure 2.5. At its widest TE is roughly 40 km across. Towards the center of the bay the average depth ranges between 1.5 - 2.0 m. TE is similar to Barataria Bay and Breton Sound in many respects. It is dominated by the same vegetation species, typically *Spartina patens* or *Spartina alternaflora* with stands of *Distichlis spicata* and *Avicennia germinans* (Sasser

et al., 2014). It also lacks a sufficient supply to maintain sub-aerial land cover and is rapidly subsiding. TE is also cut off from the GoM by a low elevation barrier island chain. The surficial sediment in Terrebonne Bay is similar to that of Breton Sound and Barataria Bay as discussed in Section 2.1.1.

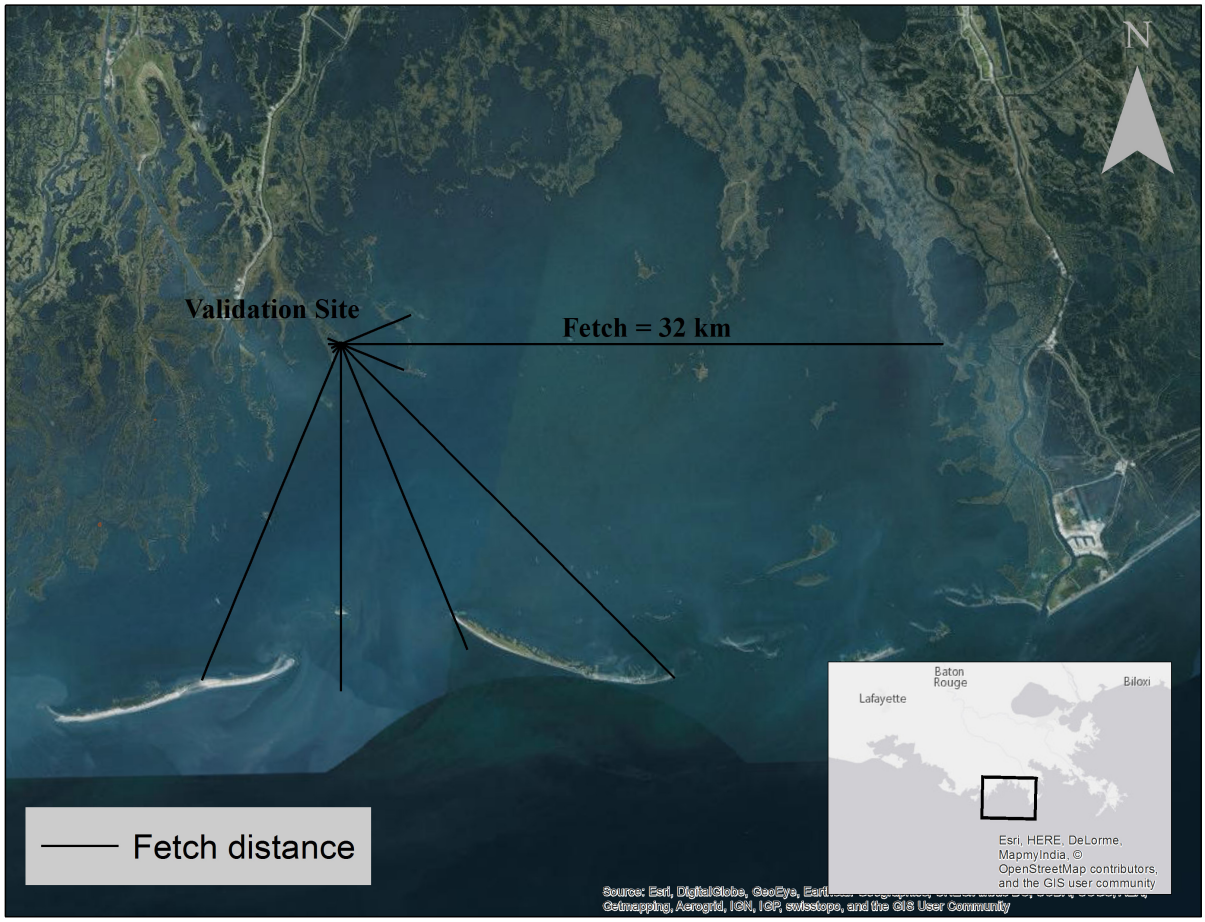

Figure 2.5: Terrebonne Bay, LA. Study area for erosion rate versus wave power relationship.

Erosion rates

As mentioned in Section 1.2, Allison et al. (2015) analyzed shoreline retreat rates throughout coastal Louisiana. This study only considers those retreat rates determined for TE and which line on the west, north, and east coastal marshes (rates determined for the back barrier marshes are excluded). The time period of analysis (2004 - 2012) was divided into three periods according the dates of the aerial photographic surveys. A marsh edge retreat rate (R) was determined for every period. See Allison et al. (2015) for details on

Table 2.3: Time periods of marsh edge retreat rate analysis

Period	Start date	End date	Time elapsed (years)
A	1-19-2004	10-27-2005	1.8
B	10-28-2005	10-29-2008	3.0
C	10-30-2008	11-14-2012	4.0
Total	1-19-2004	11-14-2012	8.8

the technique of determining the retreat rate. Table 2.3 contains the start and finish date for each period of analysis within the larger study and Figure 2.6 portrays the spatial and temporally variable marsh edge retreat rates within TE.

The length of the time periods involved argue for using the erosion rate averaged over the enttire study period. The rates determined from the intervals within the study period may represent time periods which may be of too short duration. It is considered more reasonable to use longer averaging periods in order to relate erosion rates to mean wave power. This will smooth out spikes in erosion rates due to high energy events and other events which the model does not consider but indeed happen in nature (Marani et al., 2011; Bendoni et al., 2016). However, this study is investigating the variability in erosion rates. The variability in retreat rate at a given MEE site through time far exceeds that of the temporal variability in mean wave power at the same site. This could be due to the exposure of soils with different properties to wave attack as the marsh is progressively eroded. Thus, the decision was made to form a composite marsh edge erosion retreat rate data set out of the periods of analysis A, B, and C.

The accuracy of the aerial photography is 1 m (Allison et al., 2015). Accordingly, any erosion rates which were less than 1 m yr^{-1} were removed from the data set. Further, there are many processes at play in the geomorphodynamics of TE. Subsidence, local currents, interior marsh degradation and the opening up of inland ponds into the bay may produce high rates of erosion which are not entirely due to wind waves.

Within the time period analyzed by Allison et al. (2015) some marsh edge retreat rates

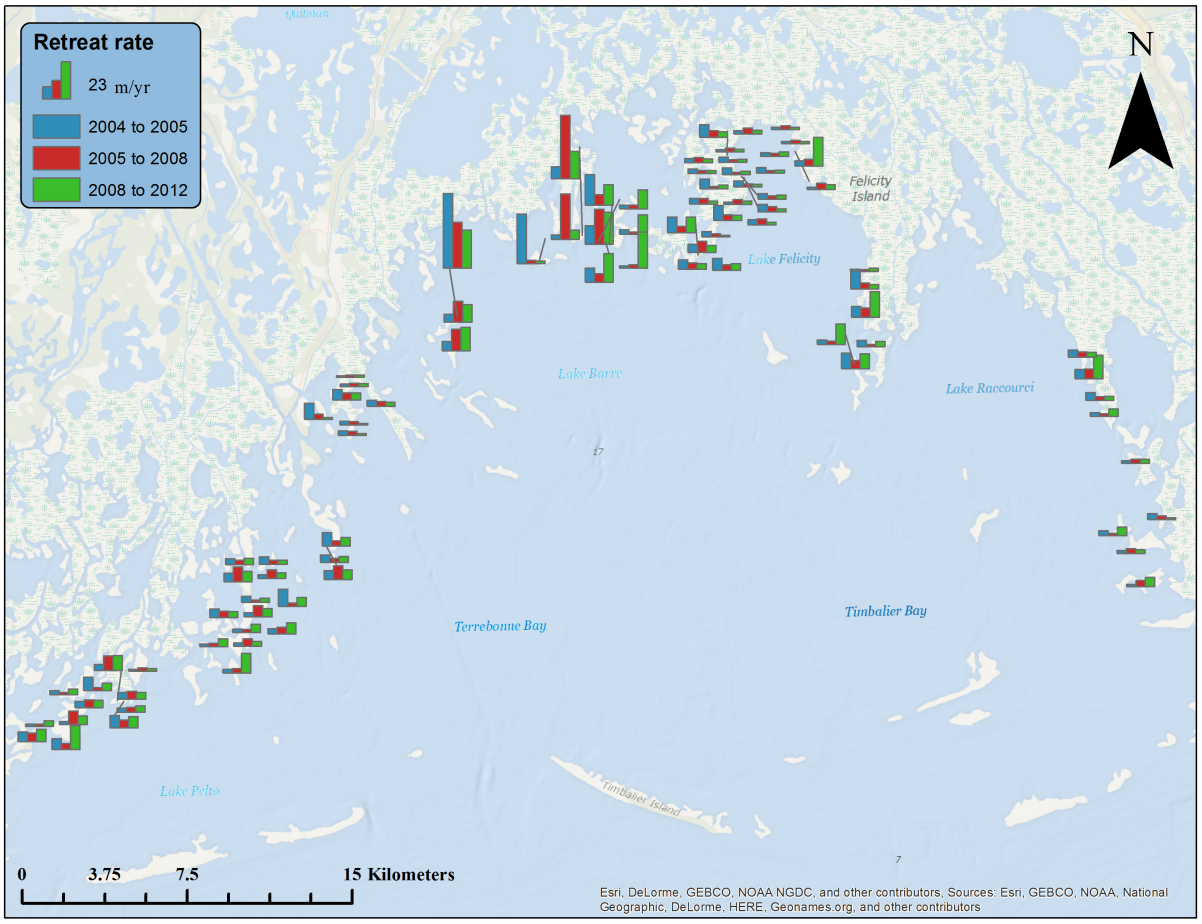

Figure 2.6: Spatial and temporal distribution of marsh edge retreat rates in Terrebonne Bay. Only retreat rates which are greater than 1 m are shown in order to avoid cluttering the map.

were found to be as high as 45 m yr^{-1}. Assuming that these extreme observations were not the result of errors, then it is highly unlikely that wind waves could cause the entirety of this erosion. Unless the marsh in this area was abnormally thin (the marsh scarp hieght, h, is unknown at these sites and assumed to be 0.5 m), then these high rates of retreat would have produced volumetric erosion rates far outside the bounds observed by other researchers (Schwimmer, 2001; Marani et al., 2011; Leonardi et al., 2015). Thus, marsh edge retreat rates in excess of 20 m yr^{-1} were also excluded from the analysis. Many of the high erosion rates were localized in northwest TE which appeared to be the results of an interior lake opening up into the bay (see Figure 2.6).

2.2.2 Wave Hindcasting

The parametric wave generation model developed by Young and Verhagen (1996) was used to hindcast the wave parameters. Young and Verhagen (1996) is an empirical model for simulating wave generation in depth limited water. These formulae are used widely to estimate sea states in shallow coastal environments such as estuaries and embayments (Allison et al., 2015; Bendoni et al., 2016; Marani et al., 2011; Mariotti and Fagherazzi, 2013). The geomorphology of TE is well suited for this approach.

Young and Verhagen (1996) collected wave height, peak period, and meteorological measurements for Lake George, Australia. Lake George is a linear inland water body with a well described bathymetry. By employing a rigorous program of quality control of their measurements they developed well characterized and steady-state meteorological forcings, i.e. winds fields with a near constant magnitude and orientation. All unsteady and non-stationary observations were removed from the data set. They modeled the effect of fetch, depth, and wind speed on wave generation by measuring wave height and peak wave period along transects of sensors when wind conditions were steady. Consequently, the fetch, mean depth, and wind speed responsible for the generation of a given wave observation were well characterized. They proposed the following set of equations.

$$H_{m0}^{*} = a_1 \left[\tanh\left[b_1 (d^{*})^{\alpha_1}\right] \tanh\left\{ \frac{c_1 (X^{*})^{\beta_1}}{\tanh\left[b_1 (d^{*})^{\alpha_1}\right]} \right\} \right]^{\gamma_1} \tag{2.2}$$

$$T_{p}^{*} = a_2 \left[\tanh\left[b_2 (d^{*})^{\alpha_2}\right] \tanh\left\{ \frac{c_2 (X^{*})^{\beta_2}}{\tanh\left[b_2 (d^{*})^{\alpha_2}\right]} \right\} \right]^{\gamma_2} \tag{2.3}$$

where $H_{m0}^{*} = \frac{gH_{m0}}{U_{10}^2}$ is the dimensionless zero-moment wave height, $X^{*} = \frac{gX}{U_{10}^2}$ is the dimensionless fetch, $T_{p}^{*} = \frac{gT_p}{U_{10}}$ is the dimensionless peak wave period, $d^{*} = \frac{g\overline{d}}{U_{10}^2}$ is the dimensionless depth, and $\overline{d}$ is the water depth averaged over the fetch distance given (see Eq. (2.4)), X is the fetch distance, g is the force due to gravity and U_{10} is the wind speed at 10 m elevation above the water surface.

Table 2.4: Young and Verhagen (1996) best fit wave generation parameters

	a	b	c	α	β	γ
1	0.24	0.49	0.0031	0.75	0.57	0.87
2	7.54	0.33	0.00052	1	0.73	0.37

$$\overline{d} = \frac{1}{X} \int_0^X d_x(x) dx \tag{2.4}$$

where d_x is the water depth along the fetch distance. The values for $a_{1,2}, b_{1,2}, \alpha_{1,2}, \beta_{1,2}$ and $\gamma_{1,2}$ are best fit parameters. The parameters used in this work are those originally proposed by Young and Verhagen (1996) and are given in Table 2.4. Other researchers have reanalyzed the data and proposed different values, see Breugem and Holthuijsen (2007) for a tabulation. Thus, for a given steady state wind field, a wave field can be estimated if the geomorphology of the water body is known.

2.2.3 Wave Power Calculation

Linear Wave Theory

Marsh edge erosion studies typically employ small-amplitude water wave theory, or linear wave theory (LWT), because its level of approximation is suitable for the processes involved. LWT was developed by Sir George Biddle Airy in the early 19$^{\text{th}}$ century. Its formulation begins with the assumptions of potential flow, i.e. an incompressible and irrotational fluid. A periodic solution is assumed. The Laplace equation is then solved in the vertical plane, with linearised kinematic and dynamic boundary conditions, to yield the linear dispersion relationship and a velocity potential function.

From these two equations, formulas for the kinematic and dynamic quantities of regular waves can be derived (Dean and Dalrymple, 1991). The quantities of interest to this study are wave energy flux or wave power density (P) and radiation stress (S_{xx}) in the direction of wave propagation. These as are given by Eq. (2.5) and Eq. (2.6), respectfully.

$$P = C_g E = (n\frac{L}{T})(\frac{1}{8}\rho g H^2) \tag{2.5}$$

$$S_{xx} = E(2n - \frac{1}{2}) \tag{2.6}$$

where L is the wave length, T is the wave period, C_g is the wave group celerity, $E = \frac{1}{8}\rho g H^2$ is the energy of the wave, ρ is the density of the fluid, g is the acceleration due to gravity, H is the wave height, and n is the group velocity parameter.

Instantaneous wave power in itself is highly variable and an unsuitable quantity to relate to the time scales of marsh edge erosion. Furthermore, it is the quantity of incident wave energy and the work it does to the sediment and soil matrix which causes erosion. Average wave power over a suitable duration is then the best metric to capture wave forcing at erosion rate time scales. Considering average wave power in action for years or decades facilitates conceptualizing the geomophodynamic role of coastal waters as an actor at the landscape scale. This work employs two time averaging windows, daily averages and annual averages, in order to analyze wave power.

Wave Power Routine

A novel MATLAB® routine was written in order to compute hourly wave power time-series at discrete locations along the coastline. Henceforth, the coastline points used in this study are referred to as marsh edge erosion (MEE) stations or sites. The principle behind the routine is to estimate wave parameters over long time periods for which 2D numerical models, e.g. Simulating Waves Nearshore (SWAN), may prove computationally prohibitive. Also, in shallow coastal environments the performance of SWAN may not justify the computational effort, though this is just conjecture. For bathymetric (depth), geomorphic (fetch), and meteorological (wind speed and direction) observations, the wave power routine utilizes Eq. (2.2) and Eq. (2.3) to estimate the wave parameters required to partially specify the sea state. These are passed to the linear dispersion relationship and

the formulas derived from LWT in order to compute wave power and radiation stress from Eq. (2.5) and Eq. (2.6), respectfully.

The formatting of the bathymetric and geomorphic input is external to the routine. The fetch measurements were calculated using a GIS tool developed by the University of Washington (UWWaves Toolbox for ArcGIS 9.0, 2005 David Finalayson). This tool produces raster files from digitized land-water boundaries. The rasters contain gridded fetch measurements at all "wet" pixels. Wave properties calculated from LWT used a depth which is local to the site being considered. The local depths were sampled from the baythemtry at at least 150 m from the coastline and at points with a mean depth greater than 0.5 m.

The fetches are calculated as the distance from a pixel along a ray cast from a given direction before it intersects with a land-water boundary. The unit circle was divided into 16 sectors of 22.5 in order to define the bins of a wind rose. Rays were cast from each bin's median angle. Thus, 16 rasters (30 x 30 m resolution) were produced which each contained the fetch distance at any "wet" pixel. These rasters were sampled directly offshore from the MEE stations in TE. As a result, each analyzed point contained the fetch distance along 16 wind directions with a 30 m accuracy. Considering the scale of fetches in the generation of winds (tens to hundreds of km), error associated with fetch measurement is insignificant. Brady Couvillion of the USGS produced the original fetch rasters and generously allowed for their use within this work.

The bathymetric observations were produced as part of the Coastal National Elevation Database (CoNED) project (USGS, 2015). They are formatted as a 1 x 1 m resolution DEM referenced to NAD83 and NAVD88. In order to estimate $\overline{d}$ at each MEE site, the length weighted mean of the intersection between each fetch at a MEE site and the CoNED DEM was calculated with the Geospatial Modelling Environment toolbox. For each MEE site the fetch distance and mean bathymetry for each wind bin were compiled in a look up table. These tables were made searchable by wind direction. In summary, for a given wind

observation at an MEE site, one can estimate the fetch distance and mean depth governing wave generation in conjunction with the meteorological forcing.

Synchronized wind speed, wind direction, and NAVD88 referenced water level time series observations are directly passed to the routine. The meteorological forcing derived from historical observations provided by instruments located at the Louisiana University Marine Consortium (LUMCON) and the Grand Isle (GI) CO-OPs station. See Figure 2.7 for the locations of the observational stations relative to the study area. "Wave gauge" on the map indicates the location where Parker (2014) deployed a wave gauge and it marks the location of the wave record which is used in the model validation.

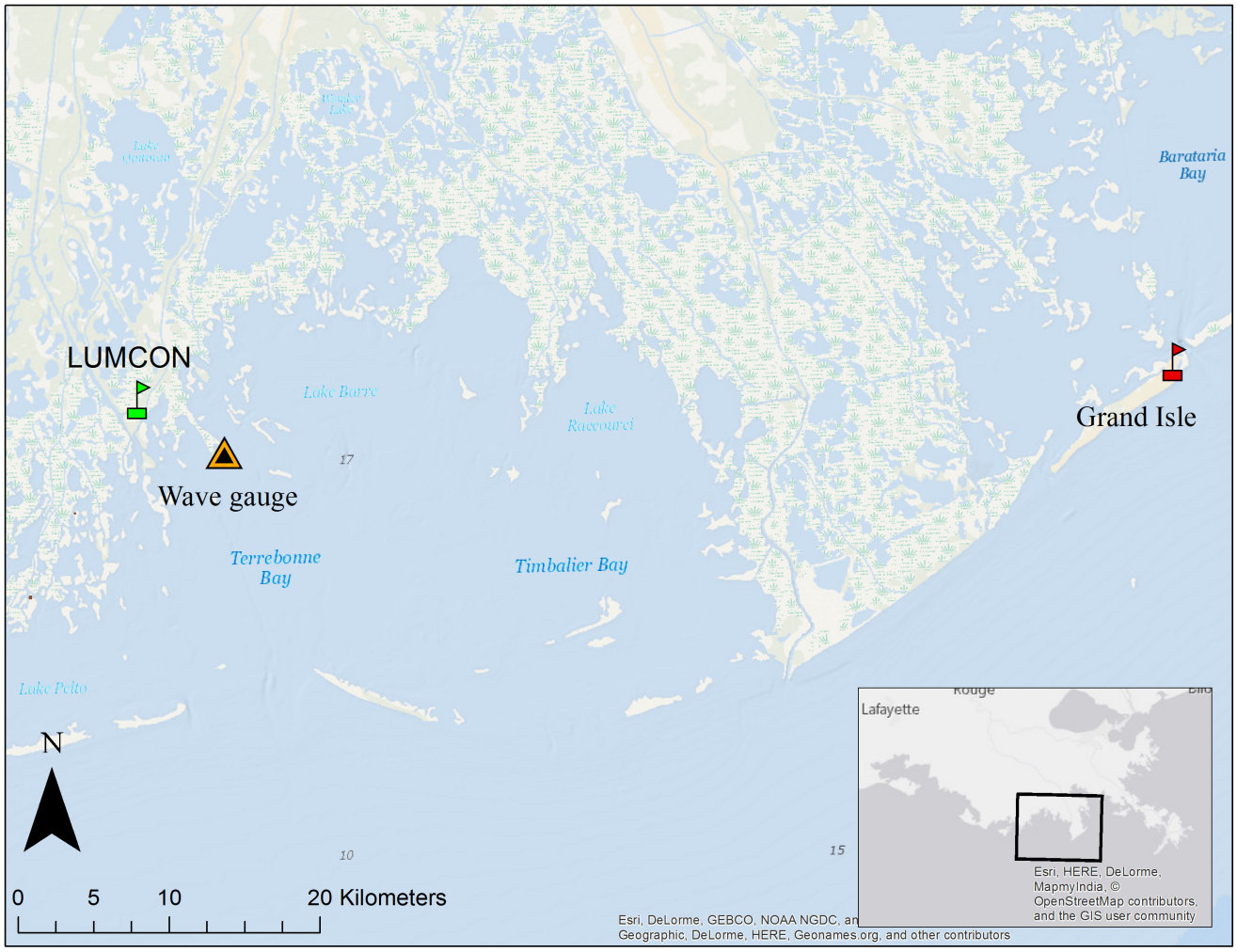

Figure 2.7: Map showing locations of meteorological and hydrological observational stations relative to wave power modeling study area.

The LUMCON station is closer in proximity to the study area and was preferentially used as input for the wind field forcing. If observations were missing from the LUMCON record, calibrated GI wind observations were used. The GI wind observations were calibrated to the LUMCON wind observations by partitioning a 10 year long record for both stations into directional bins. A linear regression was fit to synchronous points within each wind direction bin. If a wind observation from LUMCON was missing, then the wind direction was assumed to be that of the GI station and the wind speed was calibrated to LUMCON magnitude. All water level forcing was derived from the GI station. If data was missing from both stations, then this time period was removed from the computation.

The wind speed and wind directions are partitioned into intervals of "steady" winds based on the preceding-consecutive-mean criterion established in the Coastal Engineering Manual (CEM) (USACE, 2015). The mean wind direction of a "steady" wind partition is used to look up the fetch distance and mean bathymetry. The wind direction means are calculated with the Yamartino method. The difference between the mean bathymetry and the water level observations yields a fetch averaged depth time series. The values of X, $\overline{d}$, and U_{10} are used to estimate a time series of H_{m0} and T_p. P and Sxx time series are then calculated and outputted at each MEE site along with the other wave parameters used in any intermediate calculations.

2.3 Erosion Rate versus Wave Power Relationship

Based on the work of Allison et al. (2015) (see Figure 1.8), the scatter in the erosion rate as a function of incident wave power argues for the modification of the linear relationship between V and P found in Eq. (1.3). As was discussed in Section 1.2, it is plausible that this additional factor should be related to the strength of the marsh edge. It is proposed that Eq. (2.7) can adequately incorporate the influence of soil properties.

$$V = \overline{k} P \exp[-\gamma(\frac{s_u^*}{S_{xx}^*} - 1)] \tag{2.7}$$

where $V = R \cdot h$ is the volumetric erosion rate, P is the wave power,S_{xx} is the radiation stress for a given wave energy field associated with P, $s_u^* = \frac{s_u}{\bar{s_u}}$ is the local shear strength normalized by the mean shear strength for the region, $S_{xx}^* = \frac{S_{xx}}{\bar{S_{xx}}}$ is the site-specific radiation stress normalized by the mean radiation stress of the data set, and $\overline{k}$ is the slope relating V and P when these values are averaged over "regular wave power bins" (Marani et al., 2011), s_u is the site specific shear strength. γ is a calibration parameter used to relate the soil properties of one region to observed erosion rates. Note that $\frac{s_u^*}{S_{xx}^*}$ is a scaling parameter relating wave forcing to marsh edge strength.

This formula was constructed from the intuition that the relative strength of the soil will scale the effect of incident wave power on the marsh, i.e. scale the erosion rate up or down depending on the strength of the marsh. The idea is that when the site-specific S_{xx} and s_u approach their means for the region, then the scaling parameter approaches one, i.e. $\frac{s_u^*}{S_{xx}^*} \to 1$, and the exponential factor goes to one. In this case, from Eq. (2.7), the erosion rate will be linearly related to the given wave power by $\overline{k}$ which represents a relationship between V and P averaged over the region.

Radiation stress was selected as the wave property with which to relate to soil strength for two reasons. One, the units of radiation stress and shear strength are the same. Two, the spatial gradient of radiation stress is a force. Seaward of the marsh edge there exists radiation stress in proportion to the wave energy. Radiation stress is reduced to zero behind the wave marsh edge as the wave height approaches zero. The gradient in radiation stress must be opposed by a force within the marsh edge. Soil shear strength is the best candidate to represent this resisting force. However, in light of the fact that shear strength and radiation stress may be orders of magnitude different, it is necessary to normalize these values by their means. This allows for an expression of how radiation stress and shear strength vary relative to each other.

If only erosion rates and wave forcing are known for a region, i.e. regionally specific information on s_u is lacking, then an estimation for s_u in that region can be derived from Eq.

(2.7). The equation is rearranged so that it is an explicit expression for s_u. The estimation is accomplished by tuning γ until the minimum estimated value of s_u approaches the minimum observed s_u. An s_u distribution is then computed from Eq. (2.7) at the (V, P, S_{xx}) points for the region. It is expected that if the observed erosion rate is related to both the forcing in the region and the distribution of the observed s_u, then the estimated distribution of s_u will be comparable to the observed s_u distribution. This method is employed in Section 3.3 in order to assess the ability of Eq. (2.7).

From here on out, when referring to the in-situ shear strength measurements made in Breton Sound and Barataria Bay, the subscript *obs* will be used. When referring to estimated shear strength values, the subscript *est* will be employed, i.e. $s_{u,obs}$ and $s_{u,est}$ refer to observed and estimated shear strength, respectively.

Chapter 3
Results and Disucssion

3.1 Coastal Marsh Edge Soil Characterization

3.1.1 Preliminary remarks

As discussed in Section 1.2 and seen in Figure 1.5, the marsh platform is composed of two distinct layers of soil: the overlying root-mat and an underlying more mineral layer. Together these two zones are sub-units of the stratigraphic facies described by Wilson and Allison (2008) as the "Organic-rich Mud and Peat". This facies is the uppermost unit in a sequence which has been observed throughout southeastern Louisiana. Wilson and Allison (2008) call the next two units in the sequence "Massive Mud" and "Interbedded Sand and Mud", respectively.

This stratigraphic sequence is characteristic of the Holocene progradational deposits of the Mississippi delta found in southern Louisiana. The sandy layers are interpreted as delta-front deposits. After the delta switches and the area becomes a more quiescent environment, the altered energy regime allows for the deposition of mud in the interlobe water body. Subsequently, or concurrently, a sub-aerial marsh emerges which accretes and promotes the deposition of the uppermost organic later (Wilson and Allison, 2008). Wilson and Allison (2008) also discuss a "Shelly Bay-Bottom Mud" which unconformably overlies the sequence described above with an erosional contact. This unit is found in open-water cores and is interpreted as reworked sediments which are eroded from the marsh platform and then deposited on the remnants of the marsh platform. See Figure 3.1 for an idealized diagram of this stratigraphic sequence. From here on out, the stratigraphy will be referred to following Wilson and Allison (2008) and the divisions within the organic-rich mud and peat unit will be referred to as the "root-mat" and the "more mineral layer".

The soil properties of the root-mat and mineral layer are dissimilar enough to be significant for erosional processes. Bendoni et al. (2016) also conceptualize the marsh

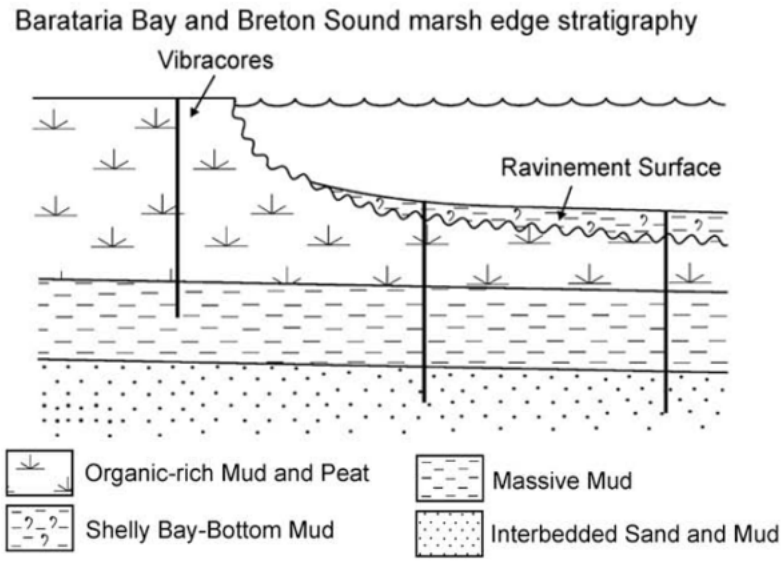

Figure 3.1: Diagram of marsh platform stratigraphy (modified from Wilson and Allison (2008)).

scarp as being composed of two distinct layers. Bendoni et al. (2016) carried out a field monitoring campaign to investigate the importance of vertical variability between the two layers in controlling erosion. Each layer of the marsh scarp, for a given location, was monitored for erosion separately and a vertically variable erosion rate was determined at each site. On average the root-mat layer exhibited a smaller erosion rate for a given incident wave field. From this it is deduced that each layer has a different erodibility. The root-mat shows a greater potential to resist erosion than the underlying mineral layer. See Figure 3.2 for schematic diagram of the two layer marsh scarp system.

Bendoni et al. (2016) argue that the relative difference in erodibility between the two layers of the marsh scarp can control the erosion rate if the incident wave field satisfies certain conditions. If the incident wave energy flux is significant at the marsh scarp, then the wave energy which does work to the marsh scarp is greater when the water level is lower in the tidal stage. This is so because the shallower depth induces wave breaking and the generation of turbulent stresses. Increased turbulence promotes sediment ablation. In this case, the more easily eroded underlying mineral layer is on average subject to a higher effective wave power and erodes at a greater rate.

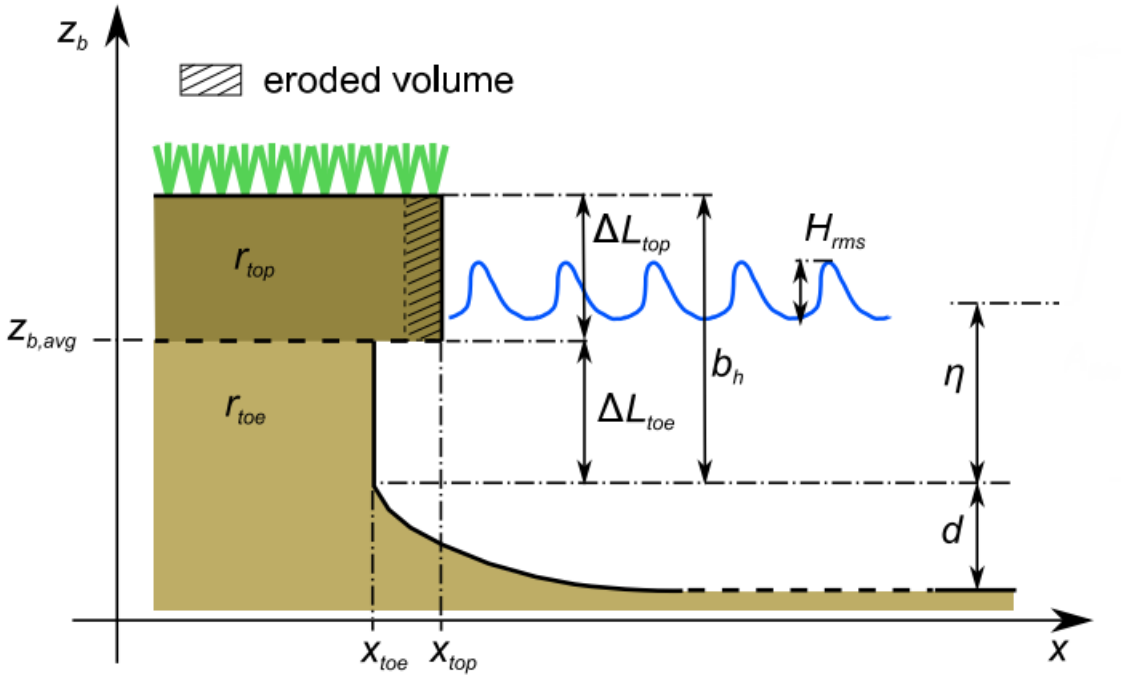

Figure 3.2: Cartoon schematizing the two layer marsh edge system (modified from Bendoni et al. (2016)).

Higher erosion of the underlying mineral layer relative to the root-mat leads to the formation of cantilevered mass failures. Higher frequencies of mass failure events may be responsible for greater net erosion rates. However, Bendoni et al. (2016) argue that the scenario of a marsh undergoing cantilevered mass failures is not all together understood at this moment. As they point out, the blocks of detached marsh may, once dislodged, protect the scarp until they are completely destroyed and their sediment is transported out of the vicinity. Further, the ability to capture the effects of mass failures is dependent on the monitoring methodology. Capturing the erosion rate associated with mass failures requires a higher frequency of observations and site visits. The more common technique of determining erosion rates from aerial photography taken at decadal frequencies tends to lower the erosion rate by averaging out the peaks in erosion which are captured in the other method (Bendoni et al., 2016). Thus, with the latter methodology, one cannot not known with certainty the significance of the mass erosional process and, with the former method, the peaks in erosion rate might tend to skew the erosion mode which is attributed

to the cantilevered mass failure to a higher rate.

It is expected then that a difference in erodibility between the two layers will appear as a difference in soil strength, where the upper root-mat should have a greater strength. It is also plausible to assume that site specific absolute or relative differences in the vertical variability in soil strength will influence the marsh edge erosion rate. However, characterizing the strength of the root-mat is difficult. The presence of the vegetation's root systems promotes a chaotic character to measurements of shear strength and bulk properties in general. Further, vegetation properties (e.g. percent cover, below ground biomass, stem density) show high spatial variability. Though it seems intuitively reasonable that the presence of vegetation will promote marsh stability, the role of vegetation is still a matter of dispute (Feagin et al., 2009; Bendoni et al., 2016).

On the other hand, the underlying mineral layer is more homogeneous and exhibits similar bulk properties between sites when comparisons are constrained to comparable environments (e.g. saline and brackish coastal marshes) (Wilson and Allison, 2008). It is then plausible to treat the mineral layer as a single type of material with a certain strength distribution. The observed variability of erosion rate for a given incident wave power can then be probabilistically modeled based on the inherent strength distribution of the "more mineral layer" within the organic-rich mud and peat layer.

The work by Wilson and Allison (2008) somewhat supports this notion. They measured cross shore elevation profiles which transected the marsh edge in Breton Sound and Barataria Bay. The transects ran from the marsh platform to approximately 300 m offshore in the adjacent water body. They also took sediment cores in cross shore transects which exhibit a similar stratigraphy to the cores sampled in this project. From the sediment cores they determined that these shoreline profiles were erosional because younger reworked sediments overlaid the horizontally continuous marsh platform layer (see Figure 3.1).

Wilson and Allison (2008) observed that the shoreline profiles were relatively uniform

within these two different regions. By considering the entire elevation data set as an aggregate, they proposed an equilibrium profile for eroding marshes shorelines and found that the bottom bathymetry decays exponentially with distance from the marsh edge. The regression fit their data with a coefficient of determination of 0.75. The similarity in shoreline profiles over such a large domain argues that the high-organic mud and peat layer may be modeled as a single material over the southern Louisiana coast.

3.1.2 Results

The geotechnical data set described in Section 2.1 was analyzed in order to determine a depth interval in the soil column representative of the transition from the organic-rich mud and peat to the underlying massive mud or interbedded sand and mud facies. In the down core direction there will be a discontinuity in sediment properties which can plausibly be inferred to define the interface between these facies. The sediment above this transition, but below the root-mat, corresponds to the portion of the marsh edge which Bendoni et al. (2016) identify as the lower lying, more erodible layer. The geotechnical and sedimentological properties of this interval in the marsh edge soil column will be critical in influencing its erodibility.

Figures 3.3 and 3.4 show down-core variation in geotechnical properties for two cores. Also shown are partial core images which provide visual evidence of significant sedimentological features (or lack thereof). Figure 3.3 shows data from a study site located on the marsh platform (i.e. a marsh edge sample), while Figure 3.4 shows data derived from an open water study site. Cores were taken from open water locations in LBA and LBR, but this sampling methodology was abandoned once the field campaign transitioned to MBA and MBR. The open water core stratigraphy is shown here in order to contrast with the features typical of the marsh edge soil column.

The stratigraphy of the two cores are significantly different. The most important feature to note is the facies contact which occurs at $z \approx 1.0$m in the marsh edge core. This is identifiable in the sediment properties (especially bulk density and organic content)

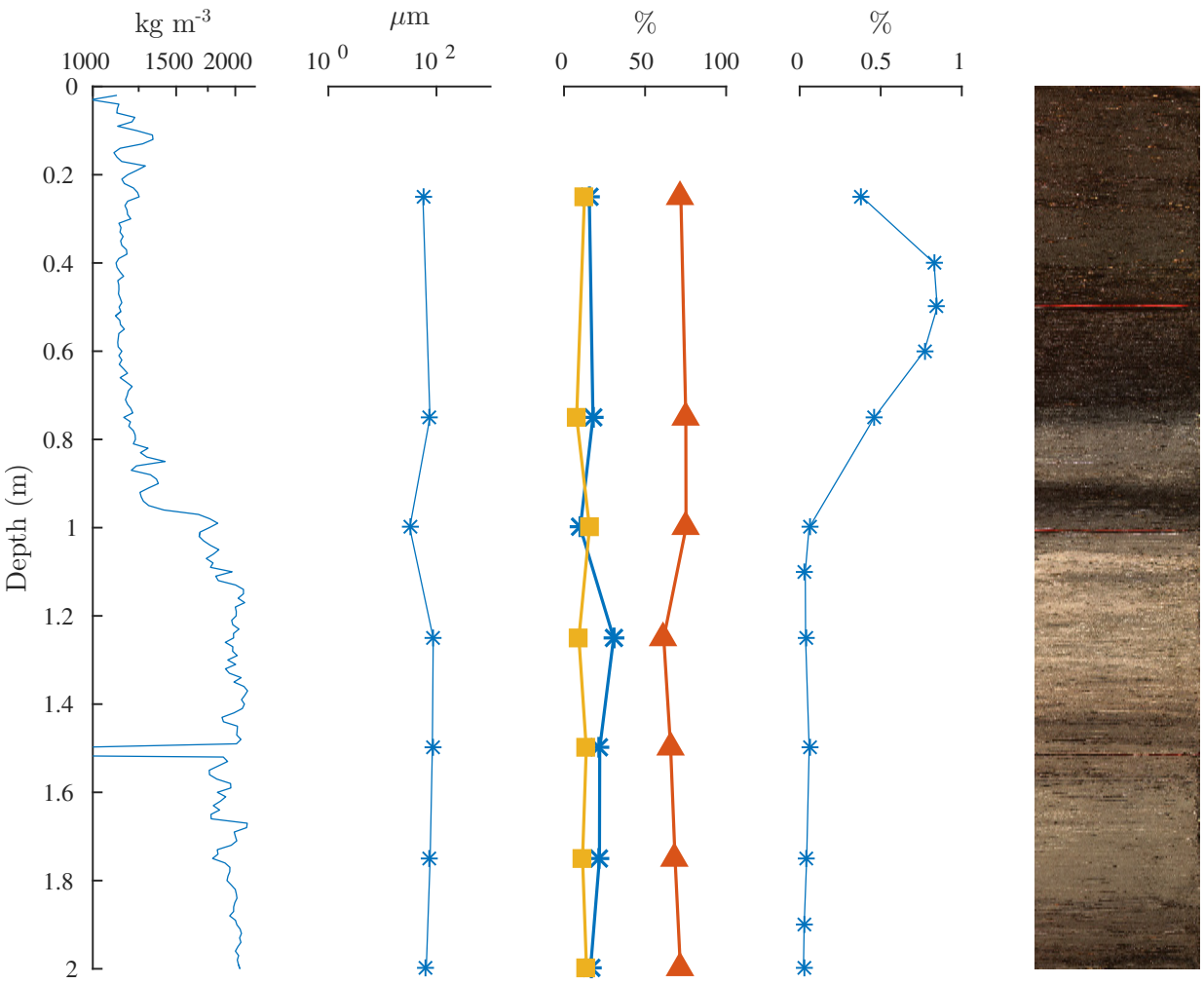

Figure 3.3: Composite sediment properties of a typical marsh edge core. From left to right the panes show: bulk density, mean grain size, sand-silt-clay composition (blue=sand; orange=silt; yellow=clay), organic content, and image of the core.

and can also be visually discerned by a change in sediment color. The transition from brown/olive sediment to light gray with interbedded tan sediment layer is described by Wilson and Allison (2008) as the transition from the organic-rich mud and peat layer (the actively accreating marsh platform) to underlying deltaic sediments.

This transition is not present, as expected, in the open water bay core. When the transition from organic-rich marsh sediments to the next layer is present in the open water cores, it is erosionally overlaid with re-worked shelly bay-bottom muds as discussed in Section 3.1.1. The core image in Figure 3.4 is illustrative of this feature. In fact, the darker portion of the open water bay core at approximately 1.0 m is probably buried organic matter

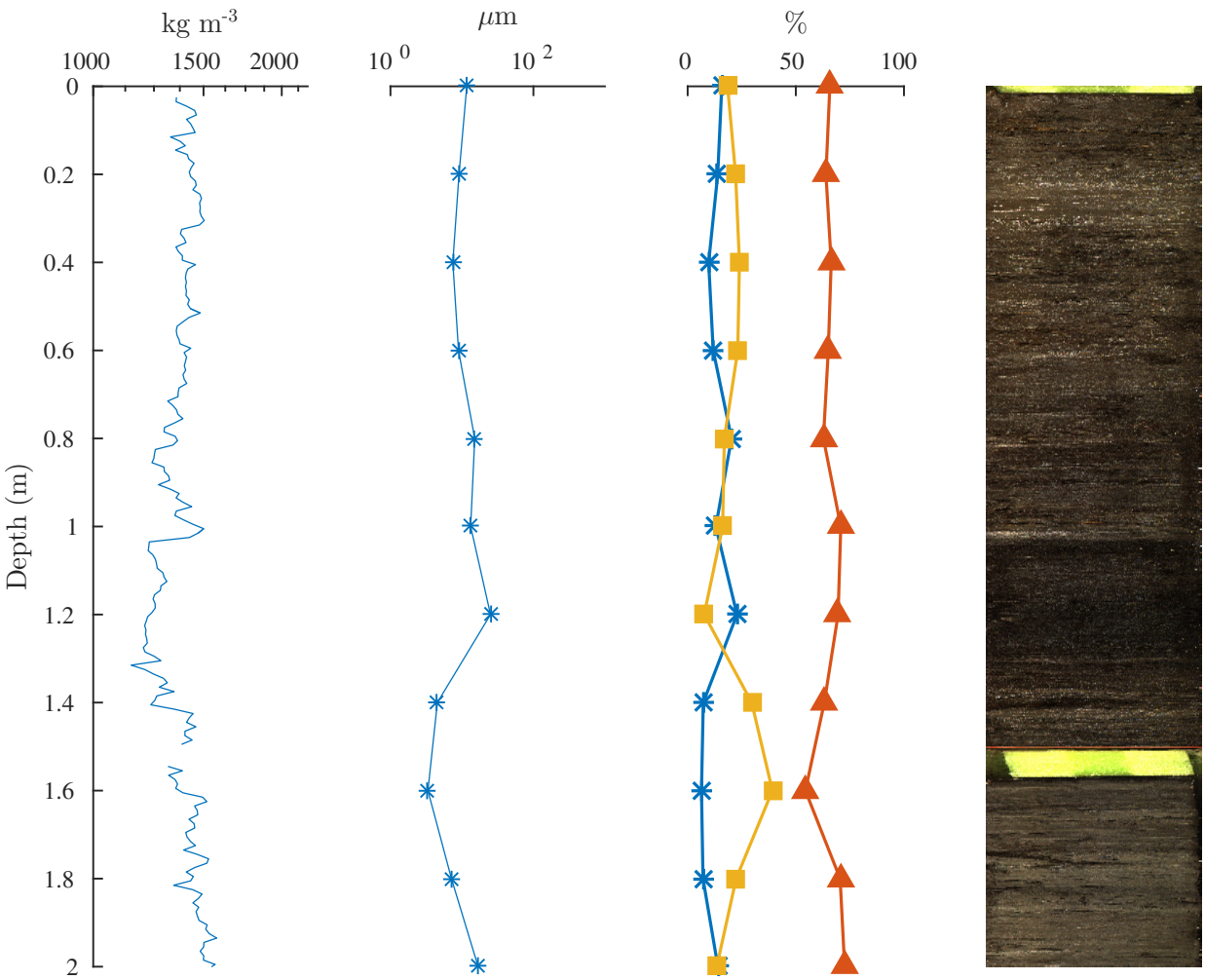

Figure 3.4: Sediment properties of a typical open water bay bottom core. From left to right the panes show: bulk density, mean grain size, sand-silt-clay composition (blue=sand; orange=silt; yellow=clay), and image of the core. No organic content was measured for this core.

undergoing the first stages of diagenesis. This organic matter is probably the remnants of the sub-aerial marsh platform which existed here prior to its erosion.

Figure A.1, A.3, A.4, and A.6, available in Appendix A, show the aggregate data of bulk density measurements for LBR, LBA, MBR, and MBA, respectfully. The data was averaged over the first 1.5 m and over the remaining length of the core as well. This was done in order to highlight the difference in soil properties between these two layers. The near vertical line present in Figure A.6 is probably the result of an operator error because it is unlikely that a marsh edge soil column would have a constant density with depth. Figures

A.2, A.5, and A.7, also available in Appendix A, show the depth averaged ($\Delta z = 0.25$ m) organic content for LBR, MBR, and MBA, respectfully. The organic content for LBA was not available.

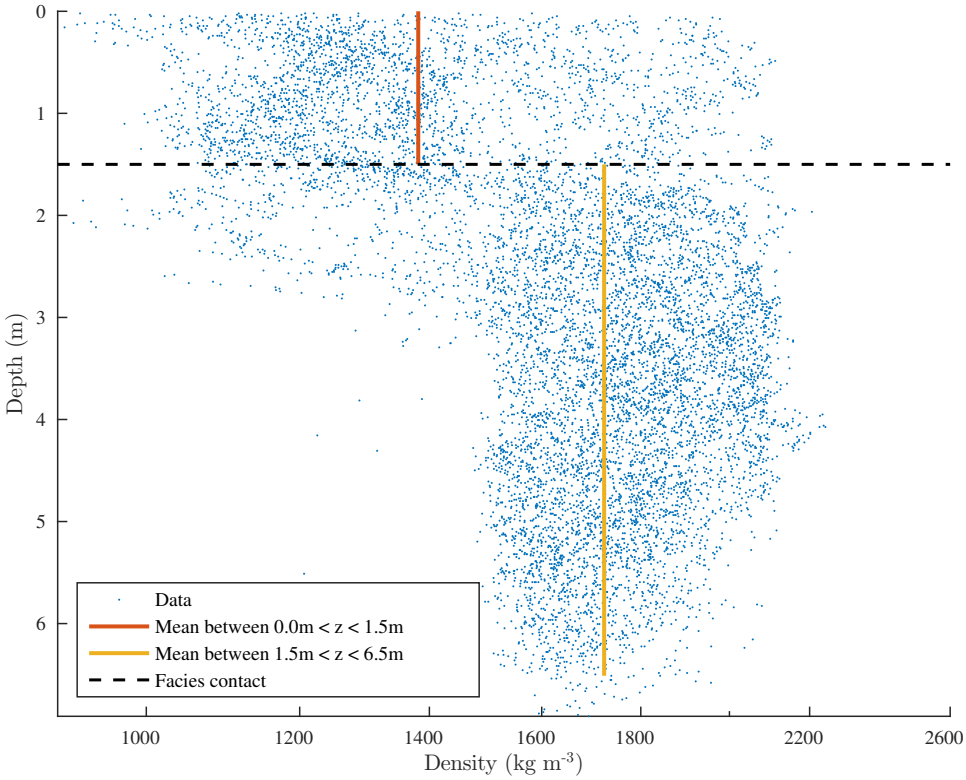

Figure 3.5: Aggregate plot of density measurements from cores samples in LBR.

The density data for LBR and the organic data for MBR is reproduced in Figure 3.5 and 3.6 in order to facilitate discussion. From the data it appears that there is generally a facies transition somewhere near $z = 1.5$ m. This is in agreement with Morton et al. (2003) and Wilson and Allison (2008) who also nominally define this contact at $z = 1.0 - 1.5$m. The facies contact could be discerned by a stratigraphic description of each core individually, however this falls outside the scope of this thesis.

Setting the facies contact at this depth, the geotechnical data can be partitioned into different soil packages for quantitative characterization. It is further recognized that the root-mat zone shows high variability due to the presence of living vegetation. The chaotic nature of the living root systems makes quantitative sediment characterizations difficult. Accordingly, the first 0.5 m is partitioned into a separate package. Table 3.1 contains the

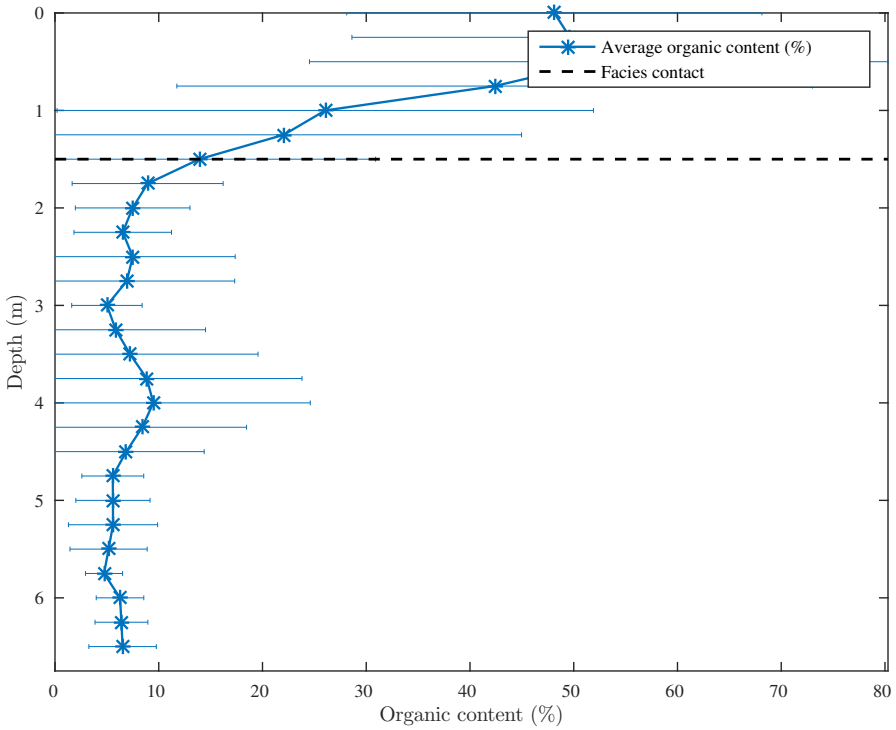

Figure 3.6: Down-core mean organic content for MBR.

statistics of these sediment packages categorized by receiving basin.

Note that the geotechnical data set was derived from a limited spatial domain (i.e Breton Sound and Barataria Bay) when compared to the entire extent of saline marshes in coastal Louisiana. However, the south eastern Louisiana coastal landscape shows a similar dominate vegetation cover, sediment source, and tidal regime. This lends plausibility to the claim that this data set can represent sedimentological trends of other shallow coastal embayments in Louisiana, in particular the study area of the marsh edge erosion modeling, i.e. Terrebonne Bay. This claim is supported by sediment cores taken from Terrebonne Bay, LA which show similar stratigraphy (Morton et al., 2003). This is also supported by the similarity in age and sediment province of Breton Sound, Barataria Bay, and Terrebonne Bay, as discussed in Section 2.1.1.

The applicability across southeastern Louisiana's coastal marsh of sedimentological characterizations drawn from this data set is further supported by a similarity in the data when it is grouped by basin. Saline and brackish marshes (LBA, LBR, and MBA) show

Table 3.1: Statistics of bulk soil properties

Basin	Depth (m)	Bulk density (kg m^{-3})		Organic content (%)		Shear strength (kPa)	
		mean	s.d.	mean	s.d.	mean	s.d.
LBA	0 - 0.5	1.123	0.175			5.9	4.3
	0.5 - 1.5	1.231	0.292			6.9	3.0
	> 1.5	1.708	0.236			10.7	7.6
LBR	0 - 0.5	1.367	0.262	16.7	3.0	6.0	2.8
	0.5 - 1.5	1.389	0.264	31.1	19.4	7.7	3.3
	> 1.5	1.723	0.222	5.8	5.4	13.9	11.7
MBA	0 - 0.5	1.194	0.156	49.4	17.8	5.2	3.3
	0.5 - 1.5	1.338	0.209	38.8	25.1	6.6	3.7
	> 1.5	1.687	0.324	16	16	10.4	7.8
MBR	0 - 0.5	1.170	0.175	48.3	19.6	6.4	3.5
	0.5 - 1.5	1.444	0.325	35.3	29.5	13.8	7.6
	> 1.5	1.875	0.298	7.6	10.1	14.7	7.2

Notes: The organic content data for LBA was not available.

similar geotechnical characteristics, as apposed to the intermediate/fresh marshes in MBR, even though these areas are remote from each other and differ to some extent with respect to ecosystem type and hydrology (See Table 3.1). As mentioned in Section 3.1.1, the similarity in marsh equilibrium profiles between Breton Sound and Barataria Bay also supports this assumption.

ANOVA one-way tests were conducted on the shear strength samples grouped by basin from sub-surface depths of $0.5\text{m} \leq z \leq 1.5\text{m}$. LBA, LBR, and MBA do not show a significant difference from each other ($p > 0.77$), but these areas all show a significant difference from the MBR sample ($p << 0.001$). Figure 3.7 shows a traditional box plot of the sample groups.

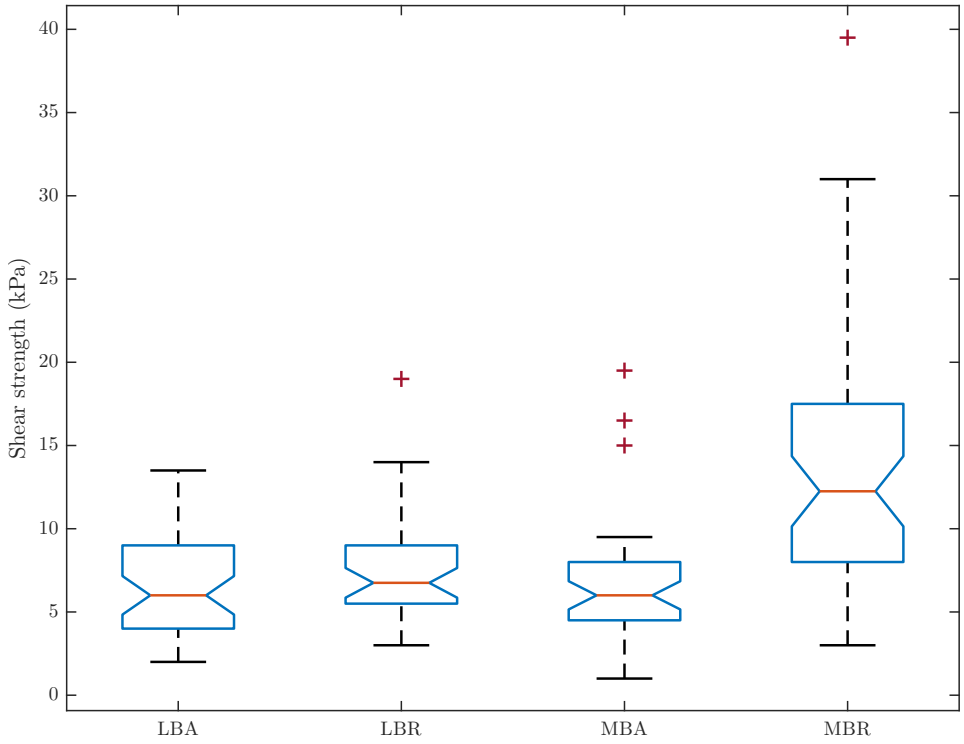

Figure 3.7: Traditional boxplot of LBA, LBR, MBA, and MBR shear strength samples

Figure 3.8 shows the difference in shear strength distributions between the LBA, LBR, and MBA populations and the MBR for $0.5\text{m} \leq z \leq 1.5\text{m}$. The upper layer of organic-rich mud and peat soils from these two populations appear to be two different materials with different properties. The former population is from here on out taken to represent coastal

saline and brackish marsh environments based on the vegetation maps of Sasser et al. (2014). The wetlands undergoing marsh edge erosion are typically saline (and possibly brackish) and dominated by similar vegetation species (Penland et al., 2000; Sasser et al., 2014). The strength distribution for the saline/brackish marshes can plausibly be extended to estimate the properties of coastal marsh edge soils exposed to erosion in Terrebonne Bay.

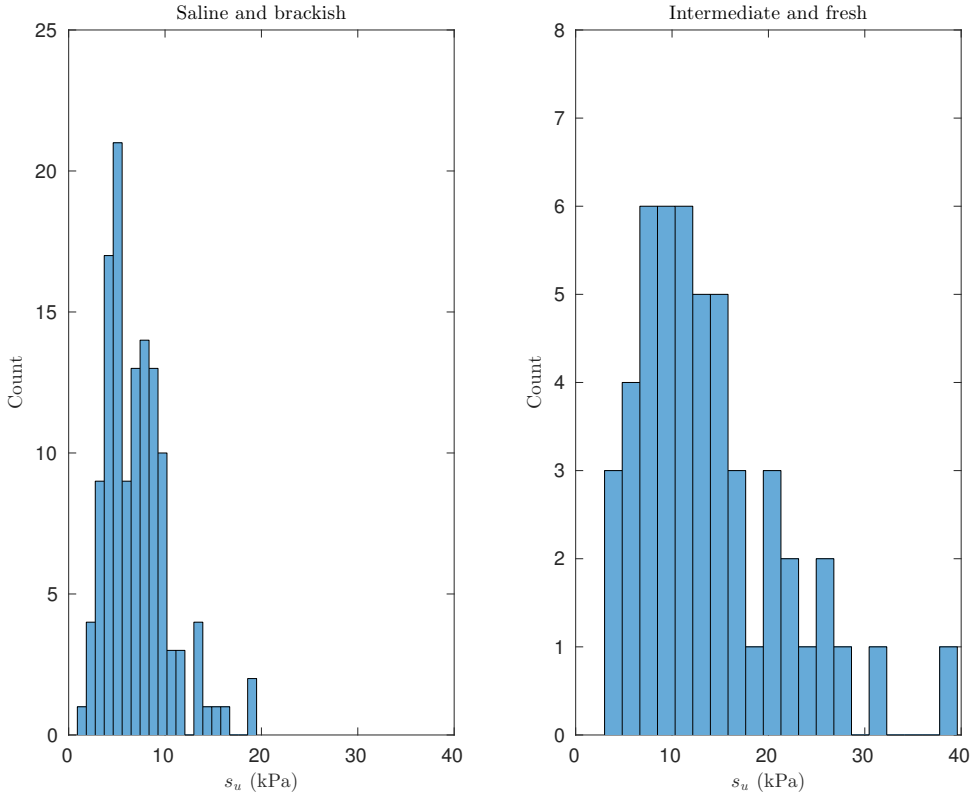

Figure 3.8: A comparison between shear strengths in saline/brackish and intermediate/fresh marsh ecosystems. The saline/brackish system comprises LBA, LBR, and MBA ($N = 126$), while the intermediate/fresh system is constituted by MBR ($N = 50$). The shear strengths were measured in between a depth of 0.5 and 1.5 meters.

In Figure 3.9 the data set was restricted to samples taken from MBA, LBA, and LBR because these basin represent saline and brackish marsh conditions (Sasser et al., 2014). The shear strength is partitioned based on depth interval. It can be seen that the distribution of shear strength varies with depth. This scheme of partitioning the marsh platform soil column is supported by the findings of Bendoni et al. (2016) and the ubiquitous observation of the overhanging root-mat. The presence of the over-hanging root-mat indicates that the root-mat responds differently to wave forcing and should be treated as a discrete

unit separate from the rest of the organic-rich mud and peat unit.

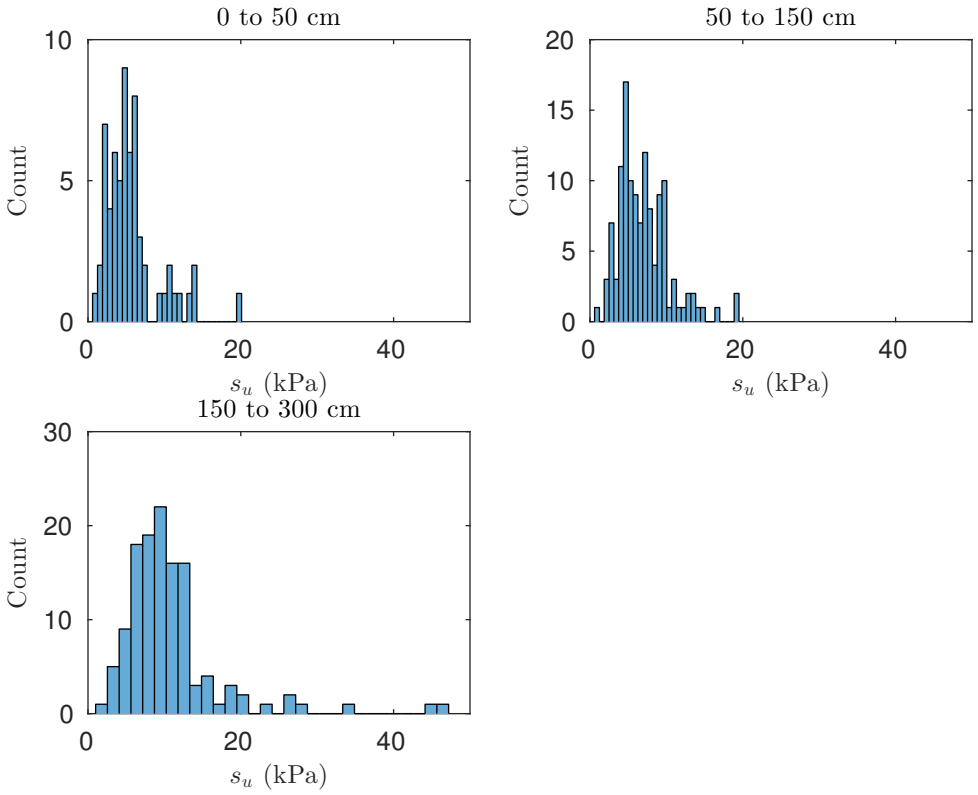

Figure 3.9: Distribution of shear strength for combined data sets of LBA, LBR, and MBA at different depth intervals. The upper left pane is constrained to the upper root layer (0 to 50 cm) N=63; the upper right is constrained to the underlying mineral layer (50 cm to 150 cm) N=126; the lower left pane is constrained to the deltaic sediments (150 cm to 300 cm) N=126.

3.1.3 Implications

Considering the inherent variability in natural systems, it is significant that the shear strength samples between LBA, LBR, and MBA for $0.5\text{m} < z \leq 1.5\text{m}$ are derived from the same population. This indicates that the organic-rich mud and peat facies, excluding the root-mat, can be treated as a homogeneous material. This facies is the primary material on which wave forcing does work in the process of erosion (Wilson and Allison, 2008; Tonelli et al., 2010). The strength of this material will characterize, at least in part, the response of the marsh edge to wave forcing.

A theoretical distribution can be selected to represent the empirical distribution of this data. The theoretical distribution can be used to estimate the probability of shear

Table 3.2: Marsh edge soil shear strength statistical model parameters and 95% confidence intervals

Shape and Scale Parameters					
Data		Lower bound		Upper bound	
a	b	a	b	a	b
4.73	1.49	3.72	1.16	6.00	1.91

strength within a 95% confidence interval. The probability density function (PDF) of this theoretical distribution can be incorporated into marsh edge erosion rate models in order to represent the influence of soil properties. However, one must allow for the assumption that this theoretical distribution can represent regions of southeastern coastal Louisiana outside the province of the geotechnical data set as discussed in Section 3.1.2.

The optimum theoretical distribution was fit to the data using the Maximum Likelihood Estimation technique (MLE). A gamma distribution was found to fit the data best. See Eq. (3.1) for an expression of the gamma PDF, Figure 3.10 for a graphical representation, and Table 3.2 for the statistics of the theoretical distribution's goodness of fit to the data.

$$f(x|a,b) = \frac{1}{b^a \Gamma(a)} x^{a-1} \exp[\frac{-x}{b}] \tag{3.1}$$

Where x is the sample data, $f(x)$ is the probability associated with a given value of x, a is the shaper parameter, b scale parameters, and $\Gamma(\cdot)$ is the gamma function.

3.2 Wave Power in Terrebonne Bay, LA

3.2.1 Model Validation

Comparison with Observations

The skill of the wave power routine and this application of the Young and Verhagen (1996) wave generation equations were assessed through a comparison with observations. The wave observations come from a deployment in TE bay undertaken by Louisiana State University (Parker, 2014). The observation span December 2011 through August 2012. The deployment site is located in west TE near the Louisiana University Marine Consortium

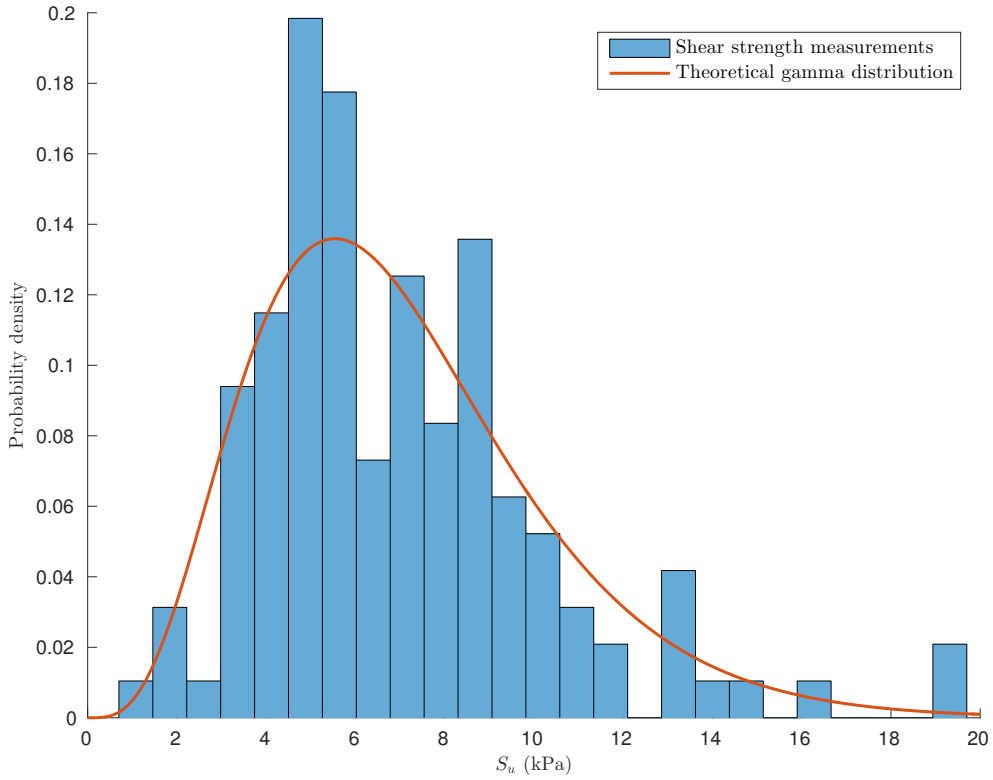

Figure 3.10: Probability density function for the shear strength of marsh edge soils. The solid line is the best fit gamma PDF.

(LUMCON) at 29'21.1"N 90'24.6"W (See Figure 2.7 for the wave gauge location).

Model skill assessment is presented in Tables 3.3 and 3.4 for zero-moment wave height and peak period, respectfully. The goodness-of-fit is assessed using model bias ($Bias$), root-mean-square error ($RMSE$), Pearson's correlation coefficient (r), the coefficient of determination (r^2), and the scatter index (SI). These are computed separately for three illustrative periods and over the entire wave record. This was done to highlight strong points and shortcomings in the model's performance. These periods are denoted good

Table 3.3: Assessment of wave model's skill for hindcasting zero-moment wave height

	Good	Fair	Poor	Entire record
$Bias$ (m)	0.00091	-0.017	0.044	0.018
$RMSE$ (m)	0.041	0.048	0.072	0.062
r	0.91	0.86	0.63	0.70
r^2	0.82	0.67	0	0.31
SI	0.19	0.25	0.59	0.49

Table 3.4: Assessment of wave model's skill for hindcasting peak period

	Good	Fair	Poor	Entire record
Bias (s)	-0.2	-0.51	-0.21	-0.33
RMSE (s)	0.33	0.68	0.53	0.60
r	0.77	0.48	0.31	0.38
r^2	0.32	0	0	0
SI	0.14	0.29	0.25	0.29

agreement, fair agreement, poor agreement, and entire record. They correspond to the intervals of 6-Mar-2012 to 22-Mar-2012, 16-Jun-2012 to 29-Jun-2012, 16-Jan-2012 to 30-Jan-2012, and 14-Dec-2011 to 20-Aug-2012, respectfully. In addition, scatter plots between modeled and observed wave height for the good agreement interval and the entire record are presented in Figures 3.11 and 3.12, respectfully, and for modeled and observed peak period in Figures 3.14 and 3.14, respectfully.

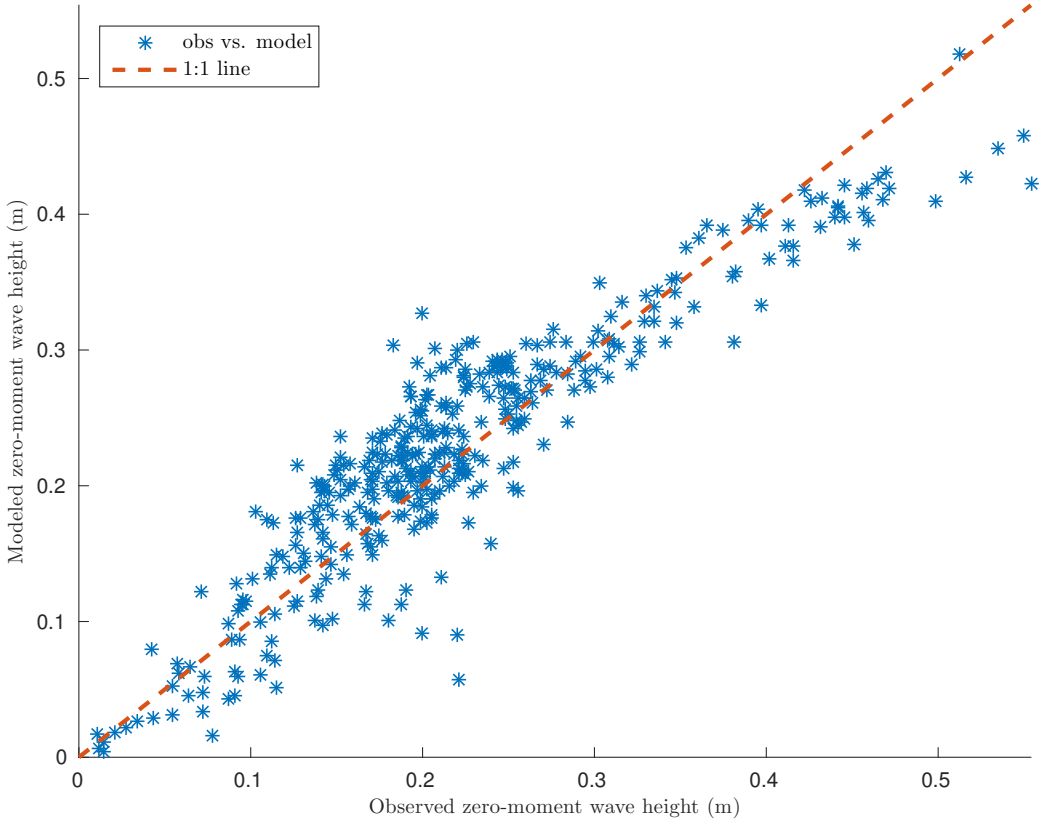

Figure 3.11: Modeled versus observed zero-moment wave height for interval of good agreement

The model performs well during the good agreement interval. A time series comparing

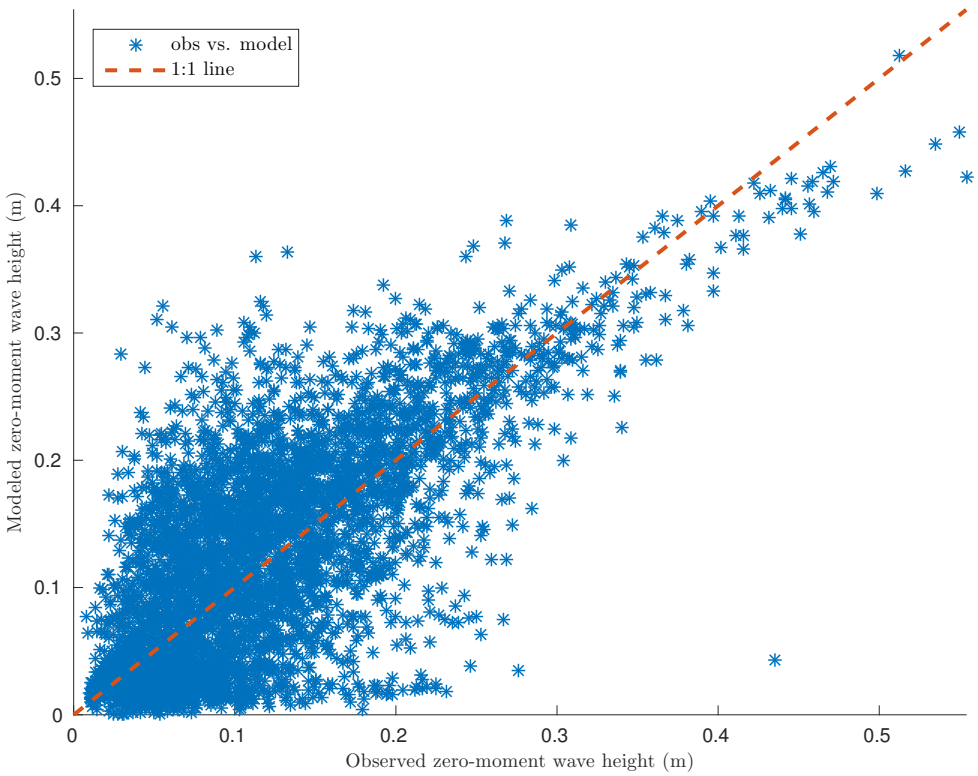

Figure 3.12: Modeled versus observed zero-moment wave height for entire observational record

model output and the wave observations (H_{m0} and T_p), along with the meteorological forcings, is presented in Figure 3.15. The wind field over this interval approached a steady state condition. It is not surprising that the wave parameters are matched well. In relation to the study site, the approach of southern winds is unobstructed. It is likely that waves approaching the wave gauge from this direction were transformed by refraction and shoaling to a limited degree. The Young and Verhagen (1996) equations are well suited to describe these sea states and the wave power routine is able to accommodate the slow variations in wind speed and magnitude.

A similar portrayal of the fair agreement period is shown in Figure 3.16. During the first part of the record (June 18$^{\text{th}}$ to June 23$^{\text{rd}}$), the agreement is satisfactory. The peak wave period is slightly underestimated. This is a well known characteristic of the Young and Verhagen (1996) equations. As the wind gradually shifts to the north there is significant underestimation of T_p. The validation site is sheltered to the north and northwest and fetch

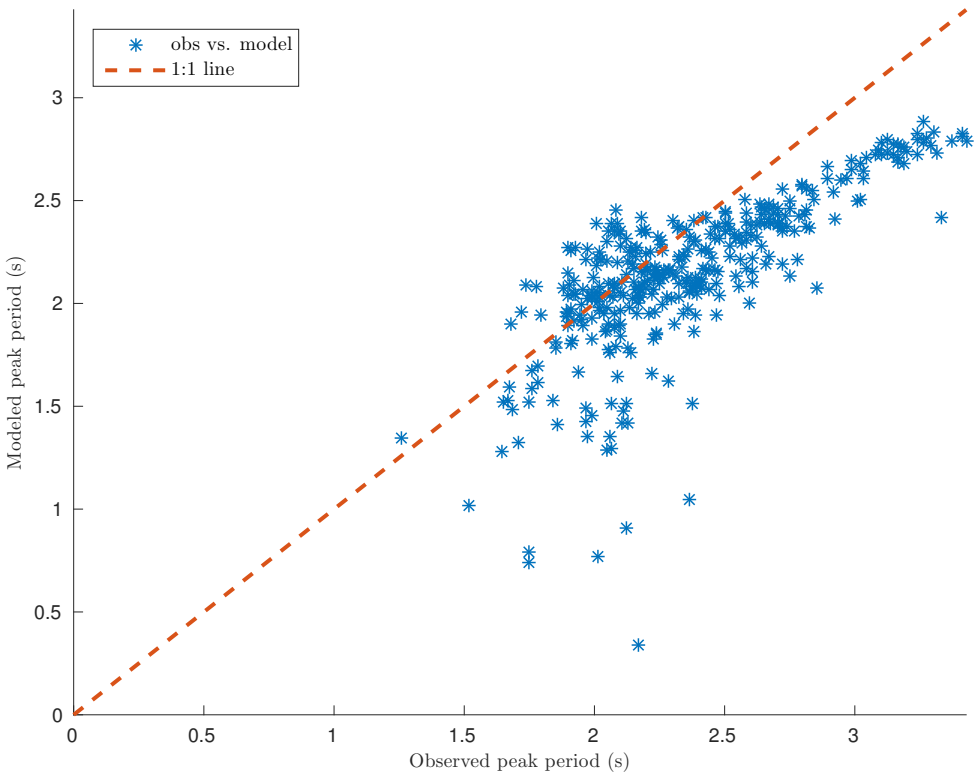

Figure 3.13: Modeled versus observed peak period for the interval of good agreement

distances are small ($X < 800$m). Consequently, the wave power routine calculates small locally generated wave though in nature there is still energy moving into the site from far field wave generation. Between the dashed vertical line the wind is rapidly changing. Due to the unsteady conditions the wave power routine has significant problems estimating the peak wave period.

Figure 3.17 shows the interval of bad agreement, a period of greater variability in the wind field. In this interval small temporal variations in wind speed cause slight over estimation of wave height. This is likely due to the consecutive-preceding-mean technique of determining steady wind conditions. If the changes in wind speed occur gradually enough, the wave power routine assumes the winds are steady. In nature, this variability may be producing a choppy wave field with increased wave interaction.

In general the wave power routine captures the zero-moment wave height. It can be noted however that the prediction of peak wave period significantly under performs for the fair, poor, and entire intervals. This is likely due to three sources of error: (1) Far field

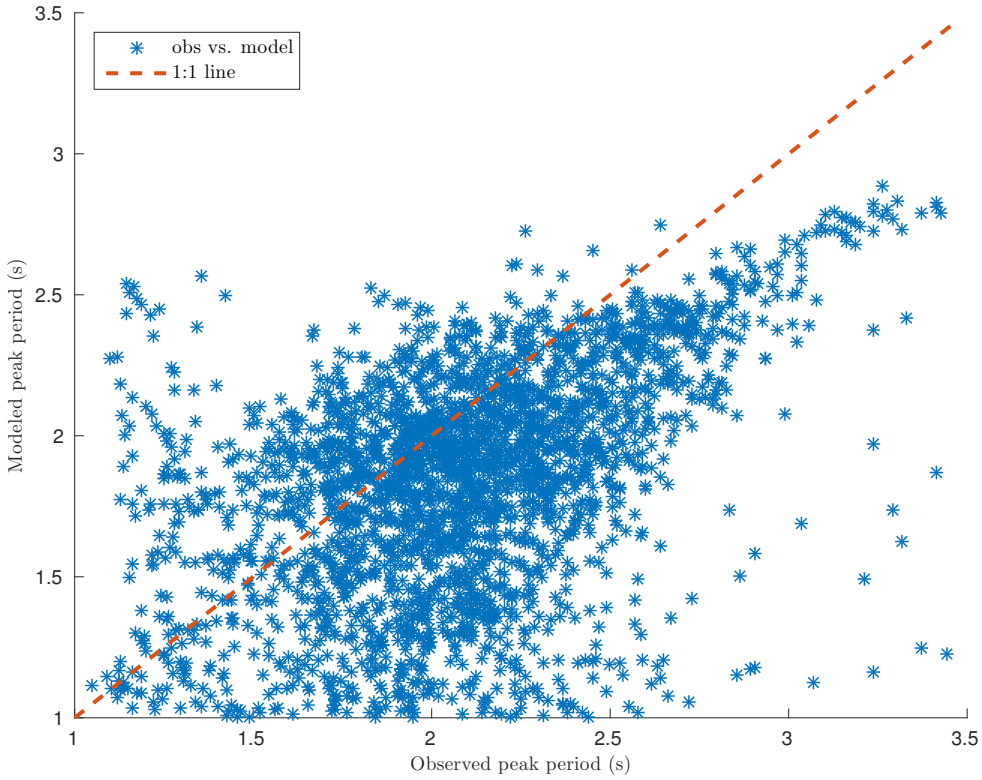

Figure 3.14: Modeled versus observed peak period for entire observational record

effects; (2) Unaccounted for swell energy; and (3) Noisy energy signal.

The first source of error stems from the inherent unsteadiness in the wind field. The Young and Verhagen (1996) equations essentially model wave generation under idealized steady state wind forcings. The wave power routine attempts to deal with unsteady conditions by determining intervals of steady wind forcing and computing wave generation as a sequence of quasi-steady states. This completely fails to consider the propagation of wave energy. For example, if the wind field rotates 90, then newly generated wave will begin to propogate energy in this direction. Concurrently, energy continues to propagate in its antecedent direction until it is generally transformed or dissipated. The wave power routine may be able to estimate the newly generated wave energy, but will not capture energy from previously generated waves.

The second source of error is essentially the same as the first. In a similar manner the wave power routine cannot not simulate the propagation of swell energy into TE.

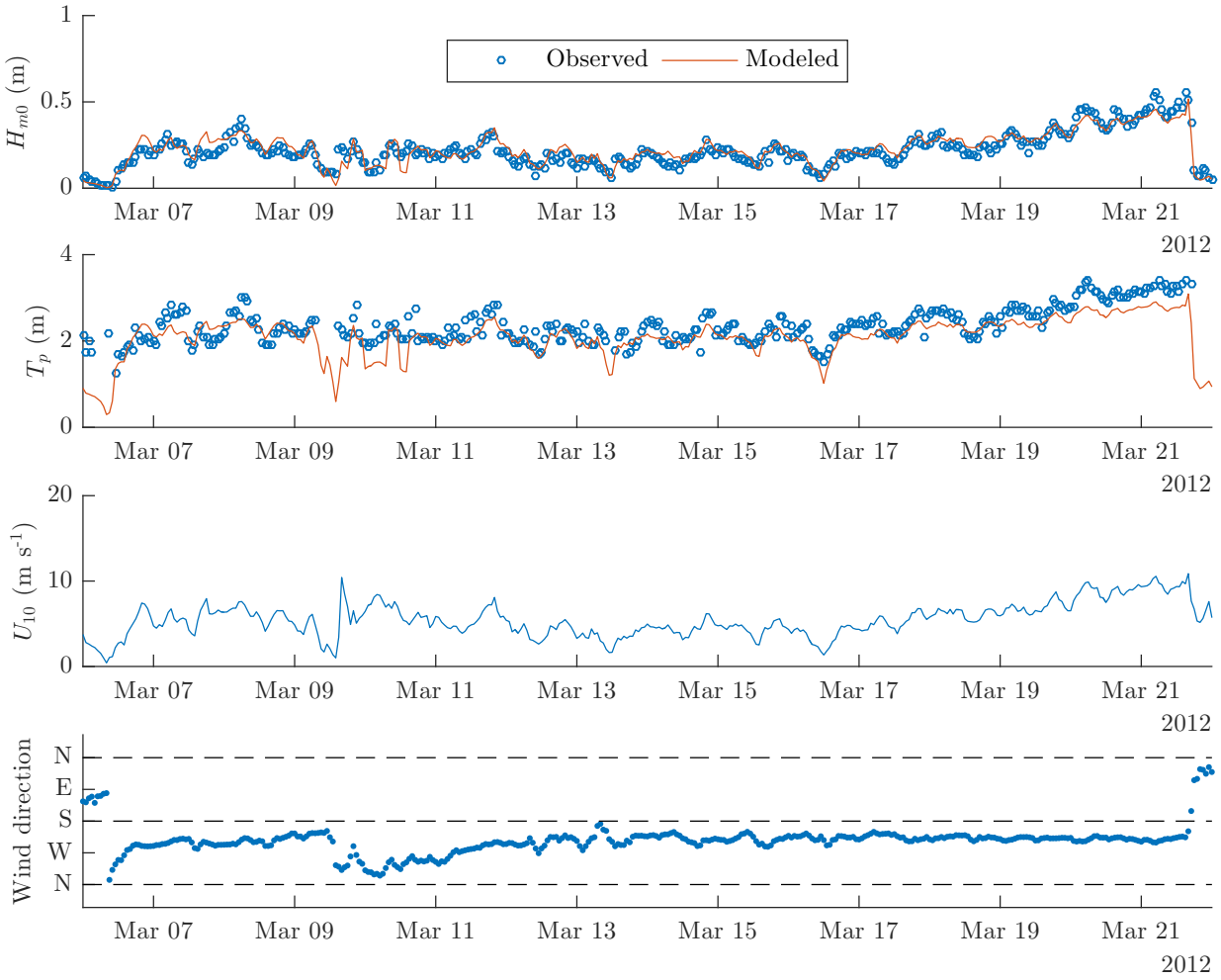

Figure 3.15: Time series comparison of meteorological forcings, wave observations, and hindcasted waves.

The presence of energy which in nature is not generated locally will appear as an under estimation in the model.

The third source of error pertains to the system being modeled itself. Wave heights are generally low in TE. At the validation site H_s ranging from 10cm to 14cm throughout the year (Parker, 2014). One feels that this is on the low end of measurable waves in the field. Further, for many intervals of wave height collection, the H_s is somewhat smaller. For these cases the power spectral density function may not conform to the canonical shape of a wave spectrum. The techniques for automated detection of wave peak period, necessary for processing hundreds of wave records, may fail to discern peak wave periods in a reliable

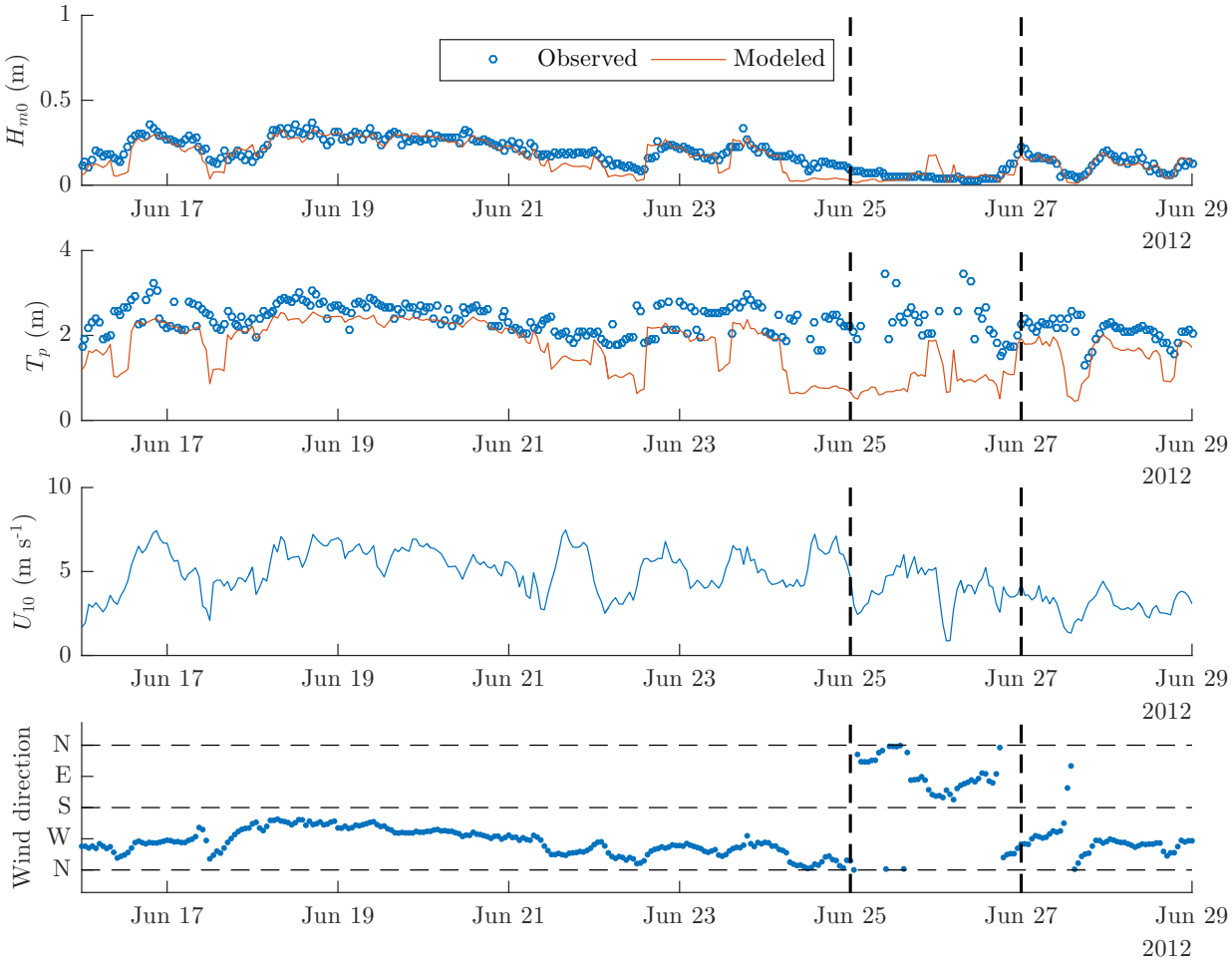

Figure 3.16: Timer series comparison showing deviation in wave height estimation

way.

The aim of the wave power routine is to estimate average wave powers over engineering time scales. The ability of the model to match the observed P at the hourly time scale will suffer from the propagation of errors. As discussed in Section 2.2.3 hourly rates of wave energy flux are not significant for marsh edge erosion. Daily averaged wave powers provide a suitable metric to assess the skill of the wave power routine. Figure 3.18 shows the

Table 3.5: Assessment of wave model's skill for hindcasting daily averaged wave power

Bias (W m^{-1})	*RMSE* (W m^{-1})	r	r^2	*SI*
5.4	30.6	0.88	0.77	0.65

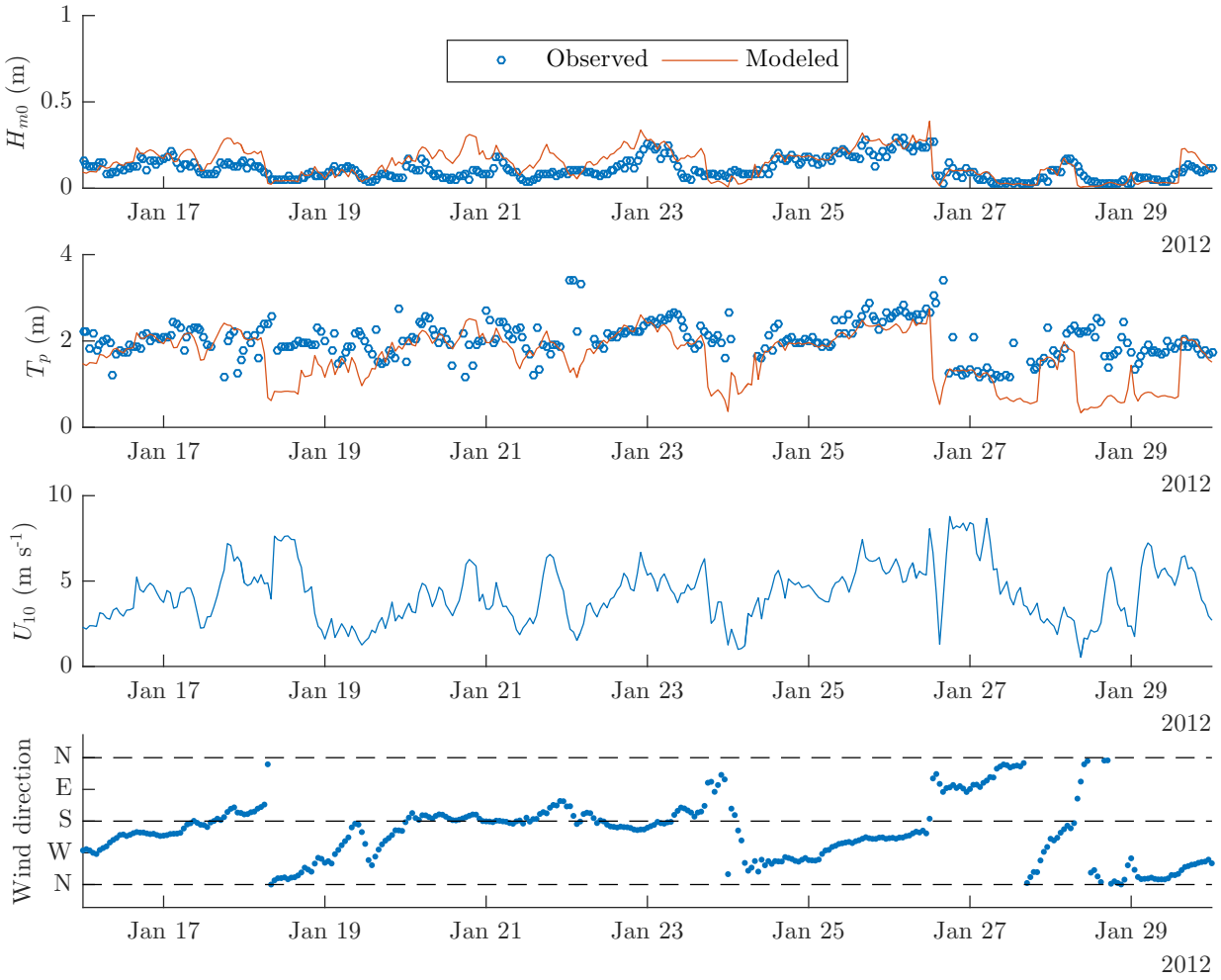

Figure 3.17: Time series comparison highlighting issues with model performance. The time period indicated by bold dashed lines indicates rapidly changing wind conditions and a low energy power density spectrum.

modeled and observed daily averaged wave powers. The wave power routine satisfactorily correlates to the data but misses some peaks. See Figure 3.19 for a scatter plot comparing observed and modeled daily average wave powers. The goodness-of-fit is presented in Table 3.5.

Comparison with SWAN

The wave power calculation routine was also validated against nearly research grade model for Terrebonne Bay, LA. Simulating WAves Nearshore (SWAN) is a phase-averaged wave model used extensively in the industry and research. It solves the wave action balance equation with a finite difference scheme. SWAN employs a variety of physics-based

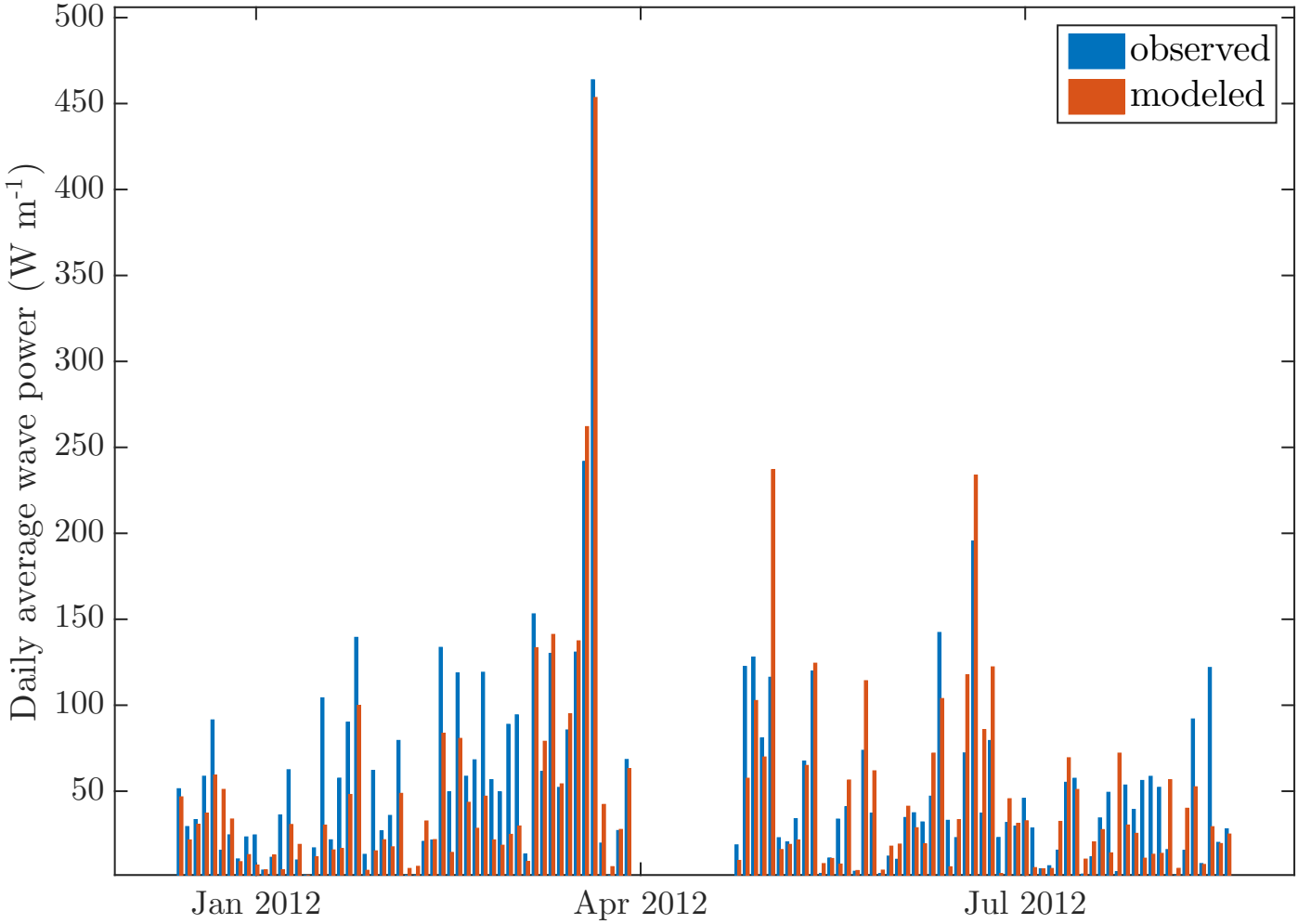

Figure 3.18: Time series of observed and modeled daily averaged wave powers

formulations to model wave generation, transformation, and dissipation in the complex bathymetry of the nearshore environment (Booij et al., 1999).

SWAN was run with identical wind forcings and bathymetry inputs for the same time period (private communication with Everett, T.). Comparing the average wave power at a point by point basis elucidated an obvious deficiency in the wave power calculation routine. The wave generation component of the routine is very sensitive to the placement of the shoreline points and the shoreline geometry. If the points are placed too close to the shoreline, then errors in shoreline digitization and the resolution of the fetch length discretization may lead to severe underestimation of the fetch lengths. In order to over come this deficiency, the shoreline points were moved out from the shore until they met a criterion

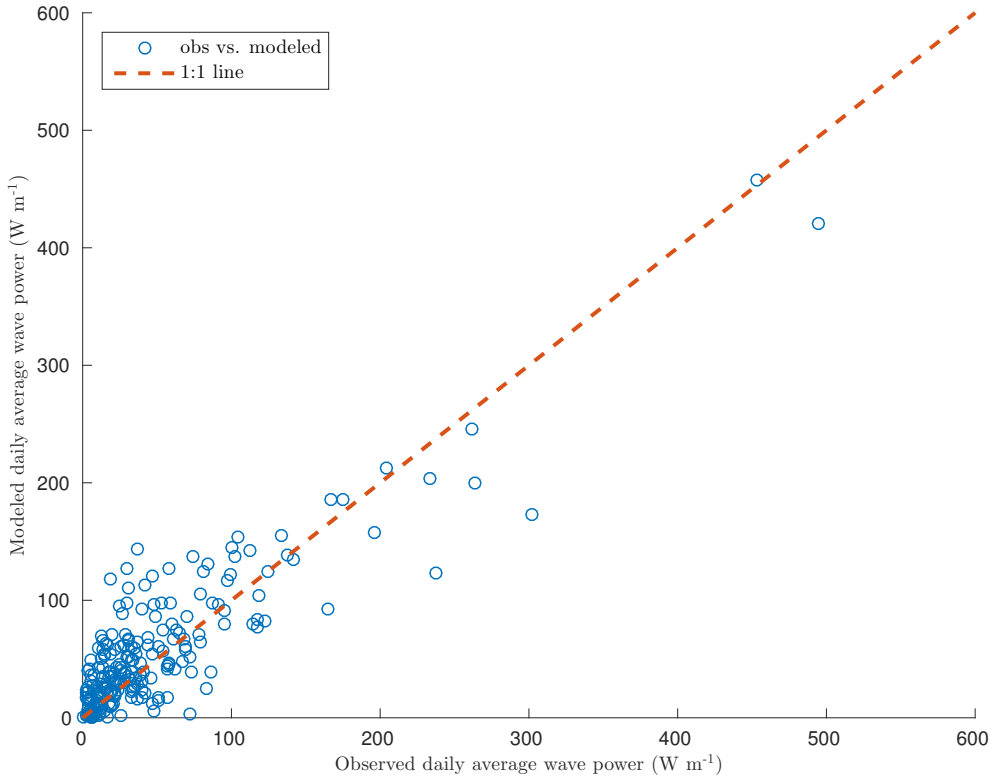

Figure 3.19: Scatter plot comparison between modeled and observed daily averaged wave power

of distance from shore and time averaged depth (T. Everett, personal communication).

Another error introduced into the wave power calculation stems from its inability to model wave propagation and transformation. If the shoreline sample points are located inside "pocket" beaches, then fetches and wave generation are quite limited. In reality, however, significant wave energy may propagate into the enclosure. In these cases, as a result, the Young and Verhagen (1996) equations are wholly inadequate to model wave power. An actively eroding and degraded marsh exhibits a highly sinuous geometry and contains many such enclosures. The coastline in Terrebonne Bay is no exception.

The mean wave power calculated from the sea energy component of the output of SWAN was compared to the output of the wave power calculation routine at each site. It was found that the wave power routine performed well for sites facing the open water and poorly for sites which were semi-enclosed. This is expected as the Young and Verhagen (1996) equations predicted limited wave growth based on the fetch of a semi-enclosed water

body and cannot capture the propagation of wave fields into the enclosure as opposed to SWAN. See Figure 3.20 and Figure 3.21 for a comparison between the SWAN output and the wave power calculation's output for a good and bad coastal geomorphology for the performance of the Young and Verhagen (1996) equations, respectively.

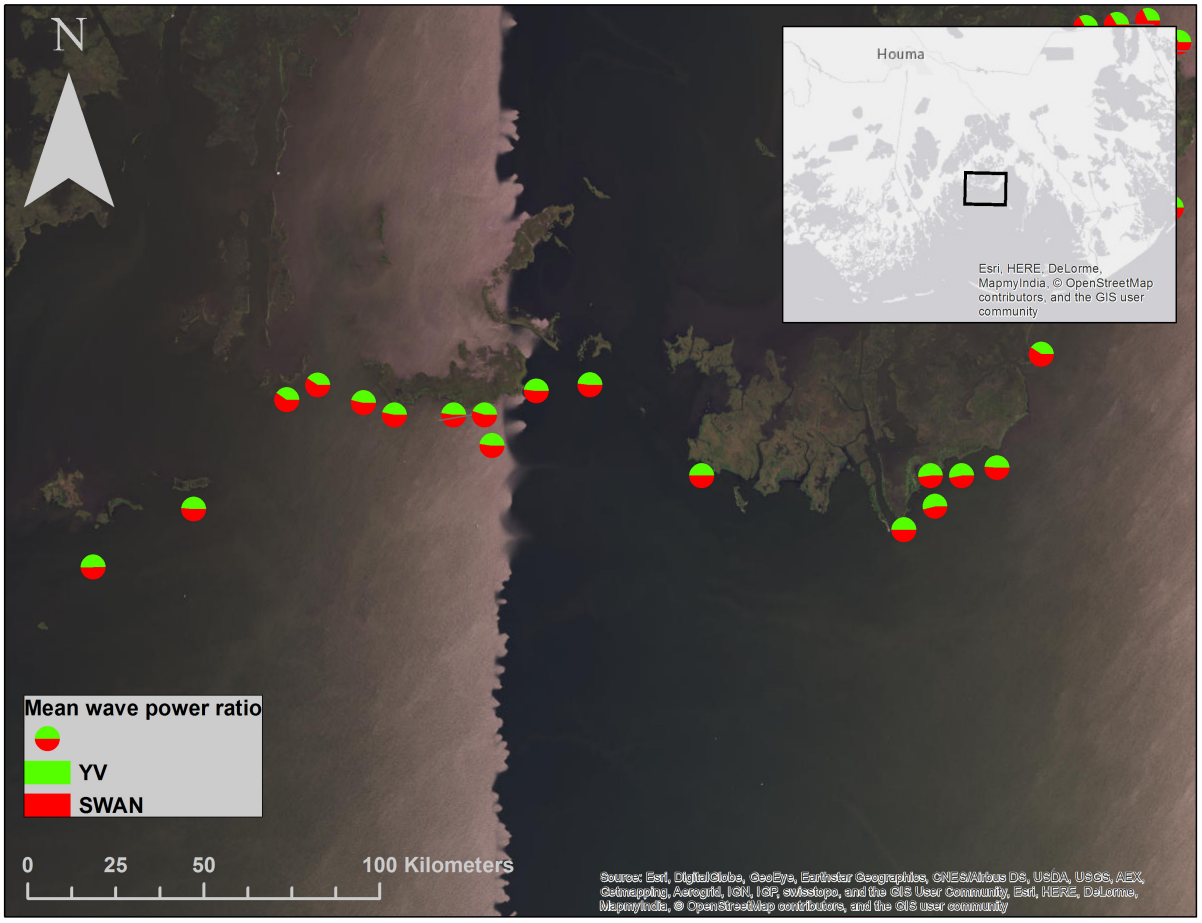

Figure 3.20: Coastline geometry which exhibits adequate performance of employing the Young and Verhagen (1996) equations to estimate incident wave power. The red proportion indicates SWAN output and the green area indicates the wave power calculation routine's output.

The pie chart symbols show the relative proportions of the different model's output to each other. These figures show clearly that within highly sinuous or embayed coastlines, the wave power calculation routine is inadequate to model incident wave power. Any points where the relative error between the SWAN output and the wave power calculation routine's output exceeded the mean error for the entire domain were eliminated because

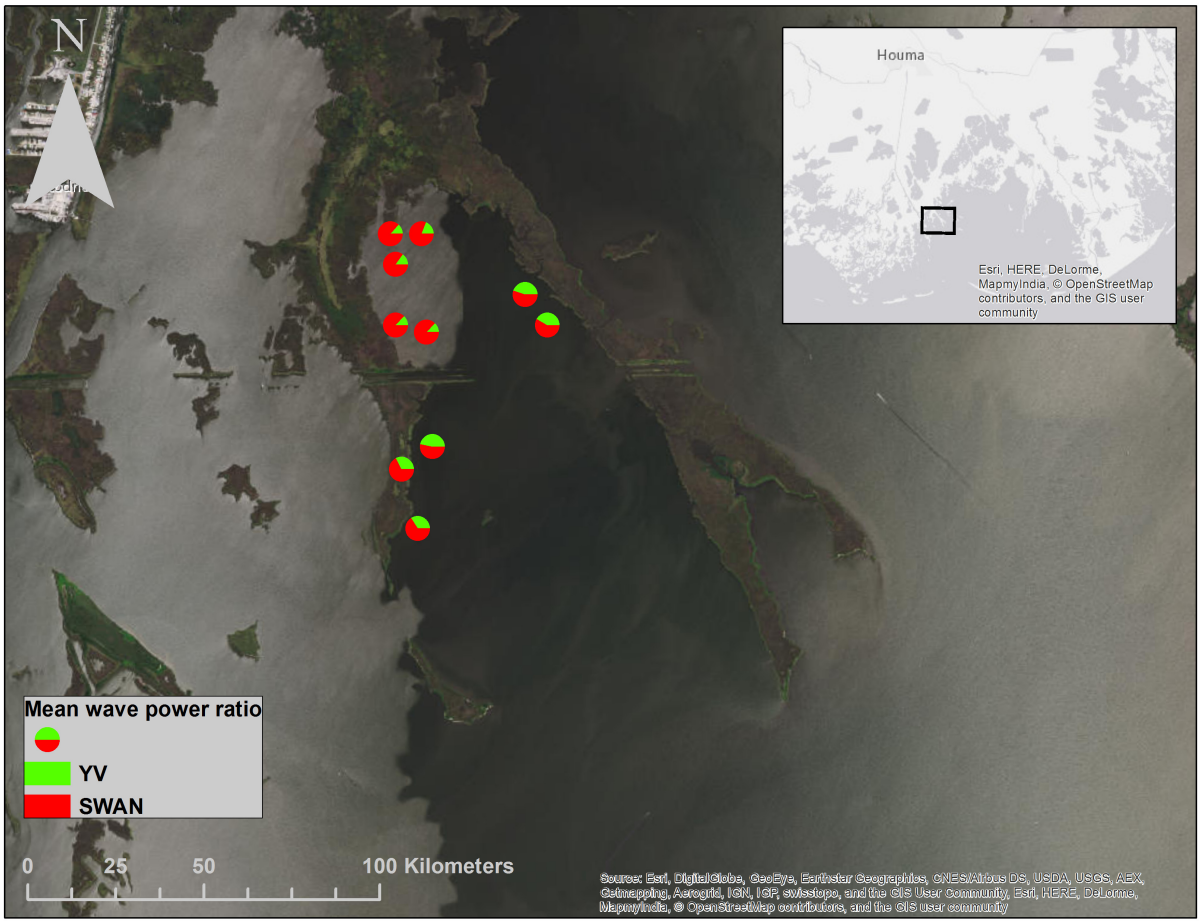

Figure 3.21: Coastline geometry which exhibits poor performance of employing the Young and Verhagen (1996) equations to estimate incident wave power. The red proportion indicates SWAN output and the green area indicates the wave power calculation routine's output.

these points would introduce an unsuitable amount of error into the erosion rate versus wave power relationship.

The wave power routine is further only able to model the wave power generated by local sea wave generated within Terrebonne Bay. Swell energy propagating into TE from the GoM, which may cause erosion, is not captured by the Young and Verhagen (1996) wave generation models. SWAN modeling results proved that some stretches of coastline within TE receive large amounts of swell energy (personal communication T. Everett). Consequently, any points which exhibited swell energy in excess of 20% of the total energy were excluded. Figure 3.22 shows the spatial distribution of excluded points and suitable

points for the erosion rate to wave power relationship. Note that most of the points in the north and north west of TE are acceptable. The agreement between SWAN and the wave power calculation routine for the sites deemed suitable is presented in Figure 3.23.

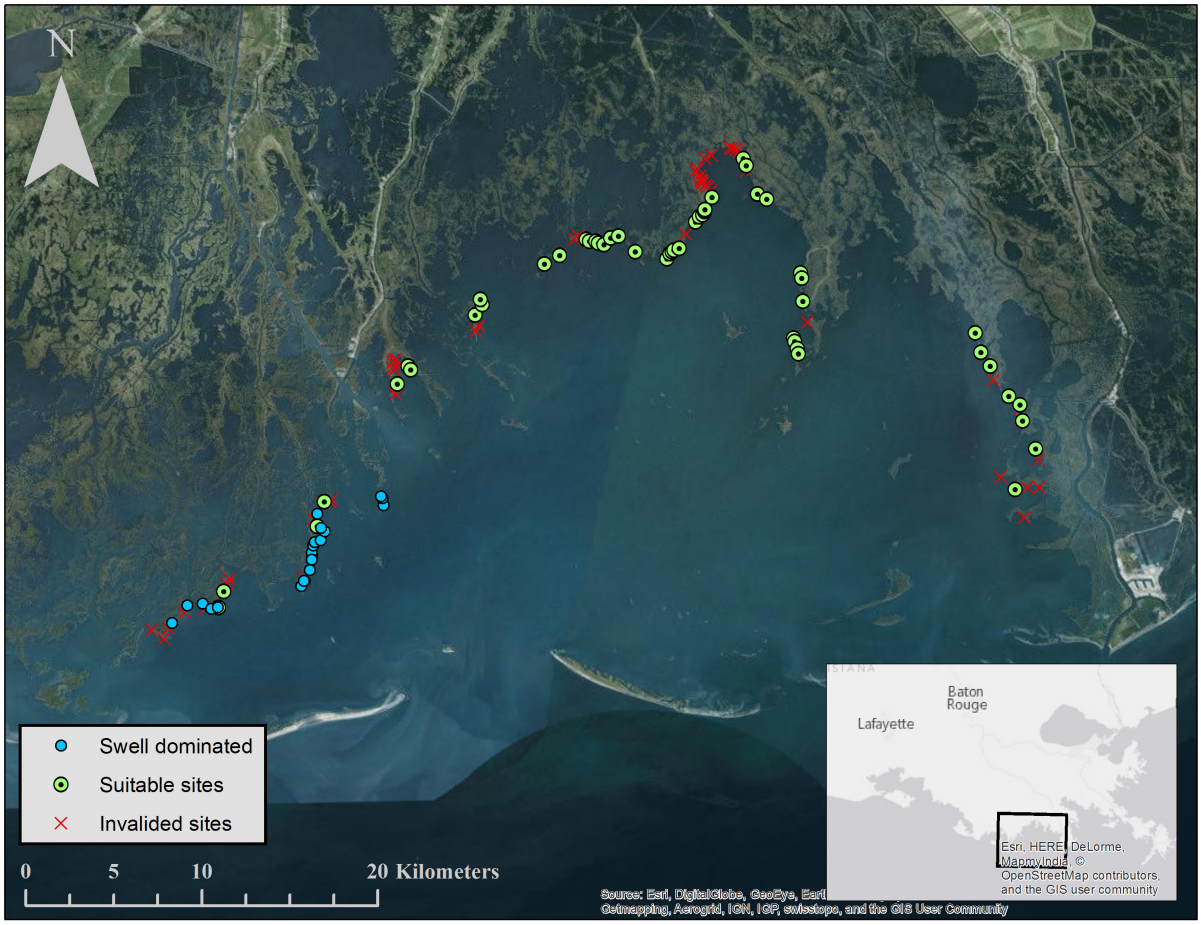

Figure 3.22: Map of Terrebonne Bay, LA showing localization of shoreline points unsuitable for parametric wave generation models.

3.2.2 Results

The wave power calculation routine was used to compute the average wave power for the points deemed suitable (see the discussion in Section 3.2.1) for 9 years of wind forcing. The 9 years were partitioned into 3 intervals in order to correlate mean wave power with the erosion rates determined between the dates of aerial photographic surveys. See Figure 3.24 for spatial and temporal distribution of average wave powers in Terrebonne Bay. Only the sites which exhibited acceptable error in comparison with SWAN are displayed. See

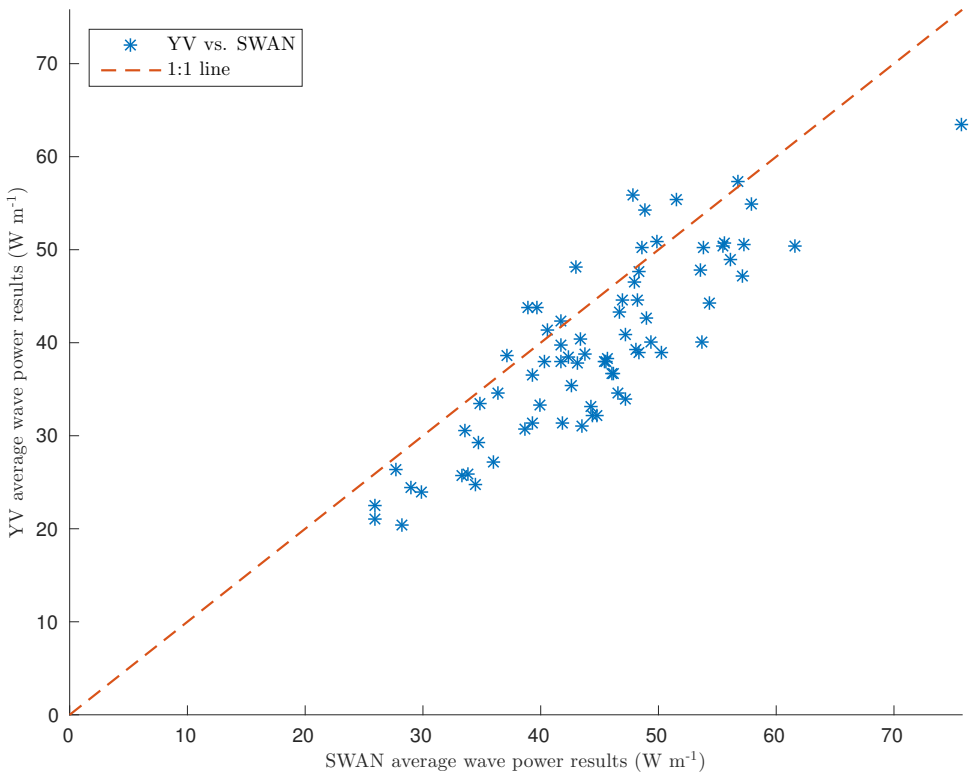

Figure 3.23: Agreement between YV and SWAN results for annual average wave power for Terrebonne Bay, LA. $r^2 = 0.35$ and $RMSE = 7.1$ (W/m).

Allison et al. (2015) for details on the aerial photography and the delineation of coastal erosion transects.

3.3 Erosion Rate and Wave Power in Terrebonne Bay, LA

3.3.1 Results

As was discussed in Section 3.2.1 and displayed on a map in Figure 3.22, only certain points in TE yielded suitable estimations of mean wave power. The marsh edge erosion rates correlated with these stations were also subject to quality control as discussed in Section 2.2.1. The final data set includes 124 points where an observed marsh edge retreat rate (R) is related to average wave energy conditions parameterized by wave power (P) and radiation stress (S_{xx}). The data set is composed of various locations throughout TE and over the three time periods of marsh edge erosion analysis. The relationship between

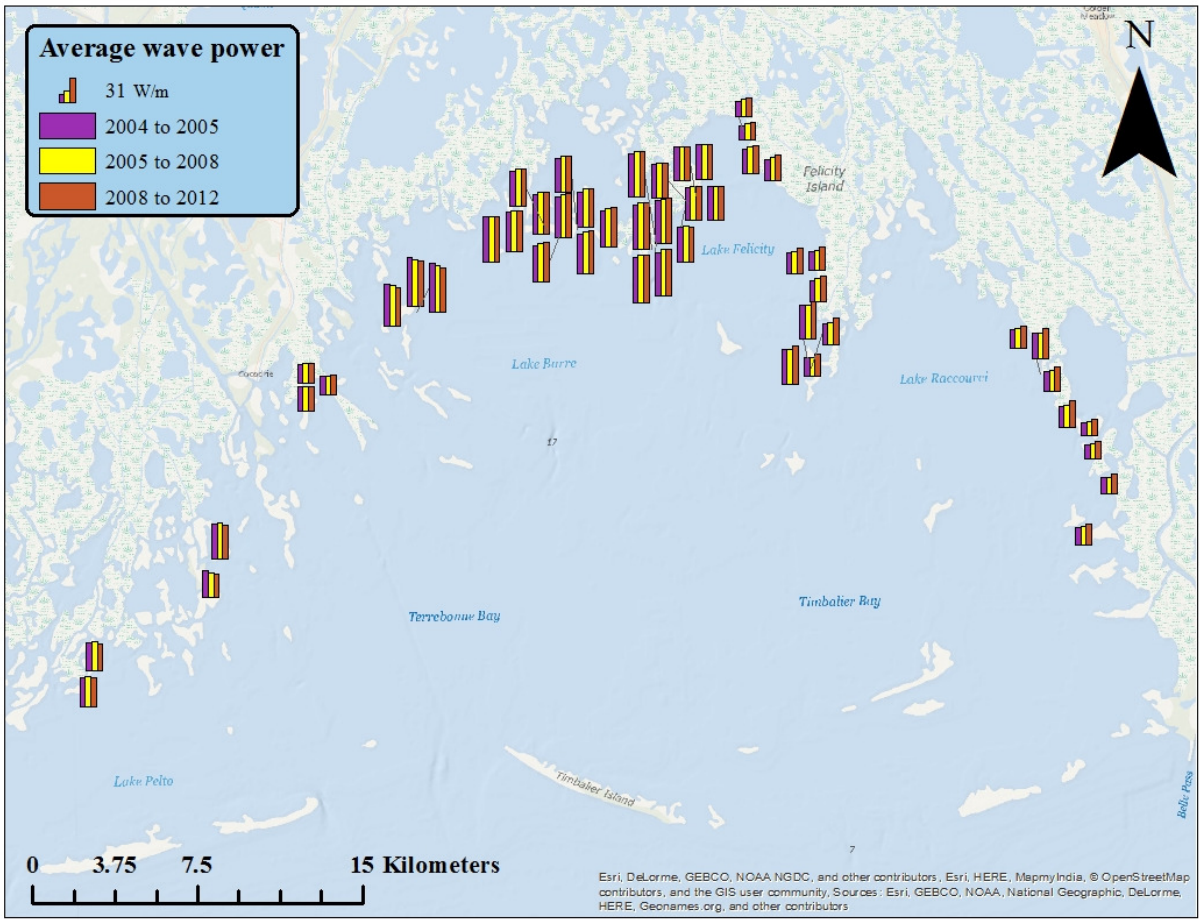

Figure 3.24: Average wave power at all suitable sites within Terrebonne Bay.

P and V for these 124 points is shown in Figure 3.25. In order to obtain a value for volumetric erosion rate, V, from the retreat rate data set, a value of h =0.5 m is assumed to represent the scarp height though out TE. It is common to assume the scarp height in regional studies because survey data for every site is unavailable. A value of 0.5 m was chosen as it reflects the tidal range in TE.

The scatter in Figure 3.25 is reasonable because these points encompass erosion rates and mean wave power determined over time intervals ranging from 1.7 to 4 years and are drawn from points distributed over 100 km of coastline. When the data is averaged over mean wave power bins, thus averaging out the variability in site-specific properties, a linear trend can be discerned. In TE for wind sea generated wave power we find that $V_{bin} = 0.0516 P_{bin}$, where the *bin* subscript denotes that these values have been bin averaged.

This relationship is similar to others reported in the literature. Marani et al. (2011) reported a bin averaged linear relationship of $V_{bin} = 0.0364 P_{bin}$.

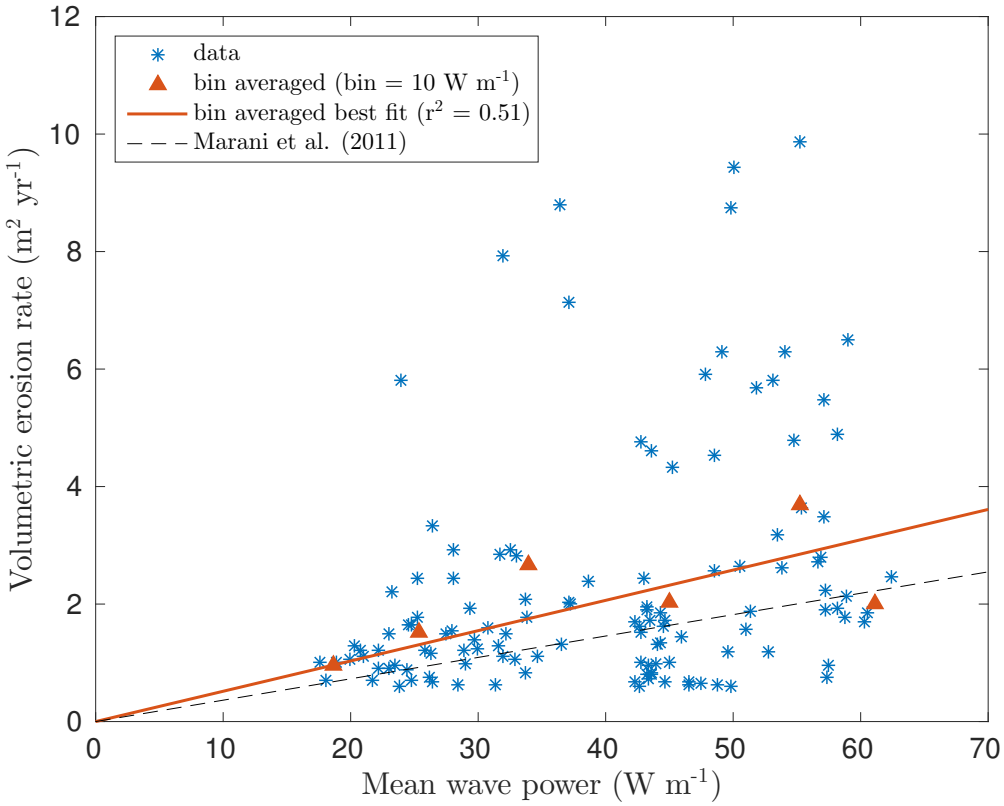

Figure 3.25: Volumetric erosion rate versus mean wave power for Terrebonne Bay

It appears that TE's coastal marshes are eroding more quickly under similar forcings than the salt marshes analyzed by Marani et al. (2011) in Venice Lagoon, Italy, shown in Figure 3.25 as a broken line. Also, the range of V between the two study regions is different, with TE undergoing erosion at twice the rate of the Venice lagoon. This could be due to natural reasons or to the manner in which P and V were computed. If the assumption that $h = 0.5\,\mathrm{m}$ is an overestimate, then the estimations of V would be inflated. For instance, it is possible that some areas of TE which were undergoing very high rates of retreat (e.g. $R > 20\,\mathrm{m\,yr^{-1}}$), were highly degraded with a marsh scarp height far less than 0.5 m. Thus, the volumetric erosion rate would not be as high as it is calculated here to be. Also, Marani et al. (2011) considers the angle of wave incidence to the shore in computing the mean wave power normal to the shoreline. This can only decrease the mean wave power as it scales

wave power in the range $[0, 1]$. Following Allison et al. (2015) this study assumes all waves are normal to the shoreline. As a result, it is likely that this study is overestimating both P and V to some degree.

The scatter in Figure 3.25 cannot be solely attributed to errors in the wave power calculation as the wave power calculation at these points were well validated. The variability in erosion rate for identical forcing is therefore due to physical factors. Eq. (2.7) is designed in order to incorporate shear strength into the relationship between V and P in such a way as to force the mean erosion rate under mean soil strength conditions and mean radiation stress. Deviations from the mean soil strength result in a greater or lesser erosion rate for given wave forcings. The variability in erosion rate is dependent on the tuning of γ which is determined by the distribution of $s_{u,obs}$ for the region of interest. The exact method of tuning γ and formulating Eq. (2.7) for TE is explained below.

$\overline{k}$ in Eq. (2.7) is determined by the slope of the bin averaged line. $\overline{s_u}$ is set to the mean shear strength of the region. Under average conditions (i.e. $S_{xx} = \overline{S_{xx}}$ and $s_u = \overline{s_u}$), the exponential factor goes to one and V is related to P by the slope of the bin averaged line. Depending on the ratio of shear strength to radiation stress, the wave power is scaled either higher or lower depending on the average conditions in the field (expressed by β). This intuitively seems correct. The gradient of radiation stress constitutes a force and this force is resisted by the soil of the marsh edge. Depending on how the marsh edge behaves on average over the region, the site specific ratio of these two quantities will influence how the marsh responds locally.

Eq.(3.2) is proposed as the model to relate wave power to erosion rate in Terrebonne Bay. This is formally the same equation as Eq. (2.7) but includes the specific values of $\overline{k}$, $\overline{s_u}$, S_{xx} and γ determined by the data collected in this study. γ was determined by minimizing the error between the minimum $s_{u,obs}$ from the geotechnical data set described in Section 3.1.2 and the minimum $s_{u,est}$. $s_{u,est}$ was calculated with the method discussed in Section 2.2.3.

$$V = 0.0516P \exp\left[-1.95\left(\frac{s_u^*}{S_{xx}^*} - 1\right)\right] \tag{3.2}$$

The best fit PDF of $s_{u,est}$ is shown in Figure 3.26 and along with the best fit PDF of $s_{u,obs}$. The mean of the resulting $s_{u,est}$ distribution is 7.53 kPa compared to the mean $s_{u,obs}$ of 7.03 kPa. A 1-way ANOVA was run against the two distributions and found that the two samples were not significantly different ($p = 0.273$). This is strong evidence that the variability in shear strength is the cause of the variability in the observed erosion rate.

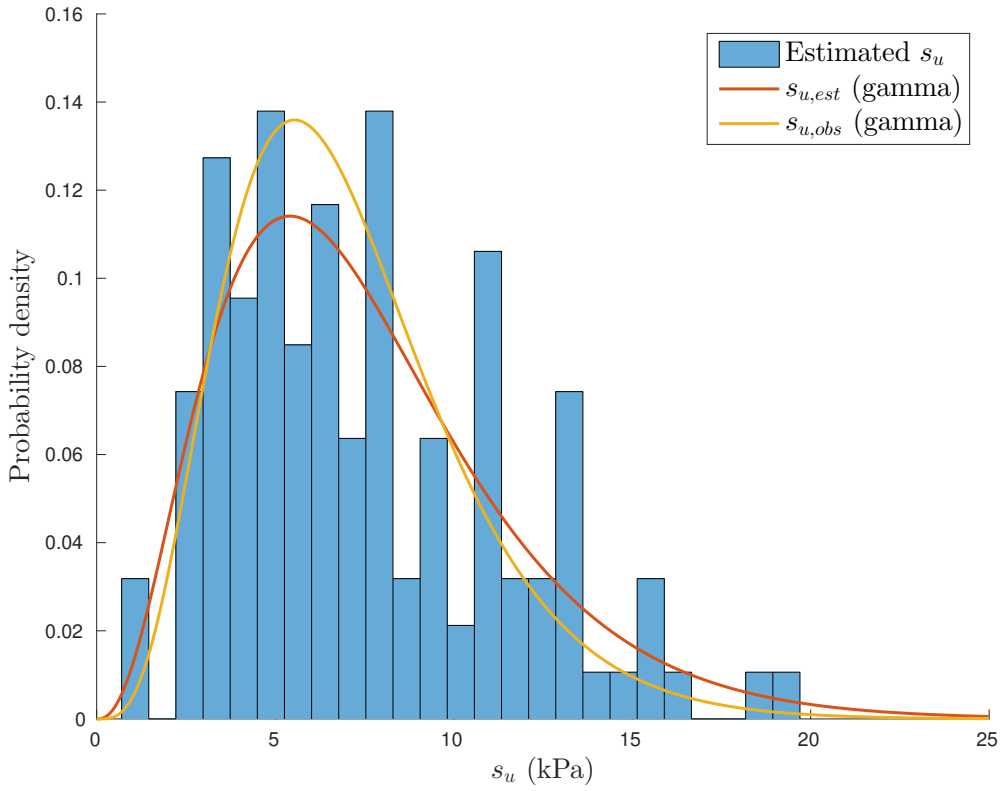

Figure 3.26: The PDF of s_u estimated from Eq. (2.7) is shown as the orange line. The PDF of the observed s_u is shown as the yellow line.

The spatial distribution of $s_{u,est}$, V, and P within TE is mapped in Figure 3.27. The value at each location has been averaged over 2004 to 2012 and then normalized by the mean of that property's data set. This was done in order to allow for a quantitative comparison between the different physical properties. In general, the distribution of the values confirms the performance of the model. In locations where their is high erosion,

relative to the mean, then the strength of the wave power will predict an estimated $s_{u,est}$ accordingly. For instance, on the eastern coast of TE, the erosion rates are slightly lower than the mean, but the mean wave power in this region is also relatively less energetic than the mean, so the model estimates a small shear strength. As opposed to this, the west coast of TE has low erosion rates but significantly larger mean wave power, and therefore a larger shear strength is estimated. Model verification would require that s_u be measured in these two contrasting regions and compared. This situation in the NW corner of TE is somewhat more complicated as within a small area there is observed a large variation in marsh edge response for a relatively constant wave forcing.

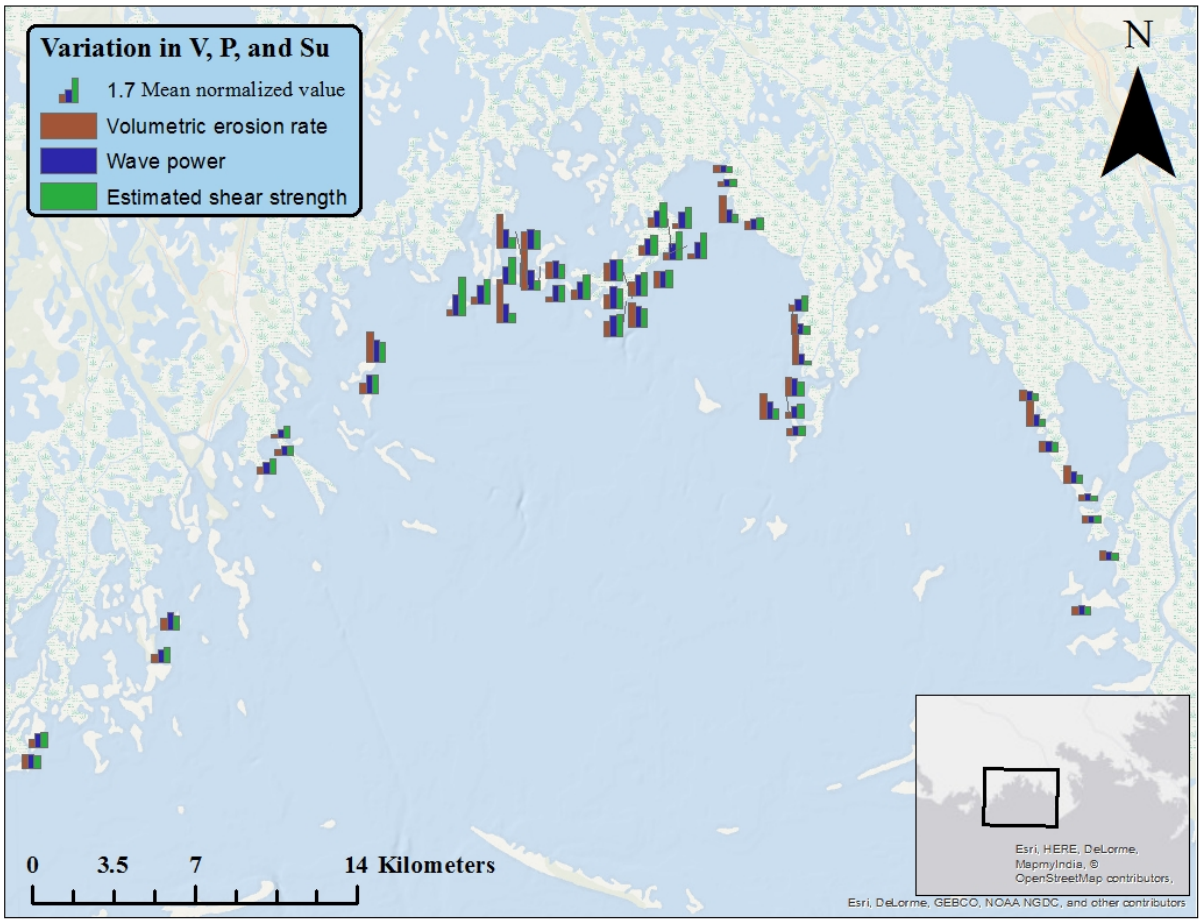

Figure 3.27: Spatial distribution of estimated shear strength, volumetric erosion rate, and average wave power within Terrebonne Bay. The values have been normalized by the mean of their respective data sets.

3.3.2 Implications

Considering the variability in natural marsh systems it may be appropriate to model the additional exponential factor probabilistically. If s_u in Eq. (3.2) is replaced by an inverse cumulative distribution function, then the maximum amount of erosion to expect or less under a given wave forcing (i.e. P and S_{xx}) can be estimated based on the probability that s_u for the region is less than or equal to a certain value.

The PDF of observed s_u was modeled with a gamma distribution as discussed in Section 3.1.3. The inverse cumulative distribution function of the gamma distribution is not given in an easy-to-write closed form. It is more felicitous gained through its computation with the parameters of the gamma PDF. The best fit gamma distribution to the shear strength data set constituting the organic-rich mud and peat layer is given as Eq. (3.3).

$$p(s_u) = \frac{s_u^{3.73}}{1.49^{4.73} \cdot \Gamma(4.73)} \exp(\frac{-s_u}{1.49}) \tag{3.3}$$

The inverse cumulative distribution function of (3.3) is computed for probabilities in the range $p = [0, 1]$ and inserted into Eq. (3.2) with mean forcings for the modeled wave power data set (P =39.9 W m^{-1} and S_{xx} =18.03 N m^{-2}). The results are plotted in Figure 3.28.

The volumetric erosion rates have been divided by $h = 0.5$ m in order to express the results in terms of a retreat rate. The figure shows probability on the x-axis and the erosion rate at which the observed erosion rate will be equal to or less than for the given probability on the y-axis. For example, the figure shows that under average forcing their is an 80% probability that the retreat rate will be roughly 2.1 m yr^{-1} or less. The mean retreat rate for the TE data set considered is $\overline{R}$ =4.37 m yr^{-1}. This agrees well with the erosion rate which the model predicts to occur half of the time or more under average wave forcing.

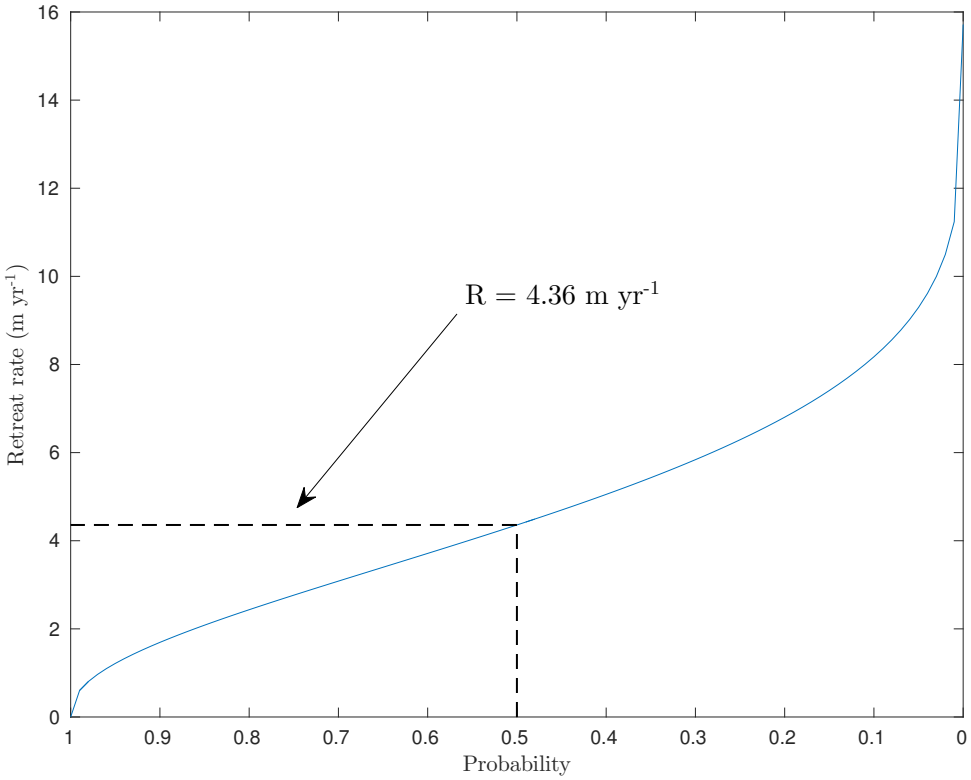

Figure 3.28: Inverse CDF for marsh edge retreat rate in Terrebonne Bay under average forcing.

Chapter 4
Conclusions

4.1 Summary

In summary, first, the possibility of modeling wave power with parametric methods on the scale of Terrebonne Bay was thoroughly investigated and answered satisfactorily. Secondly, a model which incorporates soil properties into the relationship between marsh edge erosion and wave power has been proposed. The conclusions and recommendations related to these two objectives will be discussed below.

The wave power calculation methodology proposed here was compared with an observational wave record and a state-of-the-art numerical model. The comparison showed that waves can be adequately estimated over large domains when restricted to certain logical conditions. It was found that by using parametric wave generation methods, daily wave power estimations could match observations on a point by point time series basis. After estimating wave forcing at 124 sites throughout TE over the course of 9 years, it was found that this forcing could explain the observed erosion rates. The mean wave powers ranged over 15 to 65 $\mathrm{W\,m^{-1}}$ and the erosion rates varied between 0 and 45 $\mathrm{m\,yr^{-1}}$. When wave power and erosion rate were averaged over regular wave power bins significant correlation was observed ($r^2 = 0.51$) and were related by $V_{bin} = 0.0516 P_{bin}$.

The influence of soil properties was investigated in order to further explain the variability in the relationship between erosion rate and wave power. The validation of the wave power estimations suggested that this variability is likely due to physical factors such as the strength of the marsh edge soils. The first stage of this investigation consisted of extensive field work in the lower MRD region. Undrained shear strength was measured in four distinct basins. Based on variations in organic content and bulk density with depth, an interval corresponding to the soil unit at play in wave erosion was established. This interval was 0.5 m to 1.5 m in depth.

The shear strength measurements made within this interval were partitioned into receiving basin, i.e. lower and upper Breton Sound and lower and upper Barataria Bay. A 1-way ANOVA revealed that the shear strength distribution of upper Breton Sound was significantly different than the other three basins and belonged to different sample populations. Based on regional characteristics, vegetation types, and site observations, it was proposed that shear strength measurements in upper and lower Barataria Bay and lower Breton Sound corresponded to coastal marsh environments and upper Breton Sound represented a landscape less influenced by coastal processes. The shear strengths within the depth interval mentioned above for these basins was assumed to represent marsh edge soils in general for the Louisiana coast. The mean shear strength for the marsh edge soil unit was found to be 7.03 kPa and the mean of upper Breton Sound was 13.8 kPa.

A new model was proposed relating erosion rates to mean wave power which included the influence of soil properties. The proposed model scales the effects of incident wave power by considering the wave radiation stress relative to the shear strength of the marsh. This model was used to estimate the distribution of shear strength which would be responsible for the scatter in the observed erosion rates given the modeled wave forcing at these marsh edge sites. The agreement between the estimated observed shear strength distribution was surprisingly good. The mean of the estimated shear strength distribution was 7.53 kPa and the mean of the observations was 7.03 kPa. A 1-way ANOVA was performed between the two distributions and it was found that they were not significantly different ($p = 0.273$).

4.2 Recommendations

4.2.1 The large Scale Applicability of the Wave Power Routine

The estimation of wave power over large scale domains relies on setting logical and obvious conditions on the application the Young and Verhagen (1996) equations. These restrictions are fundamental to the theory underlying the Young and Verhagen (1996) wave generation model.

These conditions are as follows:

1. Wave hindcasting with Young and Verhagen (1996) equations is sensitive to the unsteadyness of the wind field.
2. Within coastal embayments only sea wave generation may be modeled.
3. Sinuous shoreline geometry limits the placement of the study sites.

It was clearly demonstrated that when the wind forcing approaches steady-state conditions the wave power calculation routine can estimate waves satisfactorily. The rate at which the wind field shifts has a direct effect on model performance. This was due to the nature of the fundamental empirical relationships which the routine used to estimate the generation of waves.

The Young and Verhagen (1996) equations were developed from steady-state conditions. Their application to dynamic, unsteady meteorological systems stretches their viability to the breaking point in some situations. For example, the rapid reversal of wind fields associated with the passage of cold front in coastal Louisiana renders untenable results. However, for estimating wave power under the forcing of less variable wind fields the application of the Young and Verhagen (1996) equations provides acceptable results.

Conditions (2) and (3) both stem from the wave power calculation routine's inability to consider the propagation of wave energy. This may be a severe limitation where the propagation of far-field wave energy is important. Also, it may limit the ability to assess the amount of wave energy inside semi-enclosed portions.

Shallow, protected coastal embayments, such as Terrebonne Bay, are not known for exhibiting a large swell energy signature. It is typical to assume that most waves are locally generated sea and this seems to be a fair assessment. However, it is necessary to consider whether swell energy may be playing a role when performing any wave modeling. Failure to do so may result in the underestimation of wave energy. Experience alone may not be enough to provide judgement on the level of energy generated from far-field propagating into the study area.

The transformation and propagation of locally generated sea energy also needs to be

considered. It was found that within small semi-enclosed portions of the coast only estimating the wave energy based on local generation may significant underestimate the wave energy which reaches the shoreline. On the other hand, on stretches of open coast the Young and Verhagen (1996) equations perform satisfactorily. It is likely that experience and individual judgement is necessary to discern exactly where the shoreline geometry will invalidate this method of calculating incident wave power.

In summary, large scale wave power modeling is possible with the methodology of the wave power routine. Manual attention to detail is still necessary. The coastline geometry of Louisiana is too variable to expect that this methodology, when employed at the regional scale, will produce reliable results unless care is taken to select sites adjacent relative to open water. It is recommended that the domain be separated into sub-domains which allows for validation and inspection at the required scale. The following list enumerates recommendations for producing reliable wave power estimations with parametric wave generation models.

1. Compute mean wave power as a time series with hourly output.
2. Quantify the relative influence of rapidly changing wind fields and parametertize their input to mean wave power.
3. Place wave power calculation sites at least 150 m off shore in order to avoid errors in fetch distance calculation due to errors in digitizing the coastline or due to its natural sinuousity.
4. Determine the influence of swell energy at wave power calculation sites. Exclude these points based on experienced judgment or quantify and include the swell energy as well.
5. Avoid placing sites within semi-enclosed portions of the coastline.

4.2.2 The Influence of Soil Properties

As was discussed in Section 1.2 the characteristics of coastal marsh soils are complex and highly variable. Much scientific work is still required to understand their behavior.

As an engineering problem, their behavior may best be approached through a high-level conceptualization (bulk properties, empirical correlations, etc.) and probabilistic modeling. The model proposed here may serve as a guide forward in this regard.

Improving the incorporation of soil properties into erosion rate models requires additional high-level thinking. This high-level thinking should focus on the design of experiments which will eliminate uncertainties as to which physical variables are at play for a given erosion rate observation. For instance, considering the schematization of Marani et al. (2011) (see Figure 1.7), it is important to know the shoreline orientation in relationship to the wave direction and also the scarp height, as these factors scale the wave power and erosion rate, respectively. In order to confidently assess the influence of soil properties, all of these variables should be known.

Detailed, exhaustive, and more extensive field experimentation is recommended as the optimum way forward. It is likely that with a more refined and larger data set, the parameters of Eq.(3.2) would be modified significantly and the confidence intervals would be improved. A large and more well constrained data set would also allow for better validity testing of any model which proposes to incorporate soil properties into the relationship between marsh edge erosion and incident wave power. Constraining the variability in the shear strength distributions in areas which exhibit different mean erosion rates through field work would allow for a rigorous validation of Eq. (3.2).

For instance, relatively higher and lower than average erosion rates are localized in the northwest and southeast of TE, respectively (see Figure 2.6). A field campaign to develop a good s_u sample for these localities would allow for an assessment of Eq. (3.2) predictive capability. It would also allow for a modification of γ in order to reflect the soil shear strength which better characterized the marsh edge in Terrebonne Bay. If successful, γ could be optimized for several shallow coastal environments of interest. This would allow for estimations of erosion rate through out coastal Louisiana with a high degree of confidence.

References

Alexander, J. S., R. C. Wilson, and W. R. Green (2012). A Brief History and Summary of the Effects of River Engineering and Dams on the Mississippi River System and Delta. Technical report.

Allison, M., Q. J. Chen, B. Couvillion, A. Freeman, M. Leadon, A. McCorquidale, E. Meselhe, C. Ramatchandirane, D. Reed, and E. White (2015). 2017 Coastal Master Plan: Model Improvement Plan, Attachment C3-2 - Marsh Edge Erosion. Technical report, Coastal Protection and Restoration Authority, Baton Rouge, Louisiana.

Barbier, E. B., S. D. Hacker, C. Kennedy, E. W. Koch, A. C. Stier, and B. R. Silliman (2011). The value of estuarine and coastal ecosystem services. *Ecological Monographs 81*(2), 169–193.

Barras, J. A. (2007). Satellite images and aerial photographs of the effects of hurricanes Katrina and Rita on coastal Louisiana.

Bendoni, M., S. Francalanci, L. Cappietti, and L. Solari (2014). On salt marshes retreat: Experiments and modeling toppling failures induced by wind waves. *Journal of Geophysical Research: Earth Surface 119*(3), 603–620.

Bendoni, M., R. Mel, L. Solari, S. Lanzoni, S. Francalanci, and H. Oumeraci (2016). Insights into lateral marsh retreat mechanism through localized field measurements. *Water Resources Research 52*(2), 1146 – 1464.

Blum, M. D. and H. H. Roberts (2009). Drowning of the Mississippi Delta due to insufficient sediment supply and global sea-level rise. *Nature Geoscience2 2*(7), 488–491.

Bomer, E. J., J. E. T. Hughes, A. A. Heath, S. J. Bentley, and K. Xu (2016). SEDIMENTATION DYNAMICS AND STRATIGRAPHY OF BRETON SOUND ESTUARY: IMPLICATIONS FOR THE IMPLEMENTATION OF SEDIMENT DIVERSION STRUCTURES ALONG THE MISSISSIPPI RIVER. *Geological Society of America Abstracts with Programs. 48*(1).

Booij, N., R. C. Ris, and L. H. Holthuijsen (1999). A third-generation wave model for coastal regions: 1. Model description and validation. *Journal of Geophysical Research 104*(C4), 7649–7666.

Breugem, W. A. and L. H. Holthuijsen (2007). Generalized Shallow Water Wave Growth from Lake George. *Journal of Waterway, Port, Coastal, and Ocean Engineering 133*(June), 173–182.

Cahoon, D. R. (1994). Recent Accretion in Two Managed Marsh Impoundments in Coastal Louisiana. *Ecological Applications 4*(1), 166–176.

Chen, Q. and H. Zhao (2012). Theoretical Models for Wave Energy Dissipation Caused by Vegetation. *Journal of Engineering Mechanics 138*(2), 221–229.

Coleman, J. M., H. H. Roberts, and G. W. Stone (1998). Mississippi River Delta : An Overview. *Journal of Coastal Research 14*(3), 698–716.

Couvillion, B. R., J. A. Barras, G. D. Steyer, W. Sleavin, M. Fischer, H. Beck, N. Trahan, B. Griffin, and D. Heckman (2011). Land area change in coastal Louisiana 1932 to 2010.

CPRA (2012). Coastal Master Plan 2012. Technical report.

Day, J. W., L. D. Britsch, S. R. Hawes, G. P. Shaffer, D. J. Reed, and D. Cahoon (2000). Pattern and process of land loss in the Mississippi Delta: A spatial and temporal analysis of wetland habitat change. *Estuaries 23*(4), 425–438.

Day, J. W., G. P. Kemp, D. J. Reed, D. R. Cahoon, R. M. Boumans, J. M. Suhayda, and R. Gambrell (2011). Vegetation death and rapid loss of surface elevation in two contrasting Mississippi delta salt marshes: The role of sedimentation, autocompaction and sea-level rise. *Ecological Engineering 37*(2), 229–240.

Dean, R. G. and R. A. Dalrymple (1991). *Water Wave Mechanics for Engineers and Scientists*. Hackensack, NJ: World Scientific Publishing Co. Pte. Ltd.

Fagherazzi, S. (2014). Coastal processes: Storm-proofing with marshes. *Nature Geoscience 7*(10), 701–702.

Fagherazzi, S., G. Mariotti, P. Wiberg, and K. J. McGlathery (2013). Marsh collapse does not require sea level rise. *Oceanography 26*(3), 70–77.

Feagin, R. A., S. M. Lozada-Bernard, T. M. Ravens, I. Möller, K. M. Yeager, and A. H. Baird (2009). Does vegetation prevent wave erosion of salt marsh edges? *Proceedings of the National Academy of Sciences of the United States of America 106*(25), 10109–10113.

Francalanci, S., M. Bendoni, M. Rinaldi, and L. Solari (2013). Ecomorphodynamic evolution of salt marshes: Experimental observations of bank retreat processes. *Geomorphology 195*, 53–65.

Grabowski, R. C. (2014). Measuring the shear strength of cohesive sediment in the field. *Geomorphological Techniques 1*, 1–7.

Howes, N. C., D. M. FitzGerald, Z. J. Hughes, I. Y. Georgiou, M. a. Kulp, M. D. Miner, J. M. Smith, and J. a. Barras (2010). Hurricane-induced failure of low salinity wetlands. *Proceedings of the National Academy of Sciences of the United States of America 107*(32), 14014–14019.

Hughes, J. E. T., F. R. Crawford, E. J. Bomer, S. J. Bentley, and K. Xu (2016). GEOLOGIC CHARACTERIZATION OF THE MIDDLE BARATARIA BAY RECEIVING BASIN: THE INFLUENCE OF STRATIGRAPHY ON SEDIMENT DIVERSION PROJECTS. *Geological Society of America. Abstracts with Programs 48*(1).

Kirwan, M. L. and J. P. Megonigal (2013). Tidal wetland stability in the face of human impacts and sea-level rise. *Nature 504*(7478), 53–60.

Leonardi, N. and S. Fagherazzi (2015). Effect of local variability in erosional resistance on large-scale morphodynamic response of salt marshes to wind waves and extreme events. *Geophysical Research Letters 42*(14), 5872–5879.

Leonardi, N., N. K. Ganju, and S. Fagherazzi (2015). A linear relationship between wave power and erosion determines salt-marsh resilience to violent storms and hurricanes. *Proceedings of the National Academy of Sciences 113*(1), 64–68.

Marani, M., A. D'Alpaos, S. Lanzoni, and M. Santalucia (2011). Understanding and predicting wave erosion of marsh edges. *Geophysical Research Letters 38*(21).

Mariotti, G. and S. Fagherazzi (2010). A numerical model for the coupled long-term evolution of salt marshes and tidal flats. *Journal of Geophysical Research: Earth Surface 115*(1), 1–15.

Mariotti, G. and S. Fagherazzi (2013). Wind waves on a mudflat: The influence of fetch and depth on bed shear stresses. *Continental Shelf Research 60*, S99–S110.

McLoughlin, S. M., P. L. Wiberg, I. Safak, and K. J. McGlathery (2014). Rates and Forcing of Marsh Edge Erosion in a Shallow Coastal Bay. *Estuaries and Coasts 38*, 620–638.

Morton, R. A., G. Tiling, and N. F. Ferina (2003). Causes of hot-spot wetland loss in the Mississippi delta plain. *Environmental Geosciences 10*(2), 71–80.

Parker, K. R. (2014). *FIELD AND NUMERICAL INVESTIGATION OF WAVE POWER AND SHORELINE RETREAT IN TERREBONNE BAY , SOUTHERN LOUISIANA*. Masters of science (m.s.), Louisiana State University.

Penland, S., L. Wayne, L. D. Britsch, S. J. Williams, A. D. Beall, and V. C. Butterworth (2000). Proccess classification of coastal land loss between 1932 and 1990 in the Mississippi river delta plain , southeaster Louisiana. Technical report, Woods Hole, MA.

Reed, D. J. (1995). The Response of Coastal Marshes To Sea-Level Rise: Survival or Submergence? *Earth Surface Processes and Landforms 20*(1), 39–48.

Roberts, H. H. (1997). Dynamic Changes of the Holocene Mississippi River Delta Plain: The Delta Cycle. *Journal of Coastal Research 13*(3), 605–627.

Roberts, H. H. (1998). Delta Switching : Early Responses to the Atchafalaya River Diversion. *Journal of Coastal Research 14*(3), 882–899.

Rodriguez, A. (2013). Measuring Marsh Accretion using Pb-210.

Sasser, C. E., J. M. Visser, E. Mouton, J. Linscombe, and S. B. Hartley (2014). Vegetation types in coastal Louisiana in 2013. Technical report.

Schwimmer, R. A. (2001). Rates and Processes of Marsh Shoreline Erosion in Rehoboth Bay, Delaware, U.S.A. *Journal of Coastal Research 17*(3), 672–683.

Temmerman, S., P. Meire, T. J. Bouma, P. M. J. Herman, T. Ysebaert, and H. J. D. Vriend (2013). Ecosystem-based coastal defence in the face of global change. *Nature 504*, 79–83.

Tonelli, M., S. Fagherazzi, and M. Petti (2010). Modeling wave impact on salt marsh boundaries. *Journal of Geophysical Research: Oceans 115*.

Twilley, R. R., S. J. Bentley, Q. Chen, D. A. Edmonds, S. C. Hagen, N. S. N. Lam, C. S. Willson, K. Xu, D. W. Braud, R. Hampton Peele, and A. McCall (2016). Co-evolution of wetland landscapes, flooding, and human settlement in the Mississippi River Delta Plain. *Sustainability Science 11*(4), 711–731.

USACE (2015). *Coastal Engineering Manual*. Washington, D.C.: U.S. Army Corps of Engineers.

USGS (2015). CoNED TOPOBATHY Data for Entity ID: TBDEMNGOM00034. Technical report, U.S. Geological Survey (USGS), Earth Resources Observation System (EROS), Sioux Falls, SD USA.

Watzke, D. A. (2004). *Short-Term Evolution of a Marsh Island System and the Importance of Cold Front Forcing, Terrebonne Bay, Louisiana*. Master of science (m.s.), Louisiana State University.

White, C. (2016). INFLUENCES OF HURRICANES, FLOODS, AND ORGANIC PRODUCTION ON RIVER DELTA EVOLUTION. *Geological Society of America Abstracts with Programs. 48*(1).

Wilson, C. A. and M. A. Allison (2008). An equilibrium profile model for retreating marsh shorelines in southeast Louisiana. *Estuarine, Coastal and Shelf Science 80*(4), 483–494.

Young, I. and L. Verhagen (1996). The growth of fetch limited waves in water of finite depth. Part 1. Total energy and peak frequency. *Coastal Engineering 29*(1-2), 47–78.

Appendix A
Marsh Edge Soil Column Figures

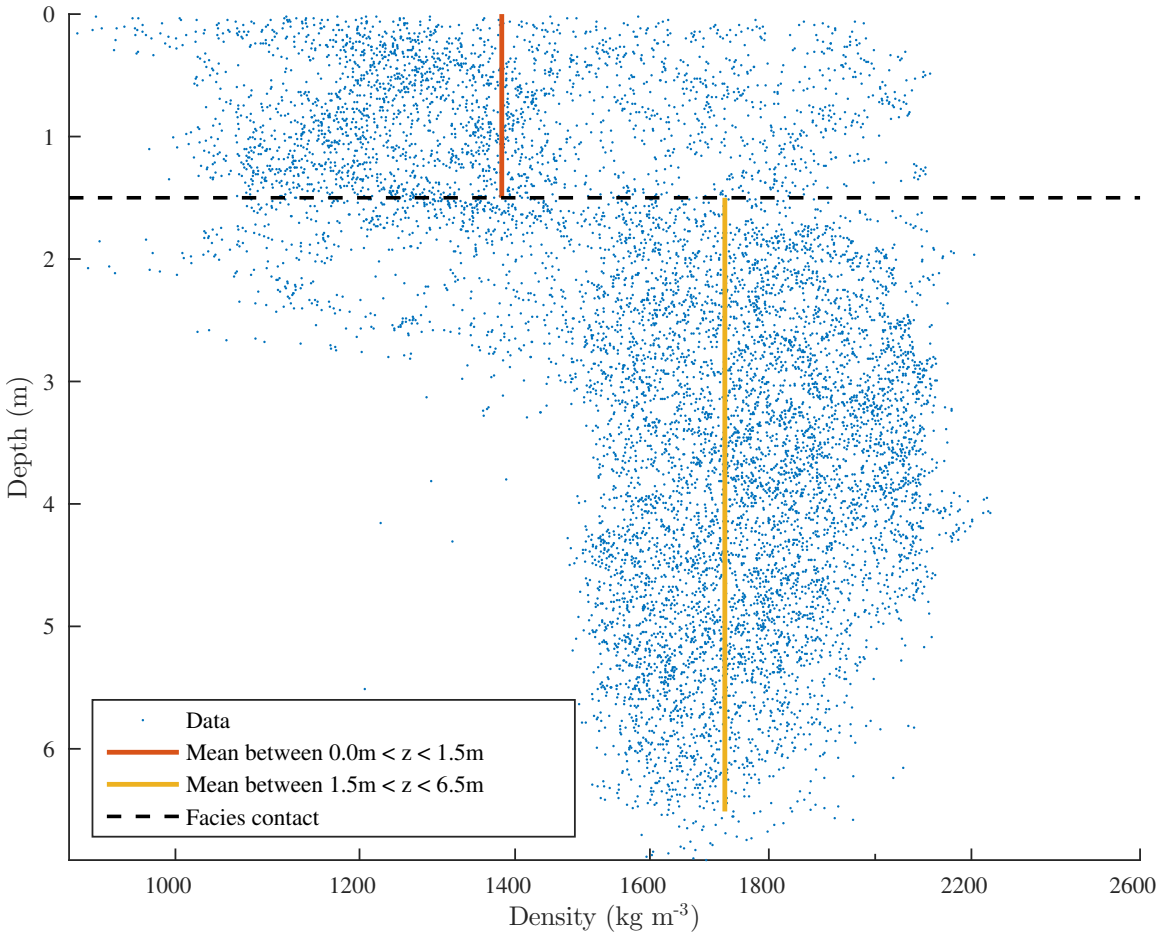

Figure A.1: Aggregate plot of density measurements from cores samples in LBR.

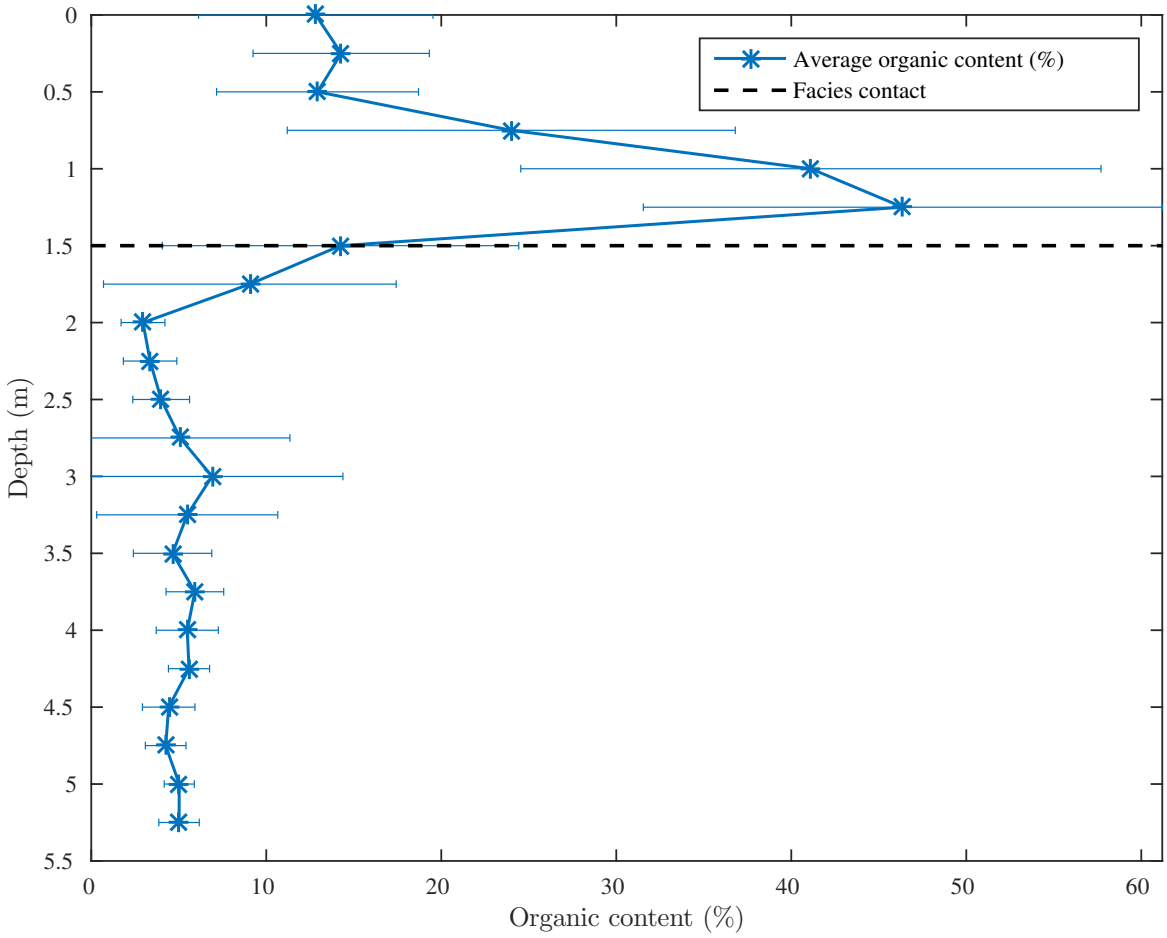

Figure A.2: Down-core mean organic content for LBR.

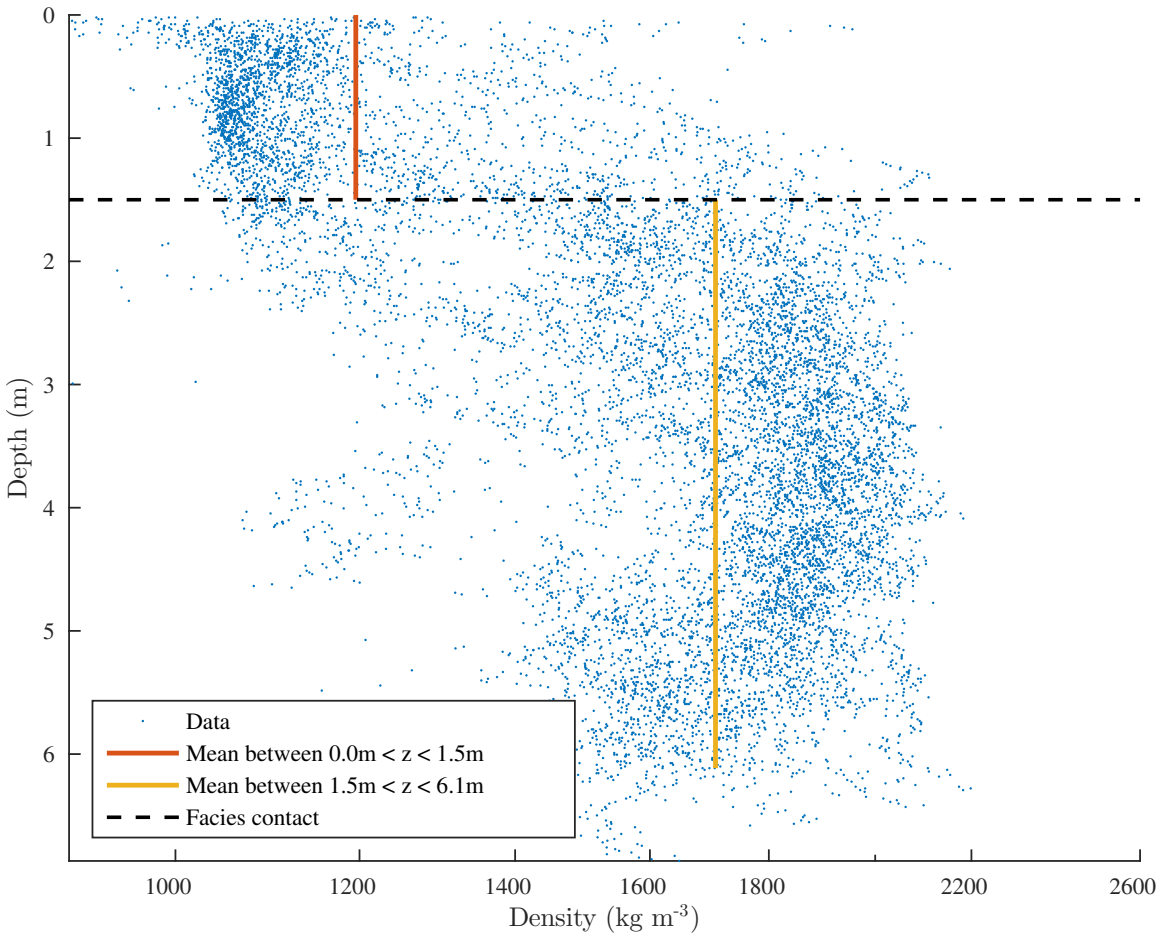

Figure A.3: Aggregate plot of density measurements from cores samples in LBA.

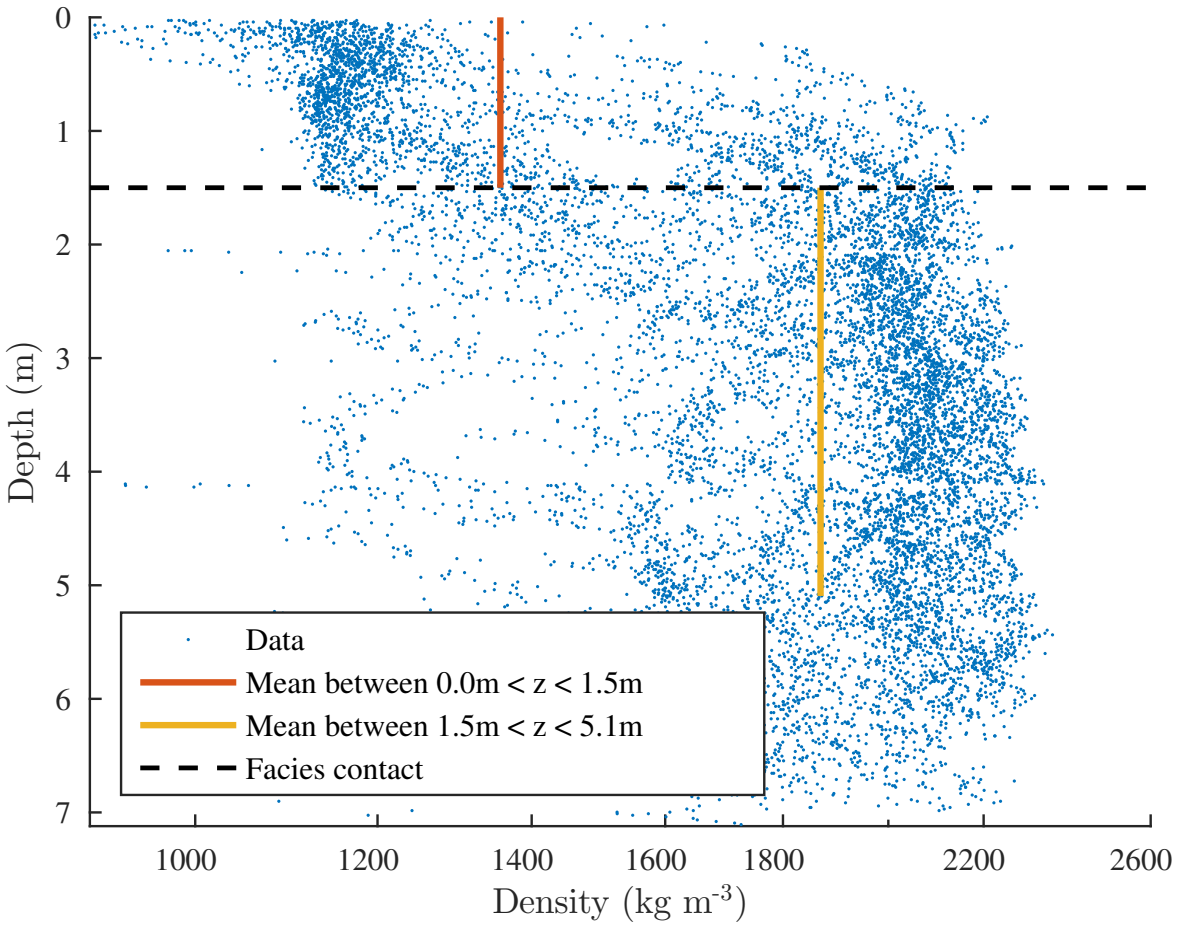

Figure A.4: Aggregate plot of density measurements from cores samples in MBR.

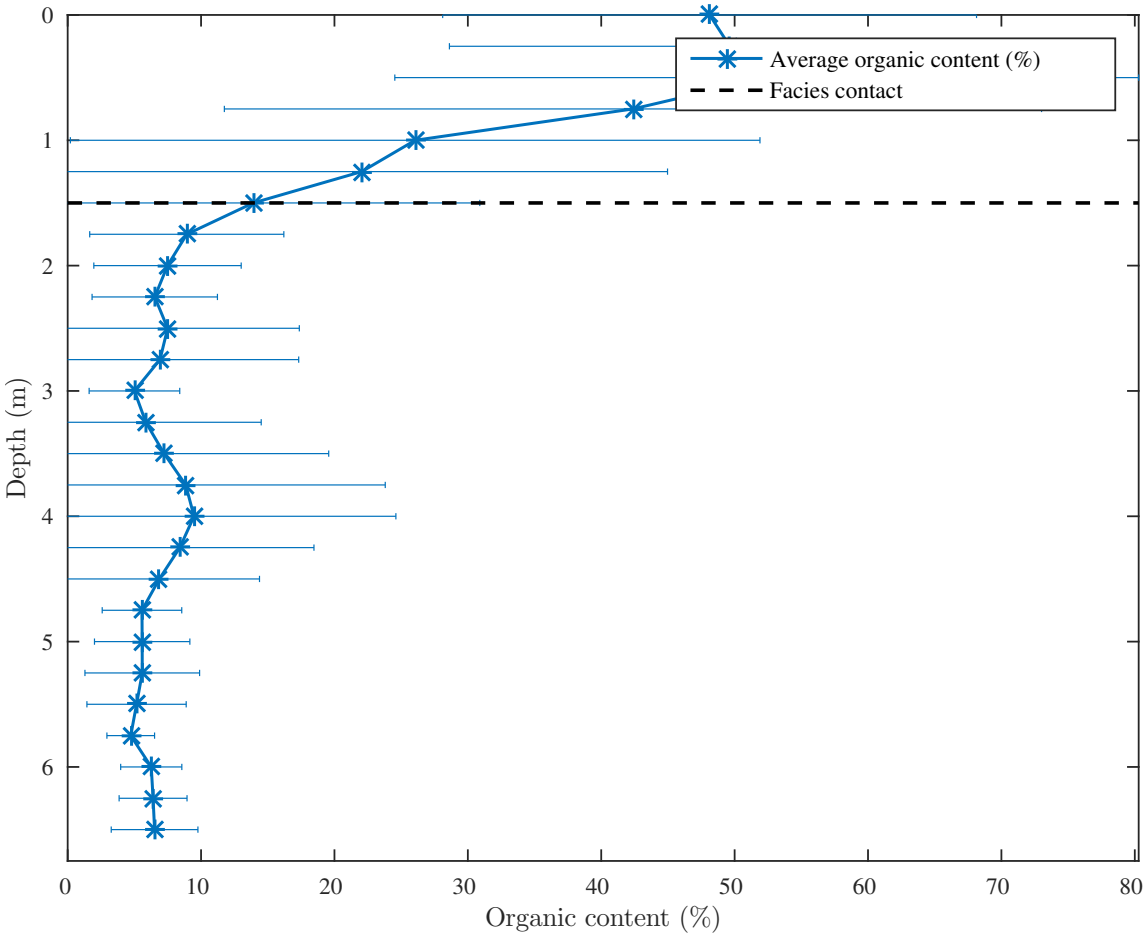

Figure A.5: Down-core mean organic content for MBR.

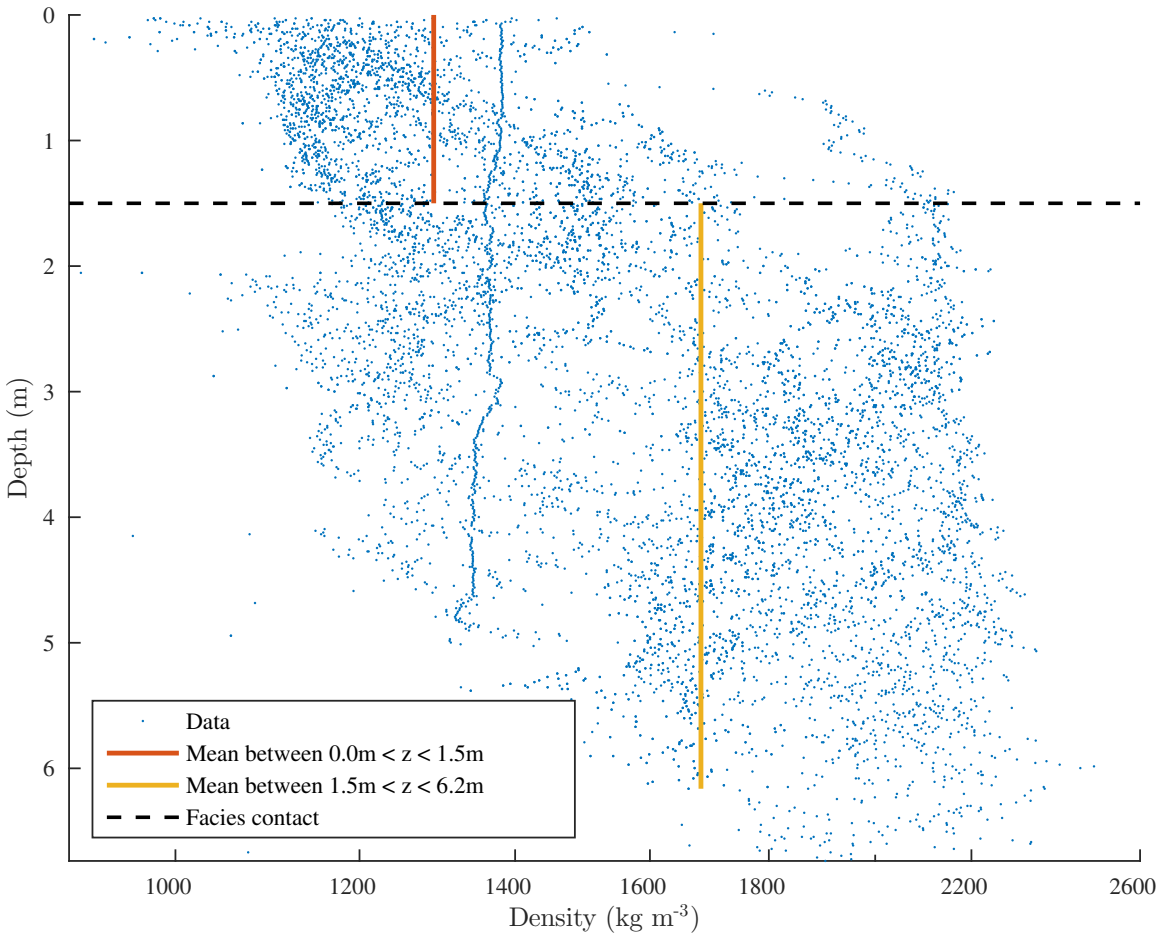

Figure A.6: Aggregate plot of density measurements from cores samples in MBA.

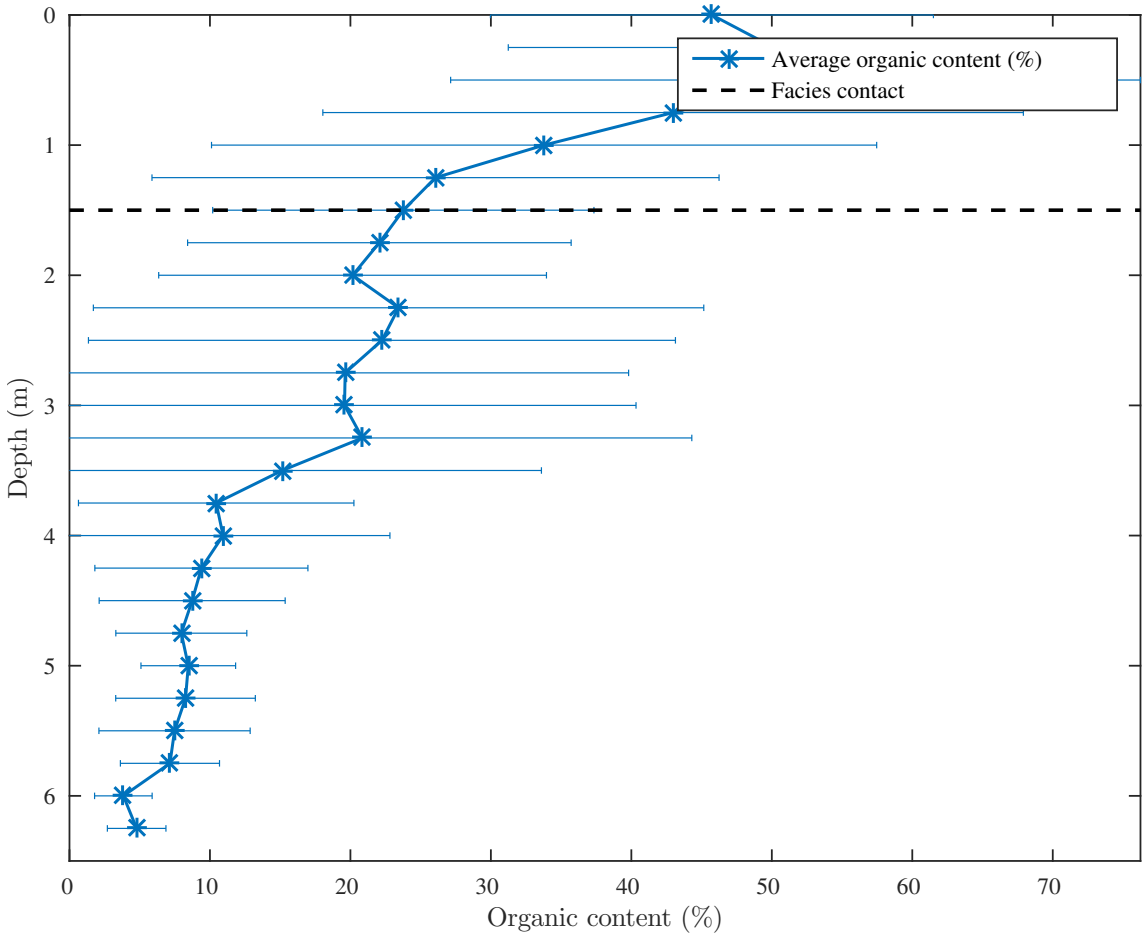

Figure A.7: Down-core mean organic content for MBA.

Appendix B
Retreat Rates and Wave Forcing
B.1 1/19/2004 to 10/27/2005

Site ID	Easting (m)	Northing (m)	Retreat rate (m yr^{-1})	Wave power (W m^{-1})	Radiation stress (N m^{-2})
1412	719600	3223235	4	37.3	17.1
1411	719900	3224135	0.2	35.8	16
1389	725200	3227810	3.6	33.8	17.2
1394	725600	3229210	3.7	44.3	15.1
1005	729750	3235935	2.6	31.5	16.5
1013	730375	3236885	0.7	23.6	10.7
1014	730525	3236710	0.2	23.4	10.6
1015	734175	3239810	0.8	53.4	19.3
1018	734575	3240435	45.9	62.1	31.6
1019	734475	3240710	4.9	62.5	33.2
1024	738125	3242735	30.5	57	28.9
955	738975	3243210	1.2	49.8	22.3
952	740500	3244110	0.4	44.4	19.1
947	740675	3243985	2.4	49.6	19.9
948	741050	3243960	8.7	45.2	17.4
949	741175	3243935	18.9	50.1	19
950	741500	3243835	11.3	51.9	22.8
951	741875	3244210	1.2	42.6	13.3
956	742330	3244326	2.7	44.2	15
957	743275	3243410	0.4	45.5	21.7
1025	745075	3243035	5.6	56.9	20
1026	745250	3243310	7.3	55.4	24.7
1027	745375	3243385	9.6	54.7	24.8
1028	745475	3243485	5.3	53.9	25.1
958	745775	3243560	0.2	54.5	25.8
959	746725	3245085	9.2	43.6	22.4
960	746925	3245360	0.4	42.4	20.7
961	747125	3245485	3.4	42.3	20
962	747225	3245710	3.3	42.7	24.7
963	747250	3245760	1.3	42.3	24.8
964	747650	3246485	1.6	43.6	17.3
1372	749425	3248660	0.4	18.8	8.2
1374	749600	3248285	1.4	18	7.3
979	750225	3246735	3.2	30.7	14.9
980	750750	3246435	1.5	26.1	13
1375	752675	3242185	1.4	26.5	13.2

Site ID	Easting (m)	Northing (m)	Retreat rate (m yr^{-1})	Wave power (W m^{-1})	Radiation stress (N m^{-2})
1376	752750	3241910	11.6	24	12
1377	752800	3240610	6.7	26.4	11.7
1379	752275	3238485	2.7	44	16.4
1380	752350	3238285	9.5	42.7	16.7
1381	752500	3237935	0.3	27.6	11.7
1382	752550	3237560	1.8	23	11.1
981	762625	3238835	4.4	23.3	10.5
982	762925	3237660	5.7	31.7	15.6
983	763450	3236860	4.9	25.2	11.6
985	764525	3235235	0.4	26.4	11.5
986	765150	3234735	0	16.7	5.9
988	765300	3233785	0.5	18	8.6
989	766050	3232210	0.2	20.7	8.9
1000	764875	3229860	1.8	22.1	9.7

B.2 10/28/2005 to 10/29/2008

Site ID	Easting (m)	Northing (m)	Retreat rate (m yr^{-1})	Wave power (W m^{-1})	Radiation stress (N m^{-2})
1412	719600	3223235	4.8	38.6	18.2
1411	719900	3224135	2.6	36.5	16.8
1389	725200	3227810	1.2	31.4	16.7
1394	725600	3229210	2.9	45.9	15.9
1005	729750	3235935	2.2	31.9	17.3
1013	730375	3236885	1.2	23.9	11.2
1014	730525	3236710	1.9	23.4	11
1015	734175	3239810	3.2	51	18.9
1018	734575	3240435	28.4	59	31.3
1019	734475	3240710	13.0	58.9	32.7
1024	738125	3242735	1.9	57.5	30.2
955	738975	3243210	0.4	51.9	23.8
952	740500	3244110	1.4	46.6	20.6
947	740675	3243985	2.4	52.8	21.6
948	741050	3243960	5.1	48.5	19
949	741175	3243935	6.3	53.4	20.6
950	741500	3243835	21.6	54.9	24.7
951	741875	3244210	2.0	44.9	14.1
956	742330	3244326	1.3	47.5	16.3
957	743275	3243410	1.2	48.7	23.8
1025	745075	3243035	3.7	60.6	21.6
1026	745250	3243310	3.6	58.8	26.8
1027	745375	3243385	3.9	58.1	27
1028	745475	3243485	7.0	57.1	27.3
958	745775	3243560	5.4	56.7	27.7
959	746725	3245085	3.5	44.7	23.7
960	746925	3245360	1.7	43.5	21.9
961	747125	3245485	3.5	43.4	21.2
962	747225	3245710	3.8	43.2	26.1
963	747250	3245760	3.0	42.8	26.2
964	747650	3246485	1.4	44.6	18
1372	749425	3248660	2.4	20.8	9.1
1374	749600	3248285	2.1	20	8.1
979	750225	3246735	4.2	33.7	16.7
980	750750	3246435	3.8	29.3	14.8
1375	752675	3242185	1.2	28.4	14.3
1376	752750	3241910	3.6	25.3	12.8
1377	752800	3240610	5.8	28.1	12.6
1379	752275	3238485	2.0	43.9	16.6
1380	752350	3238285	4.9	43	17

Site ID	Easting (m)	Northing (m)	Retreat rate (m yr^{-1})	Wave power (W m^{-1})	Radiation stress (N m^{-2})
1381	752500	3237935	2.0	29.1	12.5
1382	752550	3237560	1.0	23.1	11.4
981	762625	3238835	3.3	24.8	11.4
982	762925	3237660	5.8	32.5	16.3
983	763450	3236860	2.4	25.8	12
985	764525	3235235	4.9	28	12.3
986	765150	3234735	2.0	17.6	6.2
988	765300	3233785	2.0	18.9	9.1
989	766050	3232210	2.6	20.3	8.9
1000	764875	3229860	3.0	23	10.3

B.3 10/30/2008 to 11/14/2012

Site ID	Easting (m)	Northing (m)	Retreat rate (m yr^{-1})	Wave power (W m^{-1})	Radiation stress (N m^{-2})
1412	719600	3223235	4.1	37.1	17.3
1411	719900	3224135	2.2	34.7	15.8
1389	725200	3227810	2.4	28.9	15.1
1394	725600	3229210	3.9	43.2	14.9
1005	729750	3235935	1.0	30.8	16.4
1013	730375	3236885	1.4	24.8	11.5
1014	730525	3236710	1.7	24.4	11.3
1015	734175	3239810	34.9	48.0	17.6
1018	734575	3240435	23.6	56.9	29.6
1019	734475	3240710	10.9	57.1	30.9
1024	738125	3242735	1.5	57.3	29.7
955	738975	3243210	3.7	51.4	23.4
952	740500	3244110	1.3	46.6	20.4
947	740675	3243985	11.6	53.1	21.6
948	741050	3243960	17.5	49.8	19.4
949	741175	3243935	12.6	54.1	20.7
950	741500	3243835	19.7	55.2	24.7
951	741875	3244210	22.2	44.9	14.0
956	742330	3244326	11.8	47.8	16.4
957	743275	3243410	5.3	50.6	24.5
1025	745075	3243035	3.4	60.3	21.4
1026	745250	3243310	4.2	58.9	26.7
1027	745375	3243385	9.8	58.2	26.7
1028	745475	3243485	4.5	57.2	27.1
958	745775	3243560	3.8	57.2	27.6
959	746725	3245085	3.2	44.5	23.3
960	746925	3245360	1.4	43.4	21.5
961	747125	3245485	1.9	43.3	20.9
962	747225	3245710	1.6	43.2	25.6
963	747250	3245760	2.0	42.8	25.7
964	747650	3246485	0.7	44.6	17.9
1372	749425	3248660	1.0	22.6	9.8
1374	749600	3248285	1.4	21.7	8.8
979	750225	3246735	17.6	36.4	17.9
980	750750	3246435	3.0	32.1	16.1
1375	752675	3242185	2.1	32.8	16.3
1376	752750	3241910	2.8	29.7	14.8
1377	752800	3240610	15.8	31.9	14.2
1379	752275	3238485	12.6	49.2	18.3
1380	752350	3238285	9.1	48.5	19.0

Site ID	Easting (m)	Northing (m)	Retreat rate (m yr^{-1})	Wave power (W m^{-1})	Radiation stress (N m^{-2})
1381	752500	3237935	1.7	33.7	14.2
1382	752550	3237560	3.0	27.5	13.3
981	762625	3238835	3.1	28.0	12.7
982	762925	3237660	14.3	37.1	18.3
983	763450	3236860	2.5	30.0	13.8
985	764525	3235235	5.6	33.0	14.2
986	765150	3234735	2.2	21.0	7.2
988	765300	3233785	2.4	22.1	10.5
989	766050	3232210	3.3	24.5	10.5
1000	764875	3229860	2.3	26.3	11.6

Vita

Cody Johnson grew up in Florida and developed an appreciation for the coastal environment. He attended Florida State University and received a B.S. in geology. His career now focuses on the application of science in the conservation and engineering of the coastal landscape.

In his spare time, he tries to keep up with the advancements of technology, enjoys the game of soccer, and strives to understand the effects of climate change.